DEVELOPMENT OF A MULTILAYER VASCULAR GRAFT WITH TARGETED CELLULAR INTERACTIONS AND IMPROVED MECHANICAL PROPERTIES

A Dissertation

by

ALLISON DAVIS POST

Submitted to the Office of Graduate and Professional Studies of
Texas A&M University
in partial fulfillment of the requirements for the degree of

DOCTOR OF PHILOSOPHY

Chair of Committee,	Elizabeth Cosgriff-Hernandez
Co-Chair of Committee,	Melissa Grunlan
Committee Members,	Daniel Alge
	Magnus Hook
Head of Department,	Michael McShane

December 2018

Major Subject: Biomedical Engineering

ABSTRACT

Limited long-term patency of synthetic small diameter vascular grafts has driven considerable research to address their two main failure modes: thrombosis and re-occlusion of the vessel due to intimal hyperplasia. To address these limitations, our lab has created a multilayered graft with a hydrogel inner layer that promotes post-implantation endothelialization for initial and sustained thromboresistance and an electrospun outer layer with arterial compliance matching to limit intimal hyperplasia. In this work, we provide improvements in cellular interactions, outer layer mechanics, and hydrogel design to increase the graft's potential for long term patency.

First, we further characterized cellular interactions with the inner layer that promote thromboresistance upon endothelialization. To optimize these interactions, we investigated specific integrin targeting utilizing designer proteins and their effect on endothelial cell hemostatic regulation. Elucidation of this relationship allows for tailoring thromboresistance of our inner layer as well as other blood contacting devices. We further improved the graft by increasing outer layer compliance matching and elucidated the intrinsic relationship between compliance mismatch and the development of intimal hyperplasia. We first fabricated grafts of increasing compliance while maintaining safe burst pressures and suture retention strength by modulating electrospinning parameters without altering graft chemistry. Grafts sutured to carotid arteries were cultured for two weeks before interrogation of early intimal hyperplasia markers. Changes in these markers were correlated to differences in wall shear stress predicted by a computational model of fluid flow changes based on dilation differences in compliance mismatch. With this relationship understanding, we created a high compliance graft that limits development of early markers for intimal hyperplasia and validated a system for rapid graft screening. Finally, we developed a suture

damage resistant hydrogel formulation that enables safe graft implantation without adversely affecting bioactivity of the inner layer. We also identified properties determinant of suture damage resistance that enable development of future hydrogel formulations.

Overall, this work improves multiple aspects of a multilayered graft for long term patency. Additionally, we have elucidated fundamental material properties and biological relationships that can be used to enhance not only the multilayer vascular graft, but also biomaterial design for other cardiovascular devices.

DEDICATION

To my mom and sister, who not only showed me what it is like to never give up, but how to persevere with hope, love, and humor.

ACKNOWLEDGEMENTS

First, I would like to thank my advisor, Dr. Elizabeth Cosgriff-Hernandez, for her instruction and patience during this process. I owe much of my knowledge of polymers, experimental planning, data interpretation, and much more to you. Thank you also for taking the considerable time to help me improve my presentation and writing skills, an ongoing process. I'm fortunate to have an advisor who pushes me to become a better scientist and leader. In addition to scientific mentorship, you have also provided invaluable guidance in life, demonstrating dedication to both work and family and providing thoughts and advice on life's opportunities and challenges. Thank you for helping me to navigate through graduate school and far beyond.

I would also like to thank my committee members, Dr. Melissa Grunlan, Dr. Daniel Alge, and Dr. Magnus Hook, for their guidance and support throughout the course of this research. Dr. Grunlan's class was one of the most beneficial of my graduate experience, and neatly laid the foundation of polymers for the remainder of my time in research. Dr. Alge has provided helpful input not only in project development, but career development as well. Dr. Hook has been an incredible resource for Scl2 consultations, as well as discussions about future career paths. It has been an honor to have you all serve as my committee.

Thank you also to my many mentors, collaborators, and colleagues. First, thank you Dr. Liezl Baloaing and Dr. Jane Grande-Allen, as you were some of the first to set me on this path and provide invaluable advice and experience. Thank you Dr. Patricia Diaz-Rodriguez (Dr. Mariah Hahn) for your collaboration and encouragement on the bioreactor work. The time spent working with you in Troy was challenging, but you made every day seem new and exciting with

your obvious love and appreciation for the work. Thank you to Dr. Sam Paulsen (Dr. Jordan Miller) for teaching me the ins and outs of the frustrating yet rewarding world of COMSOL. I would still be stuck on the welcome page if it weren't for your help and patience. Thank you, Sevinj Isgandarova and Dr. Margie Martinez-Moczygemba, for your instruction and positive collaboration on the many flow cytometry studies I performed throughout my graduate study. Your input has truly elevated the work. Thanks to Dr. Egeman Tuzun and his team for performing *ex vivo* suturing and animal studies that have led to considerable advancement in the graft design. Many thanks to Dr. Jose Rivera and Dr. Wen Liu (Dr. Magnus Hook) for all of their help in production and troubleshooting of the Scl2 proteins. Thank you, Madeleine Gomel (Dr. Grande-Allen), for accommodating my many platelet studies in the lab. Thank you, Imran Vohra and Alyssa Shapiro (Dr. Rebecca Richards-Kortum), for being my "vampires" and for making yourselves available any time to do a blood draw.

My graduate school experience has been shaped by my incredible lab mates. Dr. Alysha Kishan, thank you for being an amazing work buddy and friend. Your reassurance and patience for my all too frequent panic have enabled me to stay on this roller coaster, and your lab competence and productivity set a high bar to reach for. Thank you, Stacy Cereceres, for your laughter and encouragement even during challenging times and for your creative crafts that bring everyone a smile. Dr. Michael Whitely, your high quality of work has pushed me to become a better researcher and presenter. Thank you Dr. Thomas Wilems, for reading and editing hundreds of pages of writing and for keeping the lab running. Thank you Prachi Davhalikar and Taneidra Buie for your long-distance help in data collection. Thank you Dr. Nick Sears for "nickaneering" so many crucial tools for my work. Dr. Siliang Wu, thank you for all of your electrospinning work. Thank you to Megan Wancura, Ziyang Lan, and Gabriel Rodriguez, for bringing fresh new

perspectives and fun to the lab. I will miss working with you all. I would also like to thank my hard-working undergrads Nico Medellin, Job Shiach, and Ellen Wang- it was a pleasure to work with you.

I have been blessed with many friends who are like my family. Thank you, Michaela Lindsay, for your life-long friendship, limitless optimism, and daily reminders that we do, in fact, got this. You are wonderfully kind to have me crash any time I had a last minute trip to Austin, even having food and drinks on hand. Thank you Chris Norwood and Rory Pearce for being my caretakers and for reminding me I have strength when I thought it was gone. I'm so glad you all are here to help celebrate the wins and recoup the losses with a good Sunday Funday. Tyler Young, thank you for getting me through the first half of this journey and for your continued love and support. Thank you to my Houston crew- Katie Dollinger, Alex Garza, Phil Adam, Andrew McDermott, Billy Hered, and Ari Ince, for providing much-needed diversion and entertainment with great company and a cold beer. Thank you to my long distance other halves: Barb Thorne-Thomsen, Nicole Orchard, Gabi Larus, Emily Romano, and Maria Failla, for your virtual love and encouragement in the form of endless texts, calls, and FaceTimes, even as you are just as busy pursuing new careers and degrees. You each truly inspire me. Hopefully I will now be able to travel more for reunions!

Finally, words cannot express my boundless gratitude to my family, who have been fundamental to my success. Mom (Patricia Post), Cat (Catherine Post), Manu (Manuel Kronhaus), and Michael Bell, thank you for your never-ending support, love, and understanding. Mom, you and Dad have always been my biggest cheer leaders, and I'm so fortunate you made sure we had every opportunity to reach our full potential. I would not have made it this far without your encouragement and guidance during all the times I felt lost. Thank you for all you

have taught me and for being an incredible role model. Cat, I'm so thankful to have you for my sister. Your humor and wit have always lifted my spirits, and your bravery and tenacity are something I aspire to. Many thanks to you and Manu for the fun Javi videos and for commiserating with me on FaceTime. And Michael, thank you for being a pillar of support and enabling this work by picking up all of my slack while I worked seemingly constantly. I can't begin to tell you how many of my days you have made so much better with your calm reassurance, wonderful meals, and thoughtful advice. I am forever grateful. In addition to these brilliant people, I have been gifted with many who are my unofficial family- thank you to my DeRidder Aunts, my Second Moms, and my Lake Charles family. I am lucky and grateful to have so many wonderful people in my life to support and encourage me.

CONTRIBUTORS AND FUNDING SOURCES

This work was supported by a dissertation committee consisting of Dr. Elizabeth Cosgriff-Hernandez (chair), Dr. Melissa Grunlan (co-chair), and Dr. Daniel Alge of the Department of Biomedical Engineering and Dr. Magnus Hook of the Institute of Biosciences and Technology.

The *ex vivo* organ culture system and histological data analyzed for Chapter III and the whole blood platelet adhesion data in Chapter IV was provided by Dr. Mariah Hahn of the Rensselaer Polytechnic Institute. The carotid artery suturing depicted in Chapter IV was performed by Dr. Egeman Tuzun. All other work conducted for the dissertation was completed by the student independently.

Graduate study was supported by the Diversity Fellowship from Texas A&M University and by NIH grants R01 EB013297 and R21 EB020978.

TABLE OF CONTENTS

Page

LIST OF FIGURES

Page

LIST OF TABLES

Page

CHAPTER I

INTRODUCTION AND LITERATURE REVIEW

1.1 Clinical Need and Current Graft Options

Coronary artery bypass grafting (CABG) surgery is one of the most common procedures performed in the U.S. with over 427,000 surgeries performed each year.[1] Autologous vessels typically harvested from the saphenous vein are the clinical gold standard. However, these vessels are unavailable in up to 85,000 patients each year due to previous grafting procedures, systemic vascular disease, or a size mismatch between the graft and the artery to be grafted.[2-4]

Many approaches have been taken to address the limitations of current clinically available grafts. These approaches include cadaver grafts, tissue engineered constructs, and synthetic grafts, each with their own advantages as well as drawbacks. Cadaveric grafts are readily available as an autograft alternative, but CABG procedures with these grafts have been met with limited success. Cadaveric grafts include both human and animal vessels, and all must be heavily processed in order to eliminate immunogenic concerns. In one such process, cryopreservation is utilized to reduce antigenicity concerns with little success. This process contributes to creating a more brittle graft that can cause early rupture of the grafts.[5,6] Even with the use of immunosuppresants, these grafts have high failure rates.[7,8] Decellularized grafts reduce immunological concerns, but require pre-endothelialization for long term success.[9,10]

Tissue engineered grafts have demonstrated increasing success in longer term studies. These grafts are typically protein based, such as those made from collagen, elastin, or fibrin.[11-15] The most successful grafts to date are in vitro cultured vascular grafts.[16-18] Notably, Niklason et al. utilize a bioreactor to culture smooth muscle cells (SMCs) on a tubular, biodegradable

polyglycolic acid (PGA) scaffold. ECs are then seeded onto the scaffold after 8 weeks of culture. These grafts exhibit high burst pressure, but have proven difficult to translate to human cells, requiring additional cellular modifications.[19] Although initial data for these grafts is promising, the extensive preparation time is not conducive to clinical translation.

Synthetic grafts are easily stored and require little to no preparation before implantation. Synthetic vascular grafts composed of expanded polytetrafluoroethylene (e.g. Gore-tex®) or polyethylene terephthalate (e.g. Dacron®) have demonstrated satisfactory long-term outcomes in large- (>8 mm) and medium-diameter (6 - 8 mm) arteries, but poor patency limits their application in small-diameter vessels (< 6mm) and has been attributed to thrombosis and the development of intimal hyperplasia.[20] In order to reduce the thrombogenicity of synthetic grafts, various coatings have been introduced to the surfaces of the grafts.[21,22] Drug coatings such as Persantin or heparin have been investigated. Although the short term results are promising, there is little long-term data to establish this as an effective strategy to reduce thrombogenicity.[23] Another promising short term approach is incorporating nitric oxide (NO) into the graft, which inhibits platelet aggregation.[24-26] Most delivery methods for NO are limited to relatively short time frames, restricted by the amount of NO producer that can be incorporated into a graft material.

In summary, the limited availability of autografts and the low patency rates of synthetic grafts, typically lasting no more than 5-10 years, has established a strong clinical need for new small-diameter graft design.[27] As mentioned above, synthetic grafts typically fail either due to thrombosis or reocclusion due to intimal hyperplasia. Improvements to the vascular graft design would require an effective thromboresistance strategy that does not necessitate additional medication as well as improvement of mechanical properties in order to limit the onset of intimal hyperplasia.

1.2 Hemostatic Regulation

1.2.1 Importance of hemostatic regulation

A critical limitation of synthetic vascular grafts and other early blood-contacting medical devices was their propensity to fail due to thrombosis. Aggregation of activated platelets can occlude blood vessels and lead to downstream morbidity due to emboli that travel to the patient's lungs or brain. These early failures led to a critical investigation of methods to prevent thrombosis, namely the generation of anti-thrombotic coatings for medical devices. Current research aims to understand and recapitulate the body's anti-thrombotic surfaces to improve the patency of blood-contacting medical devices. The endothelium provides dynamic hemostatic regulation of all blood-contacting surfaces in the body. Thus, promoting endothelialization of cardiovascular devices is a popular strategy for generating long-term thromboresistance and controlling hemostasis without the need for systemic anti-platelet therapies. Endothelial cells prevent platelet activation, provide a protective and selective barrier to underlying tissues, respond to injury, and activate clotting when necessary.[10,28-30] Importantly, the endothelial cell layer is a dynamic system that accomplishes all of these tasks by responding to cues not only from circulating blood but also from the underlying extracellular matrix (ECM).[31] These environmental cues, such as biochemicals, shear stress, and attachment matrix constituents, are responsible for changes in endothelial cell phenotype and determine which anti- or pro-thrombotic constituents are released from the cells into the blood stream to regulate hemostasis.[32-46,47] Fundamental understanding of how the ECM influences endothelial cell hemostatic regulation would enable enhanced cellular interactions with small diameter vascular grafts by providing specific targets for cell adhesion, allowing for optimized biomaterial design.

1.2.2 Endothelial cell hemostatic regulation

Endothelial cells have several mechanisms for regulating coagulation and inflammation.[48,49] In addition to providing a physical barrier to the pro-thrombotic ECM, endothelial cells are responsible for the initiation or direct regulation of coagulation, platelet function, and fibrinolysis to minimize adverse consequences of vascular injury, as well as maximize vascular repair capabilities.[29,50,51] Disruption of these regulatory functions can lead to cardiovascular disease or sudden cardiac death, highlighting the importance of the endothelial layer in cardiovascular systems.[28-30,52-60]

In controlling coagulation, the endothelial cells bind antithrombin III that is responsible for inactivation of thrombin, Factor Xa, and Factor IXa in the coagulation pathway, slowing coagulation.[29] The ECs also express thrombomodulin, which in turn promotes the activation of protein C in concert with endothelial protein C receptor.[61] Protein C is an anticoagulant that limits the conversion of Factor VIII to Factor VIIIa and prevents the conversion of Factor V to Factor Va.[61] Endothelial cells also prevent coagulation by expressing tissue factor pathway inhibitor (TFPI) which inhibits the conversion of Factor VII to Factor VIIa.[62] Without these controls, the coagulation pathway would proceed unchecked and clotting would be prolific in the body leading to increased rates of stroke, embolisms, and heart attacks.[28,29]

Platelets play a critical role in coagulation with fibrin-stabilized platelet aggregates able to rapidly form hemostatic plugs upon vessel damage.[63] Endothelial cells can rapidly promote platelet adhesion and activation by producing and releasing von Willebrand factor (vWF). vWF is a blood glycoprotein that binds to Factor VIII as a stabilizing agent against protein C, platelet surface glycoproteins, and constituents of the ECM. vWF exists in two compartments in endothelial cells: constitutively secreted pathway where dimerized vWF is exported to the plasma and

subendothelial matrix, and residing in a granular store containing very highly multimerized vWF that can be mobilized rapidly in response to agonists such as thrombin.[64] Endothelial cells also produce ADAMTS13, which cleaves the ultra-long vWF strings (ULVWF) that form to capture platelets.[43,65-68] Platelets also reduce platelet activation by producing prostaglandin I2 (PGI_2) and endothelial nitric oxide synthase (eNOS).[69] Synthesis of these molecules is triggered by increases of intracellular calcium ion concentrations in endothelial cells. PGI_2 and nitric oxide (NO) are both potent vasodilators and inhibit platelet activation. The powerful anti-aggregatory and vasodilator properties of PGI2 and nitric oxide make them critical regulators of hemostasis.

Endothelial cells also play an important role in fibrinolysis, or the enzymatic breakdown of blood clots, an important consideration for medical devices by enabling endothelial cells to help eliminate small clots and prevent large thrombi formation. To this end, endothelial cells synthesize and acutely release tissue plasminogen activator (t-PA), a protein that is involved in the dissolution of blood clots by converting plasminogen to active plasmin. tPA is constitutively released from small granular stores that are separate from vWF stores.[70] Endothelial cells release plasminogen activator inhibitor PAI-1 (the main t-PA inhibitor) in activated conditions to prevent excessive fibrinolysis by blocking the action of t-PA.[70] The regulation of t-PA and PAI-1 is vital to healthy vasculature because an imbalance of either of these factors leads to hemorrhagic disease or hypercoagulable states.

Endothelial cells are responsible for releasing a number of products that trigger signaling cascades that carefully balance the cell response to maintain hemostasis. A summary of the prothrombotic and antithrombotic agents regulated by endothelial cells is provided in **Table 1.1**. When disease states are induced in endothelial cells, either from extracellular or intracellular cues,

this balance is perturbed. Therefore, it is critical to maintain endothelial cell health when attempting to recapitulate the endothelial cell environment for cardiovascular applications.

Table 1.1: Common hemostatic regulators synthesized by endothelial cells in response to environmental cues.

	Protein	**Function**
Prothrombotic Proteins	Von Willebrand Factor (VWF)	Binds platelets to form platelet thrombi when in ultra-large multimer form [da Silva 2016]
	Tissue Factor (TF)	Surface protein expressed by activated endothelial cells to initiate coagulation cascade [White 2010]
	Plasminogen activator inhibitor (PAI-1)	tPA inhibitor [Booyse 1999]
Antithrombotic Proteins	A disintegrin and metalloproteinase with a thrombospondin type I motif, member 10 (ADAMTS-13)	VWF cleaving enzyme [Shim 2008]
	Tissue factor pathway inhibitor (TFPI)	Major inhibitor of TF, Factor Xa, and thrombin [White 2010]
	Tissue plasminogen activator (tPA)	Regulator of fibrinolysis [Booyse 1999]
	Endothelial nitric oxide synthase (eNOS)	Synthesizer of nitric oxide that inhibits platelet aggregation [Warner 2016]

1.2.3.3 Basal lamina

The basal lamina is crucial for the maintenance of a confluent and functional endothelial cell monolayer that provides the dynamic hemostatic regulation described above.[55,56,71] It is typically 20-120 nm thick and can prevent the movement of cells from one layer to the next while

selectively filtering molecules that are transported across it.[28,72] The basal lamina is composed of many components that work synergistically together to not only promote cell adhesion but also influence cell phenotype and genotype.[73-75] It is composed of collagen, fibronectin, elastin, laminin, glycosaminoglycans, and proteoglycans in varying concentrations depending on the location of the tissue in the cardiovascular system.[30,76,77] Varying these components can change the cell response based on ligand type and availability.[78] Although it is the combined presentation of the individual components that drives cellular functions, understanding how each component contributes to the mechanical and biochemical characteristics of the basal lamina will allow for improved constituent selection when creating substrates for endothelial cell growth, whether for antithrombotic coatings or for investigating cell behavior. A summary of the key components of the basal lamina is provided in **Table 1.2** and detailed in the sections below.

Table 1.2: Summary of the main ECM components found in the basal lamina, their roles, and respective locations.

ECM Component	Role	Compositional Variation with Location
Collagen	Tensile strength, cell adhesion and signaling	Coarse in aortic smooth muscle cell-derived substratum; exclusive production of type IV in HUVECs; prevalence in I, III, small amounts of IV in large blood vessels; large amounts of I and III in capillaries; I and III found in smooth muscle matrix; abundant in arterial walls; present in tunica media; high relative content in tunica adventitial; mostly I, III, IV, V, VI in mice aorta.
Fibronectin	Cell adhesion, proliferation, migration, and differentiation	Exists within ECM of submucosal structures and basement membrane structures; prominent in migratory pathways for embryonic cells; present in loose connective tissue and in clots in association with fibrin; increased during fibrotic process.
Laminin	Cell adhesion, migration, and differentiation; main ECM structural organizer	Major component of basement membranes, including cardiovascular basal lamina and tumor tissue.
Elastin	Tissue recoil and elasticity	Loose layer of fibrils in aortic smooth muscle cell-derived substratum; abundant in arterial walls; mostly elastin in tunica media; present in tunica adventitia.
Other components	Hydration, cell signaling, clotting	Glycosaminoglycans, proteoglycans, thrombospondin, fibrinogen

Collagen is the most prominent constituent of the basal lamina and is responsible for tensile strength and cellular adhesion. Although 28 types of collagen have been identified, collagen type I and IV are the most prevalent types found in the cardiovascular system.[79] Collagens have a hallmark triple helical structure and are typically involved in forming fibrillar networks in the

ECM that impart strength and structure to the basement membrane.[76] Collagen's rope-like structure provides resistance to tensile forces by carrying stress.[80] Furthermore, collagen is one of the main ECM components responsible for imparting cellular adhesive properties through several receptors including binding sites for the α1β1, α2β1, α10β1, and α11β1 integrins, known as the collagen receptor subfamily of integrins.[81] Attachment to these integrins is promoted via the GFOGER peptide sequence.[79] In addition to binding via integrins, cells also bind to collagen through syndecan-1.[82] Therefore, collagen is vital to basal lamina due to providing significant mechanical strength and biochemical cues that enable cell adhesion and migration.

Fibronectin, a glycoprotein, is another major constituent of the basal lamina and is formed by two nearly identical polypeptide chains attached via disulfide bonds to form a dimer structure.[83] Fibronectin exists in both soluble and insoluble forms.[83] Soluble fibronectin circulates in the blood and other body fluids, and insoluble fibronectin is found within the ECM. Although transcribed from a single gene, fibronectin within the ECM has multiple forms as a result of alternative splicing that can generate up to 20 variants.[83] These fibronectin variants promote specific cellular and ECM interactions by generating different adhesive ligands. For instance, fibronectin facilitates cellular attachment of endothelial cells to the ECM via integrin binding sites, primarily integrin α5β1, but also αvβ3, α4β1, α4β7, and α9β1 with RGD, PHSRN, LDV, and REDV binding sites.[83] Additionally, fibronectin not only binds to cells but also promotes adhesion to other ECM components such as collagen, primarily in denatured regions of collagen triple helices through functional and structural domains, as well as heparin and fibrin through specific binding domains.[77,83] Overall, fibronectin offers complex interactions of the basal lamina with ECs and their environment.

Elastin is another major component of the basal lamina and provides elastic recovery after stretch or deformation of the tissue, a common occurrence in the body's vasculature. Elastin is made from the soluble precursor molecule tropoelastin that generate a highly insoluble crosslinked network.[80] The lysine amino acids of tropoelastin are extensively crosslinked immediately after release from the cell by oxidative deamination of the lysine side chains via the enzyme lysil oxidase with subsequent condensation linking two, three, or four side chains.[80] The elasticity of the resulting elastin network is attributed to the loose, random coil conformation of the resulting polypeptide chain. The stretching of elastin is limited by interwoven stiff collagen fibers, and the overall stress response of ECM is dictated by the interplay and concentrations of collagen to elastin. Elastin has not shown cell adhesive properties and the function appears to be limited to providing important mechanical recoil to tissues.[80]

Laminin is a key organizer of the basal lamina's structure as it can self-assemble into sheets, bringing together the other basal lamina components through crosslinking. Laminin is composed of three long polypeptide chains (an α, a β, and a γ chain) held together by disulfide bonds. 18 laminin trimers have been investigated and described, with laminin-1 as the most prominent in the basal lamina. In addition to being an important ECM crosslinker, laminin enables ECM interactions with many different cell types through its diverse binding sites for cellular surface receptors. For example, laminin has binding sites for integrins α3β1, α6β1, α7β1, and α6β4 as well as binding sites for syndecans 1, 2, and 4, creating a diverse array of cellular responses and interactions.[84]

Glycosaminoglycans (GAGs) are unbranched polysaccharide chains composed of repeating disaccharide units and are essential to the formation of the ECM as hydrophilic space-fillers. GAGs form gels at low concentrations and allow the ECM to resist compressive forces by

hydrating and filling most of the extracellular space.[80] GAGs are considered the "most anionic molecules produced by animal cells" and hydrate the ECM by attracting water molecules due to their high negative charge.[80] GAG chains can be covalently linked to a core protein, forming a proteoglycan.

Proteoglycans are abundant in the ECM and can regulate the activities of secreted ECM proteins by binding to them. They play a major role in chemical signaling between cells by changing conformations or blocking of binding sites.[80] Although many proteoglycans are secreted, some remain as trans-membrane proteins, known as syndecans, and act as receptors for ECM proteins.[85] The diverse family of GAGs and proteoglycans are responsible for not only hydration but also ECM-endothelial cell interactions that regulate cellular behavior.

In summary, the individual components of the ECM work in concert to define the biochemical and mechanical landscape of the basal lamina. Interactions of endothelial cells with these individual components then initiate signaling cascades to affect cytoskeletal organization and gene expression. Understanding the individual qualities and combined synergistic effects of the basal lamina constituents allows for tailoring of substrates for desired cell growth and behavior.

1.2.3 Effect of ECM components on endothelial cell hemostatic regulation

As discussed above, the basal lamina is the ECM that supports endothelial cells in the cardiovascular system with major components consisting of collagen, laminin, fibronectin, elastin, proteoglycans, and glycosaminoglycans.[71,76,77] Endothelial cells bind uniquely to these components using different transmembrane proteins, such as integrins and syndecans.[55,71] Integrin and syndecan binding to ligands on the basal lamina initiates intracellular signaling cascades that affect many cell behaviors including migration, proliferation, apoptosis, and hemostatic

regulation.[28,53,71,86-89,90] Elucidating key relationships between integrin binding, signaling cascades, and the corollary changes in a cellular hemostatic regulators has become an area of interest for researchers. Elucidation of the key mediators of anti-thrombotic cell behavior can provide improved material design of thromboresistant coatings for blood-contacting devices.

Integrins and syndecans are transmembrane receptors that facilitate ECM-endothelial cell adhesion. These transmembrane proteins uniquely interact with ECM ligands and provide a method for signal transduction from the exterior of the cell to the interior. Understanding which integrins and syndecans are responsible for attachment to individual ECM components in the basal lamina will elucidate the signaling cascades leading to changes in endothelial cell gene expression, **Figure 1.1**.

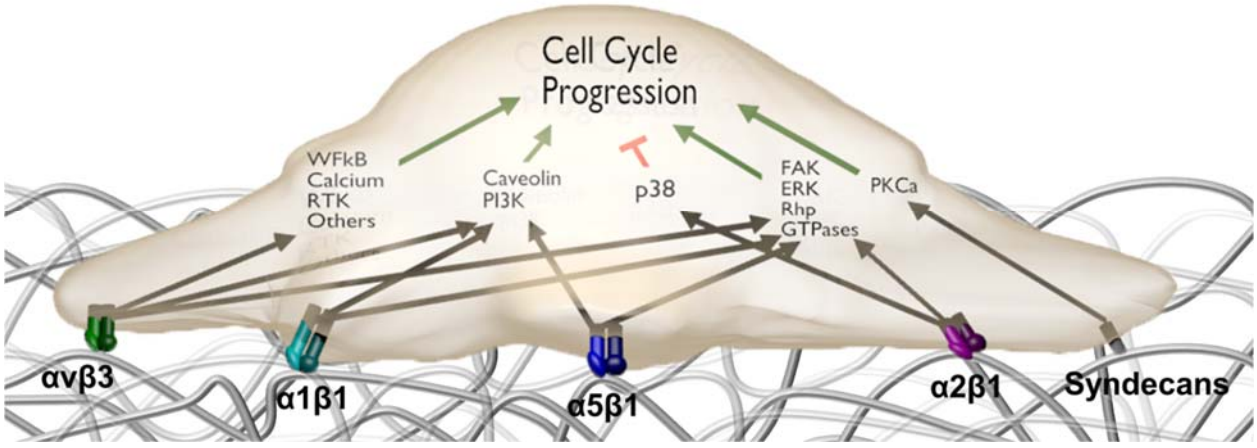

Figure 1.1: Common integrin and syndecan signaling pathways in endothelial cells.

1.2.3.1 Integrin Expression in Endothelial Cells

Integrins are critical for not only anchoring cells to the ECM and mediating migration but also important transducers of intracellular signaling that influence cell phenotype.[91,92] Integrins are a large family of transmembrane proteins that exist as heterodimers, with 18 unique α and β subunits that combine to form 24 distinct dimers that bind to specific amino acid sequences within ECM proteins.[71] A list of common integrins and their respective ligands are listed in **Table 1.3**. Endothelial cells express α1β1 that binds to collagen, α2β1 that binds to collagen and laminin, α3β1, α6β1, and α6β4 that bind to laminin, α4β1 and α5β1 that find to fibronectin, and αvβ3 and αvβ5 that selectively bind to vitronectin.[87,93,94] The extracellular portion of these transmembrane proteins links to ligands on the ECM, and the intracellular part of integrins associate with actin binding proteins, including vinculin, α-actinin, paxillin, talin, zyxin, tensin, and filamin.[95] Signaling pathways are then activated by the actin binding proteins which may lead to downstream changes in the chemical or mechanical composition of the ECM, or affect cell behavior such as proliferation, migration, and differentiation.[96,97] One of the key regulators of integrin-matrix signaling includes the focal adhesion kinase, or FAK, and can play a role in inflammation and hemostasis.[98] For example, one of the major signaling pathways initiated by the Src-FAK complex is the Ras-MEK-MAPK pathway that affects the transcription of genes important to cell cycle progression.[95]

Table 1.3: Summary of relevant integrins with corresponding cell expression and extracellular ligands. Fg= fibrinogen, Coll=collagen, Fn= fibronectin, Vn= vitronectin, Tn= tenascin, Ln= laminin, Opn= osteopontin, Tsp= thrombospondin.

Integrin	Cell type	Proteins with attachment ligands
α1β1	Endothelial cells, lymphatic endothelial cells	Coll VI, Col lI, Ln
α2β1	Human platelets, lymphatic endothelial cells	Coll 1, Coll IV, Ln
α5β1	HUVECs	Fn, Fibrillin-1
αIIbβ33	human platelets	
αvβ6	epithelial cells	Fn, Fg, Vn, Tn, LAP-TGFβ, Fibrillin-1
αvβ1	SMCs, fibroblasts, endothelial cells	Ln, Fn, Opn, Vn
αvβ3	Human platelets, endothelial cells, SMCs, fibroblasts, leukocytes	Fg, Vn, Tn, Opn, Tsp, Fn, VEFG-A, Fibrillin-1, vWF
α4β1	Endothelial cells, leukocytes	Fn
α9β1	Endothelial cells	Tn, VCAM-1, VEFG-A, VEGF-C, VEGF-D, HGF
α6β4	Endothelial cells	Ln
αIIbβ3	Human platelets	Fg, Fn, vWF
αEβ7	Leukocytes	E-cadherin
αXβ2	Leukocytes	Fg, heparin
α6β1	endothelial cells	Ln
α8β1	SMCs	Fn, LAP-TGFβ
αvβ5	Endothelial cells, SMCs, platelets, epithelial cells, leukocytes	Opn, Fg, Vn, Fn, Tsp

Not only does the type of integrin affect cell adhesion and signaling, but the location of the integrins and their abundance affect the strength of cellular adhesions and response of the cell. For example, focal adhesion complexes are strong, stable adhesions formed when integrins are clustered on the cell surface, allowing for many cytoskeletal filaments to attach at the resulting plaque.[99] Endothelial cells are dependent on these attachments for cell survival, as detachment from their substrate leads to upregulation of apoptotic signaling. Focal adhesion complexes also recruit intracellular proteins such as focal adhesion kinase (FAK), a cytoplasmic tyrosine kinase

that plays an important role in cell survival by activating essential signaling pathways critical for the prevention of apoptosis.[12,71,100-102]

There are a multitude of other focal adhesion proteins involved in establishing and maintaining cytoskeletal linkages: integrin-bound proteins that directly bind actin, such as talin, α-actinin, and filamin; integrin-bound proteins that indirectly associate with and regulate the cytoskeleton such as kindling, integrin-linked kinase (ILK), paxillin, and FAK; non-integrin-bound actin-binding proteins, such as vinculin; and adaptor and signaling molecules that regulate the interactions of the proteins of the afore-mentioned groups.[95] These molecules then go on to affect many common cellular pathways such as the Akt, ERK, JNK, RhoA, Rac1, and Cdc42 pathways. Each of these pathways then uniquely affects cell survival, proliferation, differentiation, migration, adhesion, and polarity by modulating gene expression, cell cycle regulation, focal adhesion turnover, and actin dynamics. A review by Legate et al. provides detailed information about the individual pathways and their effects.[95] For example, β1 integrins are involved in a signaling pathway with RACK that results in increased cell migration toward insulin-like growth factor 1, or IGF-1. Binding of the αvβ3 integrin has been shown to induce a β3-SHP-2 interaction that sequesters phosphatase and prolongs IGF1R signaling, that plays an important role in growth and development.[86,95,103,104]

Overall, integrins provide complex and wide-ranging modes of attachment and signaling in endothelial cells. The endothelial cell presentation and available ECM binding sites dictate the resulting cell behavior. However, it remains challenging to isolate the role of one integrin from another in order to discern the individual and synergistic contributions of these interactions. Elucidation of these roles would provide greater understanding of how cells regulate hemostasis and how specific binding events can be incorporated into material design to facilitate that process.

1.2.3.2 Syndecans

The evolving roles of syndecans, type I membrane glycoproteins composed of GAG chains covalently linked to a core protein, is becoming increasingly important in understanding ECM - endothelial cell interactions.[105] Syndecans often act as co-receptors to ligands such as vascular endothelial growth factor (VEGF) and fibronectin that have interactions of particular interest in the ECM and are relevant for tissue engineering.[106] The syndecan family is organized into four group members: syndecans-1, -2, -3, and -4, each with distinct functions as shown in **Table 1.4**. For example, syndecan-1 regulates cell-interstitial collagen adhesion and binds to fibronectin, as well as growth factors via heparin sulfate chains.[85] Syndecan-1 is down regulated in endothelial cells and can promote differentiation in vascular smooth muscle cells.[107,108] Syndecan-2 is also found in endothelial cells and binds to ECM components such as fibronectin and growth factors.[85,109] However, further research is required to understand the specific roles of syndecan-2 in cell adhesion. Syndecan-3 is predominantly found in muscle cells and neuroblastoma cells within the nervous system and binds to certain growth factors.[85] However, it has low affinity for fibronectin, collagen I, III, and laminin and therefore plays a limited role in cell adhesion to ECM.[85] Therefore, syndecan-3 is of limited interest in hemostatic regulation. Syndecan-4 is found to be ubiquitously expressed in all cell types, making it a more widespread component than the other syndecans and is known to be involved in focal cell adhesion, a tight interaction between the cell and ECM, ensuring intracellular signaling.[89] Syndecans influence cell interactions significantly in their roles in cell adhesion and binding to ligands in the ECM. Although the importance of syndecans is established, there is still much to learn about the nuances of their function.[82,85,89,110]

Table 1.4: Summary of the syndecan family and their roles as cell attachment mediators.

Syndecan	Cell type	Syndecan receptors	Reference
Syndecan-1	Vascular endothelial cells, human umbilical vein endothelial cells, microvascular endothelial cells	Fibronectin, collagen, growth factors	Hozumi 2006; Beauvais 2009;
Syndecan-2	Human umbilical vein endothelial cells, microvascular endothelial cells	Fibronectin, laminin, collagen, growth factors	Nogur 2009; De Rossi 2014; Halden 2004
Syndecan-3	Human coronary artery endothelial cells, brain endothelial cells	Matrix molecules*, growth factors	Carey 1997; De Rossi 2013
Syndecan-4	Human umbilical vein endothelial cells	Fibronectin, laminin, collagen, growth factors	Gopal 2010; Vuong 2015

1.2.3.4 Effect of each ECM component

In an effort to recapitulate the basal lamina, many ECM-mimetic platforms have been used to culture and examine the behavior of endothelial cells.[111,112] As discussed earlier, endothelial cells bind to ECM proteins via integrins and syndecans, which then initiates intracellular signaling that modulates cell behavior. Although many of the intricacies of the cell-ECM binding are not explicitly discussed in many of the studies discussed here, comparisons of behavior between various ECM components can be used to identify roles of different integrin or syndecan binding and corollary effects on hemostatic regulation.

Collagen-initiated Hemostatic Regulation

Collagen is one of the most prevalent adhesive proteins found in the body and is a commonly selected protein to promote enhanced cellular adhesion to biomaterials. Collagen

studies are typically performed using mammalian-derived collagen either as a coating or as a crosslinked gel.[113] Endothelial cell adhesion to collagen is mediated by integrins α1β1, α2β1, α10β1, and α11β1 as well as syndecans 1 and 4.[93] Studies have also been performed on collagen mimics that have more tailored integrin interactions.[114] These typically require coating studies or chemical crosslinking into another network, as they do not form networks on their own.[115]

Collagen coat studies have demonstrated a difference in not only cell behaviors such as migration and proliferation as compared to TCPS but also differences in hemostatic regulation.[116-120] For example, endothelial cells cultured on collagen-coated ePTFE demonstrated lower levels of PGI_2 and tPA as compared to endothelial cells on an un-coated ePTFE control.[16] This would indicated a less thromboresistant phenotype, but this study did not analyze the production of complementary pro-thrombotic factors in the endothelial cells cultured on these substrates.[16] Another collagen coat study noted an increase in NO production with endothelial cells on the collagen coat as compared to endothelial cells on TCPS, indicating a more thromboresistant phenotype.[116] However, like the previous study, the authors did not discuss the production of pro-thrombotic factors and how the substrate difference would affect their expression. Studies on collagen gels have shown that endothelial cells have decreased expression of PGI2 and vWF, indicating the signaling from collagen attachment is important for endothelial cell regulation of hemostasis.[120]

Scl2 Proteins

Studies on collagen mimics that allow for more specific integrin binding are utilized to further elucidate the interactions between endothelial cells and collagen. Scl2 proteins provide the unique opportunity to tune bioactivity to target specific integrin binding. Streptococcal collagen-like proteins, or Scl2, are recombinant proteins that mimic the triple helical structure of collagen

but do not require post-translational modification for helix formation.[121] The Scl2 proteins, however, are devoid of the native binding sites associated with collagen.[121] Therefore, the bioactivity of the Scl2 protein can then be customized by site-directed mutagenesis to introduce peptide sequences for specific cell surface receptor targeting.[122] For example, the collagen-derived peptide binding sequence GFPGER targets the integrins α1β1 and α2β1 and has been incorporated into Scl2 to tailor bioactivity.[122,123] Scl2 proteins with this targeting sequence are known as $Scl2_{GFPGER}$ proteins, and the binding of integrins to this peptide sequence is strengthened by the triple helical structure of the $Scl2_{GFPGER}$ protein.[124] $Scl2_{GFPGER}$ proteins have been demonstrated to not promote platelet aggregation while still promoting endothelial cell adhesion and migration.[54,86,125,126] Endothelial cells showed increased adhesion on poly(ethylene glycol) (PEG) hydrogels containing the $Scl2_{GFPGER}$ proteins compared to PEG gels alone, as well as comparable adhesion to PEG hydrogels containing collagen.[54,126] Endothelial cells seeded on these scaffolds demonstrated a decrease in NOS3 and TM gene expression, and e-selectin gene expression increased compared to collagen gels. This suggests that integrins α1β1 and α2β1 binding are responsible for these gene expression changes.[119]

Based on the evidence in the studies described above and shown in **Table 1.5**, the binding of these integrins and syndecans to collagen are responsible for the observed changes in the endothelial cell expression of hemostatic regulators. These integrins could be used as targets to increase the thromboresistance such as through increased NO production. However, parsing out the specific integrin interactions is needed to identify specific integrin binding targets for tissue engineering and cardiovascular device coatings.

Table 1.5: Summary of the effects of endothelial cell attachment to collagen on hemostatic regulator molecule expression.

Substrate Application	Cell type	Molecules tested	Results	Reference
Collagen-derived peptide coat	Human umbilical vein endothelial cell; human aortic endothelial cell	PGI2, vWF; PECAM-1, VE-Cadherin, NOS3, TM, E-selectin;	Increase in NOS3 compared to TCPS; No significant change in PGI2, vWF; PECAM-1, VE-Cadherin, TM, E-selectin	Genove 2005
Crosslinked collagen coat	Human umbilical vein endothelial cell; human saphenous vein	PGI2, vWF, tPA, PAI-1	Decrease in PGI2 and vWF secretion; No difference in basal levels of PGI2, tPA increase compared to bare	Wissink 2001; Gillis 1996
ePTFE with collagen-1 coat	Human saphenous vein; human umbilical vein	tPA, PGI2, PAI-1	Decrease in PGI2 and tPA; no difference in tPA secretion; PAI increased; Different levels of PGI2, PAI-1 and tPA between unmodified versus modified PTFE	Li 1992; Gillis 1996; Zhang 1995
Collagen derived peptide hydrogel (PEG-Scl2)	Human aortic endothelial cell	PECAM-1, VE-Cadherin, NOS3, TM, E-selectin	Decrease in NOS3 and TM on PEG-Scl2 and E-selectin increased compared to collagen; no significant change in PECAM-1	Munoz-Pinto 2015

Fibronectin and Gelatin-initiated Hemostatic Regulation

Endothelial cells bind to fibronectin via integrin α5β1, but also α4β1, α4β7, and α9β1 as well as syndecan 4.[83] When endothelial cells are seeded on fibronectin coats, a measured increase in PGI2 as well as tPA was observed as compared to uncoated ePTFE and TCPS.[16,117,118] Endothelial cells bind to gelatin also through integrin α5β1 as well as αvβ3, binding specifically to the RGD binding sequence that becomes accessible on denaturation of the collagen triple helix.[127,128] When gelatin is coated on ePTFE, there are increased levels of PGI2, PAI-1, and tPa

compared to the unmodified ePTFE, suggesting a more thromboresistant phenotype.[129] Studies are commonly performed using RGD, as it is a readily available peptide sequence. When endothelial cells are cultured on RGD that is incorporated into hydrogels, ADAMTS-13, TFPI, tPA, vWF, TF, P-selectin all increased compared to TCPS.[106] With these increases and results summarized in **Table 1.6**, endothelial cells appear to be much more activated on RGD peptides that attach to the integrins α5β1 and αvβ3. Again, these changes highlight specific integrin and syndecan targeting are influencing the endothelial cell hemostatic regulation.

Table 1.6: Summary of the effects of endothelial cell attachment to fibronectin and gelatin on hemostatic regulator molecule expression.

ECM Protein	Substrate Application	Cell type	Molecules tested	Results	Reference
Gelatin	Gelatin coat on TCPS	Bovine aortic endothelial cell; human saphenous vein endothelial cell	PGI2, PAI, tPA	Increase in NO and PAI; Decrease in PGI2 compared to TCPS	Balcells 2002; Gillis 1996
	ePTFE with gelatin coat	Human umbilical vein endothelial cell	PGI2, PAI-1, tPA	Increase in PGI2, PAI-1 and t-PA compared to bare	Lu 2001
	PEG-RGD hydrogel	Porcine aortic valvular endothelial cell	ADAMTS-13, TFPI, tPA, vWF, TF, P-selectin	ADAMTS-13, TFPI, tPA, tPA, vWF, TF, P-selectin all increased compared to TCPS	Balaoing 2015
Fibronectin	Fibronectin coat on TCPS	Bovine aortic; human umbilical vein; human saphenous vein	PGI2, vWF, tPA, PAI-1	Increase in PGI2; decreased vWF compared to TCPS; no significant change in tPA	Balcells 2002; Wissink 2001; Gillis 1996
	ePTFE with Fn coat	Human saphenous vein endothelial cell; human umbilical vein endothelial cell	tPA, PGI2, PAI-1	Increase in PGI2 and tPA compared to bare ePTFE; no significant change in PAI-1	Li 1992; Zhang 1995

Laminin-initiated Hemostatic Regulation

Endothelial cells bind to laminin via integrins α3β1, α6β1, α7β1, and α6β4 as well as syndecan 2.[93] Studies on laminin coats have demonstrated an increase in PGI2 expression, indicating a more thromboresistant phenotype of the endothelial cells.[130] Studies have also been performed on laminin-mimetic hydrogels. A laminin peptide sequence targeting syndecan binding was covalently linked to the surface of poly(ethylene glycol) diacrylate hydrogels. Cells grown on these constructs were then compared to hydrogels with RGD binding sequences linked to the surface of the gels, which interact with integrins α5β1 and αvβ3.[106] The endothelial cells grown on the laminin-mimetic gels showed ADAMTS-13, TFPI, tPA, vWF, TF, and P-selectin all increased, with NO increased compared to plate grown cells.[106] The change of gene expression of hemostatic regulators in targeting syndecan binding indicates that syndecans also play an important role in endothelial cell hemostatic regulation. The effects of laminin on endothelial cell hemostasis are shown in **Table 1.7**.

Table 1.7: Summary of the effects of endothelial cell attachment to laminin on hemostatic regulator molecule expression.

Substrate Application	Cell Type	Molecule Tested	Results	Reference
Laminin coat on TCPS	Bovine aortic endothelial cell	PGI2	Increase in PGI2 compared to TCPS	Balcells 2002
PEG-laminin peptide hydrogel	Porcine aortic valvular endothelial cell; human aortic endothelial cell	ADAMTS-13, TFPI, tPA, vWF, TF, P-selectin; NO	ADAMTS-13, TFPI, tPA, tPA, vWF, TF, P-selectin all increased; NO increased compared to TCPS	Balaoing 2015; Genove 2005

The studies discussed here have demonstrated the importance of the substrate on endothelial cell hemostatic regulation, but few have investigated specific binding interactions and the correlated changes in endothelial cell gene expression and thromboresistance. Future investigation would need to isolate integrin interactions on well controlled surfaces for the culture of endothelia cells. Using these platforms it would then be possible to analyze the changes in gene expression as well as the functional changes in endothelial cell hemostatic regulation. Once specific interactions have been correlated to changes in hemostatic regulation, mechanisms and signaling pathways can be elucidated. Understanding signaling pathways and mechanisms could lead to further tailoring of coating designs for endothelialization of biomedical devices. By elucidating the specific effects of integrin attachment on hemostatic regulation, it would then be possible to target specific endothelial cell binding mechanisms to promote a thromboresistant phenotype in an endothelial cell monolayer.

1.3 Biomechanics and Intimal Hyperplasia

1.3.1 Intimal hyperplasia

Intimal hyperplasia is characterized by intimal thickening that eventually causes vessel re-occlusion and typically occurs at the distal anastamosis of a grafted vessel.[27,131-133] This intimal thickening occurs due to many cell phenotype changes and ECM organizational changes. Central to the disease progression are the changes to vascular smooth muscle cells (VSMCs). VSMCs are highly specialized cells responsible for the contraction and regulation of blood vessel tone, blood pressure, and blood flow.[134] In normal adult arteries, differentiated VSMCs present very low proliferation rates and exhibit a contractile phenotype expressing proteins such as smooth muscle myosin heavy chain (SM-MHC), smooth muscle α-actin (SM-α-actin), smooth muscle 22 alpha

(SM22α), h-caldesmon and calponin, important for the regulation of the vessel contraction.[134-136] However, during the progression of intimal hyperplasia, VSMCs proliferate and abnormally migrate towards the innermost layer of the arterial wall promoting an increase of the wall thickness and a consequent reduction of blood flow.[98,137] When intimal hyperplasia is initiated due to trauma, changes in wall shear stress, or inflammation, VSMCs undergo a de-differentiation process towards a proliferative phenotype, associated with a higher proteoglycan-rich extracellular matrix.[133,135,136,138] Proliferative VSMCs present an increased synthetic activity with higher expression of hyaluronic acid, collagen type 1, elastin, versican, biglycan and fibronectin (interstitial matrix components) while decreasing the synthesis of basement membrane components such as laminin.[134,136,138]

Although most of the intimal hyperplasia morphological changes are associated with the phenotypic switch of VSMCs, all the components of the vessel play an important role in the modulation of the disease initiation and progression.[133] Vascular endothelial cells are key regulators of vessel homeostasis and secrete molecules able to prevent coagulation, promote vasodilation, and control VSMCs proliferation and differentiation.[133,138] However, in the absence of laminar blood flow or injury, endothelial cells become dysfunctional and secret agents that promote coagulation, vasoconstriction, switch VSMCs to a proliferative phenotype, and regulate the infiltration of inflammatory cells. Dysfunctional endothelial cells express adhesion molecules such as intercellular adhesion molecule 1 (ICAM-1), vascular cell adhesion molecule 1 (VCAM-1), E-selectin, and P-selectin.[138] Endothelial cells and infiltrated immune cells also produce cytokines and growth factors that act as inflammatory mediators and further stimulate vascular remodeling.[138,139]

1.3.2 Compliance mismatch

Poor compliance matching has been linked to low patency rates in synthetic grafts. Intimal hyperplasia causes failure of approximately 10-30% of synthetic grafts.[132] This high rate of failure has been correlated with a compliance mismatch between the grafting material and the native vasculature.[132,140] Despite this strong empirical correlation, the mechanisms by which compliance mismatch leads to intimal hyperplasia are relatively poorly understood. It is theorized that the compliance mismatch leads to a flow disruption at the distal anastomosis, that then leads to low wall shear stress.[132,141] The vessel wall, in response to the low wall shear stress, attempts to correct the flow disruption with intimal thickening, ultimately leading to re-occlusion of the vessel.[140]

It has been difficult to directly relate compliance-mismatch and the resulting changes in fluid dynamics to the development of intimal hyperplasia because of confounding factors of graft properties. For example, the often cited high-compliance grafts with improved patency are autografts as compared to the low-compliance synthetic grafts.[140] Isolation of the effect of compliance is ideally conducted on synthetic grafts that can vary compliance independent of other graft variables. Identification of the cause of intimal hyperplasia would allow for improved small diameter vascular graft design. However, in order to design vascular grafts with improved patency, the complex cascade of events that begins with changes in the endothelium and initiates the smooth muscle cell phenotypic alterations that typify intimal hyperplasia need to be elucidated.

1.4 Multilayer Vascular Graft

1.4.1 Multilayer graft design

With the limitations of current efforts toward a small diameter vascular graft in mind, there is a clear need for an off-the-shelf, post-implantation endothelialization small diameter vascular graft that can withstand physiological forces and match the compliance of native vessels. To this end,

our lab has developed a dual layered vascular graft.[86] Addressing both the mechanical and bioactivity design requirements is difficult to achieve in a single material. Therefore, we have created a layered construct to address the requirements separately. The graft consists of an electrospun polyurethane outer layer and a bioactive hydrogel inner layer.

The electrospun outer layer has been tuned to meet the mechanical demands of a vascular graft. Polyurethanes are commonly used in cardiovascular applications as they are typically biocompatible, durable, and exhibit strong fatigue resistance.[142,143] Electrospinning this material creates a fibrous scaffold with mechanical properties that can be easily modulated by tuning the electrospinning parameters to alter fiber morphology and mesh thickness. By altering these parameters, we are able to impart high compliance, matching that of the saphenous vein, while maintaining high burst pressure and suture retention strength. Increasing this compliance further would provide a compliance match to the native vasculature. Creating grafts within a range of distinct compliances can also be used to investigate the effects of compliance on the development of intimal hyperplasia. Modulating compliance is a novel and important tool for understanding disease initiation and progression of intimal hyperplasia.

The inner layer of the vascular graft is designed to impart both initial and sustained thromboresistance. The inner layer is made of a poly(ethylene glycol) (PEG) based hydrogel that provides initial thromboresistance to the graft. PEG based hydrogels have been widely established to be bio-inert and resist protein adhesion.[144-147] However, this initial thromboresistance will diminish over time. In order to promote sustained thromboresistance, endothelialization of the graft is required. To this end, $Scl2_{GFPGER}$ proteins are used to promote endothelial cell adhesion and proliferation on the hydrogel layer. $Scl2_{GFPGER}$ proteins, however, cannot self-assemble into 3D structures, and therefore require incorporation into another matrix, as is done in the vascular

graft.[126] Incorporation of the protein is accomplished by functionalizing the protein with a PEG linker that covalently crosslinks into a PEG hydrogel network.[126]

To create a multilayered graft composite, the outer layer is first electrospun onto a rotating mandrel. The tubular fibrous mesh is then subjected to an ethanol ramp to allow for penetration of the aqueous hydrogel precursor solution. The meshes are placed in a cylindrical mold with an inner glass mandrel, and hydrogel solutions are pipetted between the mandrel and the mesh, then crosslinked with UV light, as demonstrated in **Figure 1.2**. This dual layered construct has been well characterized previously, displaying no delamination between the layers and long term storage capabilities.

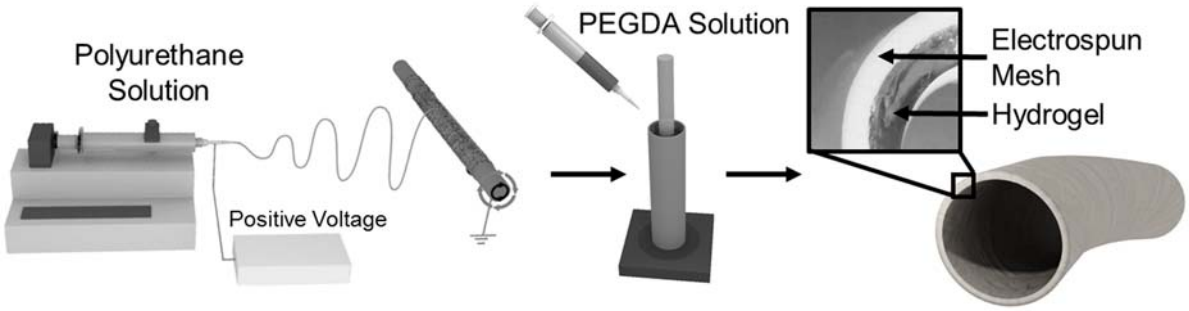

Figure 1.2: Fabrication of the multilayer vascular graft.

1.4.2 Limitations of multilayer vascular graft

The proposed graft has met many of the design requirements set forth that include initial thromboresistance and increased compliance. However, the multilayered graft required further investigation and improvement in order to be a relevant clinical alternative to the currently available synthetic grafts. The key relationships between integrin binding and endothelial cell

hemostatic regulation had yet to be elucidated. This crucial understanding is required in order to promote endothelial cell adhesion and thromboresistance simultaneously. Although the graft matched the compliance of the saphenous vein, this compliance is still lower than that of the carotid and coronary arteries to which the graft will be sutured. Presumably, the compliance mismatch still allows for the development of intimal hyperplasia. However, the relationship between compliance mismatch and intimal hyperplasia has not been definitively defined. Therefore elucidation of this relationship was required for identification of graft compliance that limits intimal hyperplasia. Finally, additional improvements were required for the inner hydrogel layer as particles are dislodged during suturing, creating pseudo-embolisms that create risk for morbidity and mortality. This would require creating a suture damage resistant hydrogel formulation.

The work presented here addresses these limitation and requirements. In Chapter II, we elucidate the effect of specific integrin binding on endothelial cell hemostatic regulation to optimize hydrogel inner layer cellular interactions for both initial and sustained thromboresistance. In Chapter III, we correlate effect of compliance on development of intimal hyperplasia and created a high compliance graft to limit the onset of intimal hyperplasia. The model used to determine this correlation will also serve has a high-throughput screening method for vascular grafts. Finally, in Chapter IV, we identify hydrogel characteristics that predict suture damage resistance and created a hydrogel for the multilayer graft inner layer that is suture damage resistant and biostable. With these improvements, we aim to increase the long term patency of the synthetic small diameter multilayer vascular graft and establish its clinical relevancy.

CHAPTER II

ELUCIDATION OF ENDOTHELIAL CELL HEMOSTATIC REGULATION WITH INTEGRIN-TARGETING HYDROGELS

2.1 Introduction

Thromboresistance is critical to the success of the small diameter multilayer vascular graft. We have previously established initial thromboresistance utilizing a hydrogel-based inner layer. In order to promote sustained thromboresistance, the inner layer must also support endothelialization.[86] As discussed earlier, endothelialization is an effective strategy to impart hemostatic regulation to the graft, and we have previously demonstrated the ability to promote endothelial cell adhesion and migration while resisting platelet adhesion.[86,125] In order to promote a thromboresistant endothelial cell layer in the lumen of the multilayer graft, it is critical to understand the integrin binding and signaling that encourages an anti-thrombotic phenotype in the endothelial cells. Although there are numerous studies focused on promoting a confluent endothelial layer, relatively few studies have investigated the downstream effects of the intracellular signaling from specific integrin binding.[106,115] Previous work has demonstrated a general increase in thrombogenicity of endothelial cells grown on gelatin that predominantly attach via the integrins α5β1 and αvβ3 in ECs.[106] A decrease in thrombogenicity has been observed in endothelial cells cultured on collagen that predominantly attach via the integrins α1β1 and α2β1 in endothelial cells.[116,148] However, many of these studies are confounded by multiple integrin interactions with individual effects not well isolated.[115] Additionally, many studies do not control for the number of adhesion sites available for binding between samples.[115] Although general trends in thrombogenicity have been explored, individual integrin binding events and their effects on

endothelial cell regulation of hemostasis have yet to be elucidated. Therefore, identification of the optimal combination of integrin binding events that promotes an anti-thrombotic phenotype in endothelial cells will allow for better design of cardiovascular devices.

In the work presented here, we utilized bioactive hydrogels to elucidate the individual and synergistic effects of integrin interactions on the anti-thrombotic phenotype of endothelial cells. To target specific HUVEC integrin interactions, we fabricated a series of bioactive hydrogels: PEGDA-collagen and PEGDA-Scl2$_{GFPGER}$ to target integrins α1β1 and α2β1, PEGDA-gelatin to target integrins α5β1 and αvβ3, and PEGDA-collagen+gelatin to target integrins α1β1, α2β1, α5β1, and αvβ3, as shown in **Figure 2.1**. We then demonstrated that cell attachment to these gels was mediated through the targeted integrins using antibody blocking. This enabled the study of the effect of integrin-mediated attachment on gene expression of hemostatic regulators. Finally, we correlated the gene expression changes induced by specific integrin attachment to changes in platelet activation and adhesion. Overall, this study provides key information on the role of integrin-interactions in endothelial cell hemostatic regulation that will enable improved biomaterial design for long term patency in blood-contacting devices, including the multilayer vascular graft.

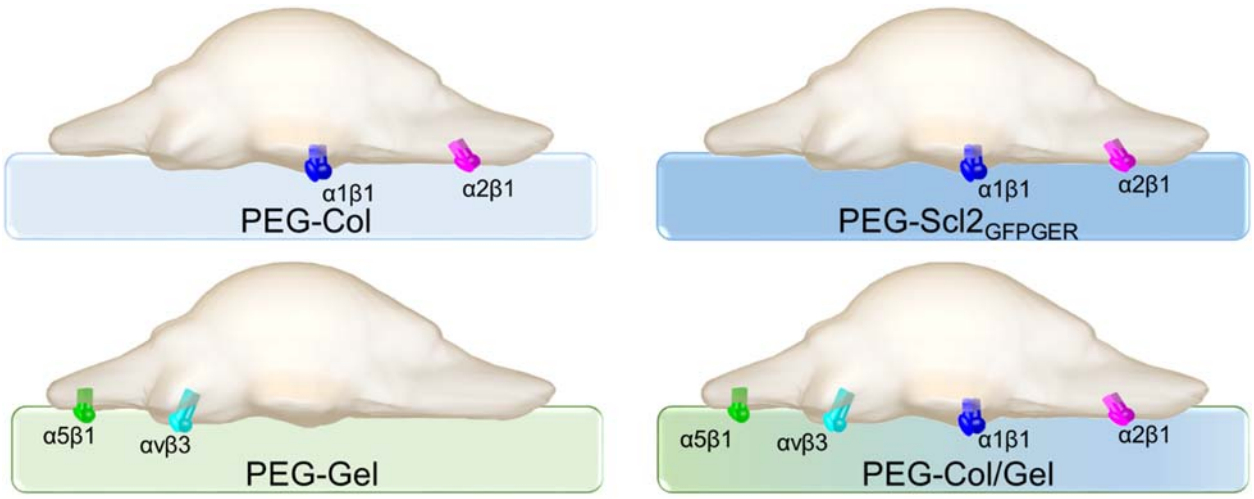

Figure 2.1: Integrins used in attachment to bioactive PEG-based hydrogels. Different platforms target specific integrins to promote attachment and intracellular signaling. Collagen and $Scl2_{GFPGER}$ target α1β1 and α2β1; gelatin targets α5β1 and αvβ3; and the combination collagen+gelatin targets α1β1, α2β1, α5β1, and αvβ3.

2.2 Materials and Methods

2.2.1 Cell culture

Human umbilical vein endothelial cells (HUVECs) at P0 were purchased from Lonza. Cells were seeded in a tissue culture treated T-75 flask with EGM-2 endothelial cell growth medium (Lonza) and allowed to grow to confluence. Cells were used between passages 2 and 8 for the following studies.

2.2.2 Integrin expression analysis by flow cytometry

Cell expression of integrins was determined by conjugated antibody staining of cells in suspension. HUVECs between passages 2 and 5 were cultured in tissue-culture treated poly(styrene) T-75 flasks to 90% confluency. HUVECs were released from the flasks using TryplE Express (ThermoFisher Scientific) 1:10 in sterile PBS. Cells were then spun down and resuspended in flow buffer (PBS with 2% FBS) at a concentration of 10^6cells/mL. Samples were

10^6 cells. Cells were then stained with fixable viability dye 450 (BD Biosciences) for 20 minutes on ice. Samples were then washed with 3mL flow buffer, spun down, and resuspended in flow buffer. Cells were then incubated with the respective integrin or syndecan antibody (anti-α1 and anti-α2 at 5µl/mL; anti-αV and anti-α5 at 2.5µl/mL) on ice for 30 minutes. Cells were again washed with flow buffer, spun down, then resuspended in 400µL 4% paraformaldehyde to fix the cells. Surface expression was then analyzed using the BD LSR II Flow Cytometer. Relative fluorescence was used to compare levels of expression.

2.2.3 PEGDA synthesis

Polyethylene glycol diacrylate (PEGDA) was synthesized according to a method adapted from Hahn, et al.[149] Briefly, acryloyl chloride (4 molar equivalents) was added dropwise to a solution of PEG diol (3.4 kDa; 1 molar equivalent) and triethylamine (TEA, 2 molar equivalents) in anhydrous dichloromethane (DCM) under nitrogen. The reaction was stirred for 24 hours, and then washed with 2M potassium bicarbonate (8 molar equivalents). After drying with anhydrous sodium sulfate, the product was precipitated in cold diethyl ether, vacuum filtered, and dried under vacuum.

2.2.4 Bioactive hydrogel fabrication

Bioactive hydrogels were fabricated by conjugating $Scl2_{GFPGER}$, collagen, and/or gelatin into polyethylene glycol diacrylate (PEGDA) gels using a photopolymerizable linker. Collagen (rat tail type I, Sigma) and gelatin (Type B, Sigma) were received as lyophilized powders and used as received. $Scl2_{GFPGER}$ is a recombinant protein based on the streptococcal collagen-like protein 2 (Scl2) that has been modified by site-directed mutagenesis to include the peptide sequence GFPGER that interacts with α1 and/or α2 integrin subunits. $Scl2_{GFPGER}$ was expressed using E. coli and purified by affinity chromatography as previously described.[121] The globular domain was

removed with pepsin cleavage in acid at a pH of 4. The protein was then dialyzed to water, frozen at -80˚C overnight, and lyophilized. $Scl2_{GFPGER}$, collagen, and gelatin were functionalized separately with an acrylate-PEG3400-NHS linker (JenKem) at a ratio of 10% of the protein's lysines. Functionalized collagen and Scl2GFPGER were dissolved at 4 mg/mL in 20 mM acetic acid, functionalized gelatin was dissolved at 4 mg/mL in water, and a 1:1 ratio of functionalized gelatin and collagen were dissolved at 4 mg/mL in acetic acid. PEG(3.4k)DA was added to each solution at 10wt% and Irgacure 2959 solution (0.01mg per 100μL 70% ethanol) was added at 1% of the polymer. Solutions were crosslinked between two glass plates on a UV plate for 6 minutes on each side to a thickness of 0.75 mm. The resulting bioactive hydrogels (PEG-Col, PEG-Gel, PEG-Col/Gel, PEG-Scl2GFPGER) and the control (PEG) were swelled overnight in sterile PBS and two additional PBS changes were performed before subsequent use in cell culture experiments.

2.2.5 Antibody blocking of integrins

Cells were cultured as described above and resuspended at 33,000 cells/mL in EGM-2 supplemented with bullet kit (Lonza). Cells were then divided into their respective sample tubes with 10,000 cells in 300 μL per sterile 0.5 mL tube. Cells were then incubated with their respective integrin or syndecan antibody at room temperature for 15 minutes (Anti-integrin α_1 (BioLegend) was used at a concentration of $1.33\mu g/10^5$ cells; anti-integrin α_2 (BioLegend) was used at a concentration of $0.665\mu g/10^5$ cells; anti-integrin α_V (BioLegend) was used at a concentration of $0.25\mu g/10^5$ cells; anti-integrin α_5 (Millipore) was used at a concentration of $0.333\mu g/10^5$ cells; anti-integrin β1 (Millipore) was used at a concentration of $0.333\mu g/10^5$ cells). 100 μL of cell/media/antibody solution was then added to the hydrogels in the 96 well plate and incubated for 30 minutes at 37°C and 5% CO_2. After incubation, gels were washed 2X with sterile PBS to remove non-adherent cells. Remaining cells were fixed with 3.7% glutaraldehyde for 10 minutes

and then washed 2X with sterile PBS. Cells were then permeabilized with 0.1% Triton X 100 in PBS and stained with rhodamine phalloidin (f-actin/cytoplasm) and SYBR green (DNA/nucleus). Representative images were taken and cell counts assessed for each substrate and integrin blocking.

2.2.6 Gene expression analysis

Cell seeding was performed as described above. Instead of fixing the cells, gels were moved to new wells for mRNA extraction using Trizol. Trizol was added to the first of three wells of each condition and left for 1 minute to lyse the cells, then pipetted up and down for mixing. The 500µL of Trizol was then moved to the subsequent wells, repeating the lysing steps for each condition. 100µL of chloroform was added to each tube of Trizol and shaken vigorously by hand for 15 seconds. Samples were then incubated for 3 minutes at room temperature, then centrifuged at 12,000 *x g* for 15 minutes at 4°C. The mRNA-containing aqueous phase was removed and placed in a new tube. 0.5mL of 100% isopropanol was added to the aqueous phase and incubated at room temperature for 10 minutes. The solution was then centrifuged at 12,000 *x g* for 10 min at 4°C. The RNA pellet was washed with 0.5ml of 75% ethanol and vortexed. The solution was again centrifuged at 7,500 *x g* for 5 minutes at 4°C and the wash discarded. The isolated RNA was resuspended in RNase-free water. Forward and reverse primers for qRT-PCR were acquired from Integrated DNA Technologies for the following hemostatic regulators in HUVECs: TF, TFPI, ADAMTS-13, vWF, tPA, eNOS, and the housekeeping gene GAPDH (**Table 2.1**). mRNA was converted to cDNA utilizing the SuperScriptIII kit and manual (Invitrogen). Briefly, 1µL of primer, 1µL of dNTP mix, up to 5µg total RNA, and DEPC-treated water to 10µL were mixed and incubated at 65°C for 5 min, then placed on ice for 1 min. cDNA Synthesis Mix was made by combining 2µL 10X RT buffer, 4µL 25mM MgCl2, 2µL 0.1M DTT, 1µL RNaseOUT, and 1µL

SuperScript® III RT. 10uL of cDNA Synthesis Mix was added to each RNA mixture, gently mixed, and incubated for 10 min at 25°C followed by 50 min at 50°C. The reactions were terminated at 85°C for 5 min and chilled on ice for 5 min. 1µL of RNase H was added to each tube and incubated for 20 min at 37°C. cDNA was then either used immediately for qRT-PCR or stored at -20°C. All gene expression is represented as a fold change compared to HUVECs attached to TCPS.

Table 2.1: Gene targets and their peptide sequences used for qrt-PCR.

	Gene	**Peptide Sequence Forward**
Pro-thrombotic	vWF	GTTCGTCCTGGAAGGATCGG
	Tissue Factor	AGAGGCAAACTGCCAGATGT
Anti-thrombotic	eNOS	CCAGCTAGCCAAAGTCACCAT
	ADAMTS-13	CACAGGCCTCTCTTCACACA
	TFPI	TGTATCACTTTCGGGACCTGTCTC
	TPA	GAAGAGAGGGCTCTGCTGTG

2.2.7 Platelet adhesion

Platelet attachment was used as an initial measure of thromboresistance of the new hydrogel formulations. Circular hydrogel specimens were punched from the hydrogel slabs and placed in a 48 well plate. Cells were grown to confluence on the protein hydrogels. Platelets were isolated from human whole blood drawn from a volunteer and mixed with ACD via inversion. The mixture was centrifuged at 990rpm for 15 minutes to isolate the protein rich plasma (PRP) layer. The PRP layer was removed and prostacyclin (Sigma Aldrich) was added at 10µL/mL and centrifuged again at 1500rpm for 10 min to form a platelet pellet. The pellet was resuspended in CGS buffer for washing and centrifuged again at 1500rpm for 10 min. The platelets were then

resuspended in Tyrode's buffer at half the original volume of PRP. Sudan B Black solution (5% in 70% ethanol) was added to the platelet solution at a 1:10 ratio for 30 minutes at room temperature. The stained platelets were then washed with PBS 3 times by resuspending the pellet in PBS then centrifuging at 1500rpm for 8 min. Platelets were counted and resuspended at a concentration of 10 x 10^6 platelets/mL in sterile PBS. 500µL platelet suspension was added in each test well, and platelets were allowed to adhere to substrate for 30 min at 37°C on a shaking incubator. Gels were transferred to new wells and washed twice with PBS, then carefully placed into microcentrifuge tubes and bound cells were lysed with 150µL DMSO for 15 min at room temperature. 150µL of PBS was added to each sample and the solution moved to a cuvette for reading on a spectraphotometer (400-650nm, SpectraMax M2, Molecular Devices).

2.3 Results

2.3.1 Integrin expression

In order to determine the relative abundance of integrins presented on the cell surface, the relative fluorescence of antibody detection was measured in flow cytometry. The lowest fluorescence was observed when staining the integrin subunit α1 (259 ± 54), and complexes most commonly with β1 to form α1β1 (**Figure 2.2**). The highest fluorescence was measured for integrin subunit α2 (1163 ± 68), and complexes most commonly with β1 to form α2β1. Both integrin subunits α5 and αv exhibited fluorescence at about half of the intensity of α2 (536 ± 48 and 650 ± 83, respectively). Integrin subunit α5 most commonly complexes with β1 to form α5β1, and integrin subunit αv most commonly complexes with β3 to form αvβ3. This data indicates that, of those analyzed, the most highly expressed integrin presented on the HUVEC surface is α2β1, with α5β1 and αvβ3 at approximately half of that expression, and α1β1 with the lowest presentation.

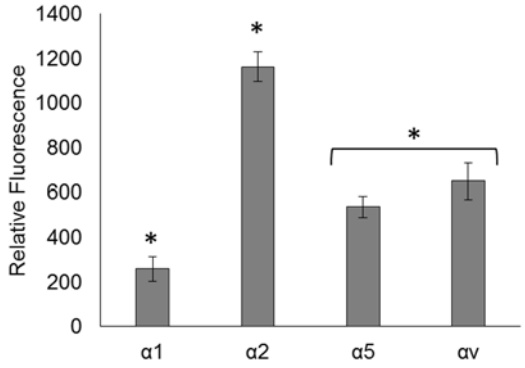

Figure 2.2: Relative abundance of major integrins involved in HUVEC attachment to extracellular matrix proteins. Relative fluorescence was measured in flow cytometry. Antibodies used for staining were administered with the following concentrations: anti-α1 and anti-α2 at 5µl/mL; anti-αV and anti-α5 at 2.5µl/mL. Data shown is average ± standard deviation. * Indicates significance from other groups, $p<0.05$, as determined by 1-way ANOVA with a post-hoc Tukey's test.

2.3.2 Antibody integrin blocking

Antibodies to these integrins were then selectively blocked to confirm the dominant integrin interactions responsible for mediating HUVEC adhesion to each of the bioactive hydrogels. When blocking integrin subunits on PEG-Col hydrogels, the largest decrease in attachment was observed when blocking α2, with only 27.5% of cells adhered. The combination α1+α2 blocking resulted in a further reduction in cell attachment to 16.5% of the control (**Figure 2.3A**). No significant decrease in cell attachment was observed with either integrin αv or α1 blocking. In contrast, the reverse trend was observed with PEG-Gel hydrogels with minimal effect on cell attachment observed when blocking α1 and α2. Significant and comparable decreases in HUVEC adhesion were observed when blocking integrin subunits αv (27.5%) and α5 (38.2%) with cell attachment almost fully eliminated with combination αv + α5 blocking (10.4%). As expected, on PEG-Col/Gel hydrogels that are designed to target integrins α1β1, α2β1, α5β1, and αvβ3,

adhesion was partially reduced (37.0%) when blocking only the integrin subunit α2 (**Figure 2.3C**). There was no significant decrease when blocking only integrin subunit αv but adhesion was reduced to less than 20% when blocking α2+αv+α5 in combination. When blocking integrin subunits on $Scl2_{GFPGER}$ hydrogels that target α1β1 and α2β1, there was no significant reduction in adhesion when blocking α5 or α1 (**Figure 2.3D**). Adhesion was reduced to less than 10% when blocking α2, and less than 5% when α1 and α2 were blocked in combination. Therefore, the findings in our bioactive hydrogel model confirm specific integrin binding in which HUVECs bind primarily to PEG-Col hydrogels with integrin α2β1 with other modes minorly contributing to attachment, bind primarily to PEG-$Scl2_{GFPGER}$ hydrogels with integrins α2β1, bind primarily to PEG-Gel hydrogels with integrins α5β1 and αvβ3, and bind to the combination PEG-Col/Gel gels through all four integrins (α1β1, α2β1, α5β1, and αvβ3).

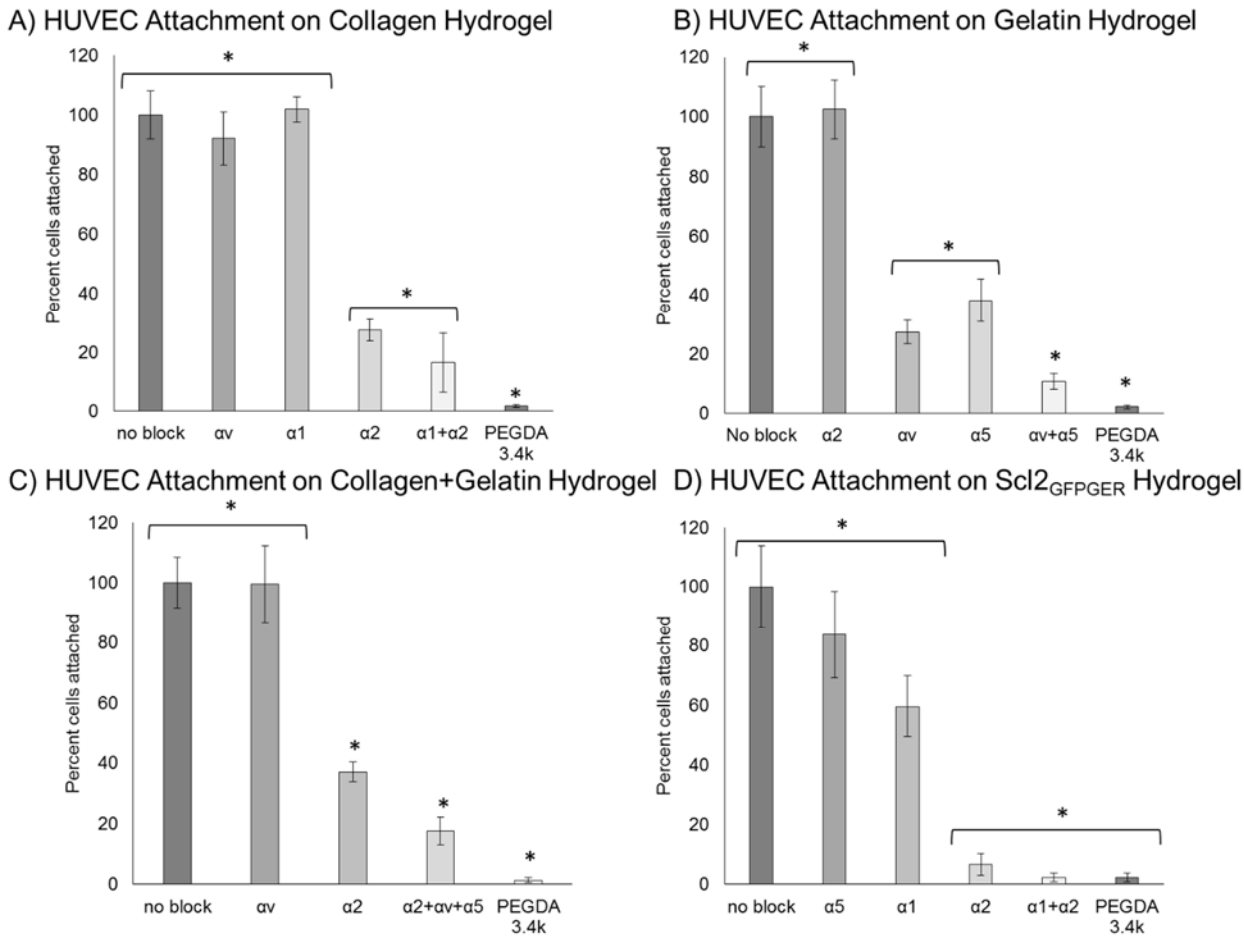

Figure 2.3: Attachment of HUVECs to extracellular matrix proteins with integrin antibody blocking. HUVEC integrins are blocked on A) collagen, B) gelatin, C) collagen+gelatin, and D) $Scl2_{GFPGER}$ hydrogels. Data shown is average ± standard error of the mean. The * indicated significance from other groups, $p<0.05$, as determined by 1-way ANOVA with a post-hoc Tukey's test.

2.3.3 HUVEC hemostatic gene expression

To test the hypothesis that integrin targeting affected hemostatic regulators, HUVEC gene expression of von Willebrand factor (vWF), a disintigrin and metalloproteinase with a thrombospondin type 1 motif, member 13 (ADAMTS-13), endothelial nitric oxide synthase (eNOS), tissue plasminogen activator (tPA), tissue factor (TF), and tissue factor pathway inhibitor

(TFPI) was examined after attachment to each substrate. Each marker was selected based on established roles in hemostasis (**Table 2.2**). The pro-thrombotic regulators selected were vWF, which mediates platelet adhesion, and TF, which initiates thrombin formation.[29,38] The anti-thrombotic regulators selected were, ADAMTS-13 as an agonist of vWF by cleaving ultra-long chains,[29,67,150] eNOS that generates the key anticoagulant of nitric oxide (NO), tPA as a protease responsible for breakdown of clots, and TFPI as an inhibitor of TF [29,38] In this study, vWF evenly expressed in HUVECs grown on PEG-Col, PEG-Gel, and PEG-Col/Gel with mixed integrin interactions, and lowest in HUVECs grown on PEG-Col and PEG-Scl2$_{GFPGER}$ that targeted integrins α1β1 and α2β1 (**Figure 2.4A**). HUVECs grown on combination PEG-Col/Gel gels exhibited expression levels intermediate to the PEG-Col and PEG-Gel. There was no observed increase in expression of TF on PEG-Gel hydrogels but the lowest expression in HUVECs was observed on PEG-Col hydrogels (**Figure 2.4B**). Unexpectedly, TF was most highly expressed in HUVECs grown on Scl2$_{GFPGER}$ hydrogels.

The expression of anti-thrombotic regulators was also dependent on which substrate the HUVECs attached. All of the hydrogels induced upregulation of ADAMTS-13, eNOS, and tPA in adhered HUVECs but only the PEG-Scl2$_{GFPGER}$ hydrogels supported upregulation of TFPI (**Figure 4C-F**). The highest expression of ADAMTS-13, TFPI, and tPA was observed in HUVECs adhered to PEG-Scl2$_{GFPGER}$ hydrogels. Although not statistically significant from the other substrates, eNOS was most highly expressed in HUVECs grown on PEG-Col hydrogels. Gene expression of anti-thrombotic regulators was statistically similar on PEG-Gel and PEG-Col/Gel hydrogels. Together, the data indicate that specific integrin targeting does in fact affect HUVEC hemostatic

regulation with differential expression of prothrombotic and antithrombotic regulators with different integrin interactions. These changes are summarized in **Table 2.3**.

Table 2.2: Hemostatic regulators measured in gene expression analysis.

	Protein	**Function**
Prothrombotic Proteins	Von Willebrand Factor (VWF)	Binds platelets to form platelet thrombi when in ultra-large multimer form [da Silva 2016]
	Tissue Factor (TF)	Surface protein expressed by activated endothelial cells to initiate coagulation cascade [White 2010]
Antithrombotic Proteins	A disintegrin and metalloproteinase with a thrombospondin type I motif, member 10 (ADAMTS-13)	VWF cleaving enzyme [Shim 2008]
	Tissue factor pathway inhibitor (TFPI)	Major inhibitor of TF, Factor Xa, and thrombin [White 2010]
	Tissue plasminogen activator (tPA)	Regulator of fibrinolysis [Booyse 1999]
	Endothelial nitric oxide synthase (eNOS)	Synthesizer of nitric oxide that inhibits platelet aggregation [Warner 2016]

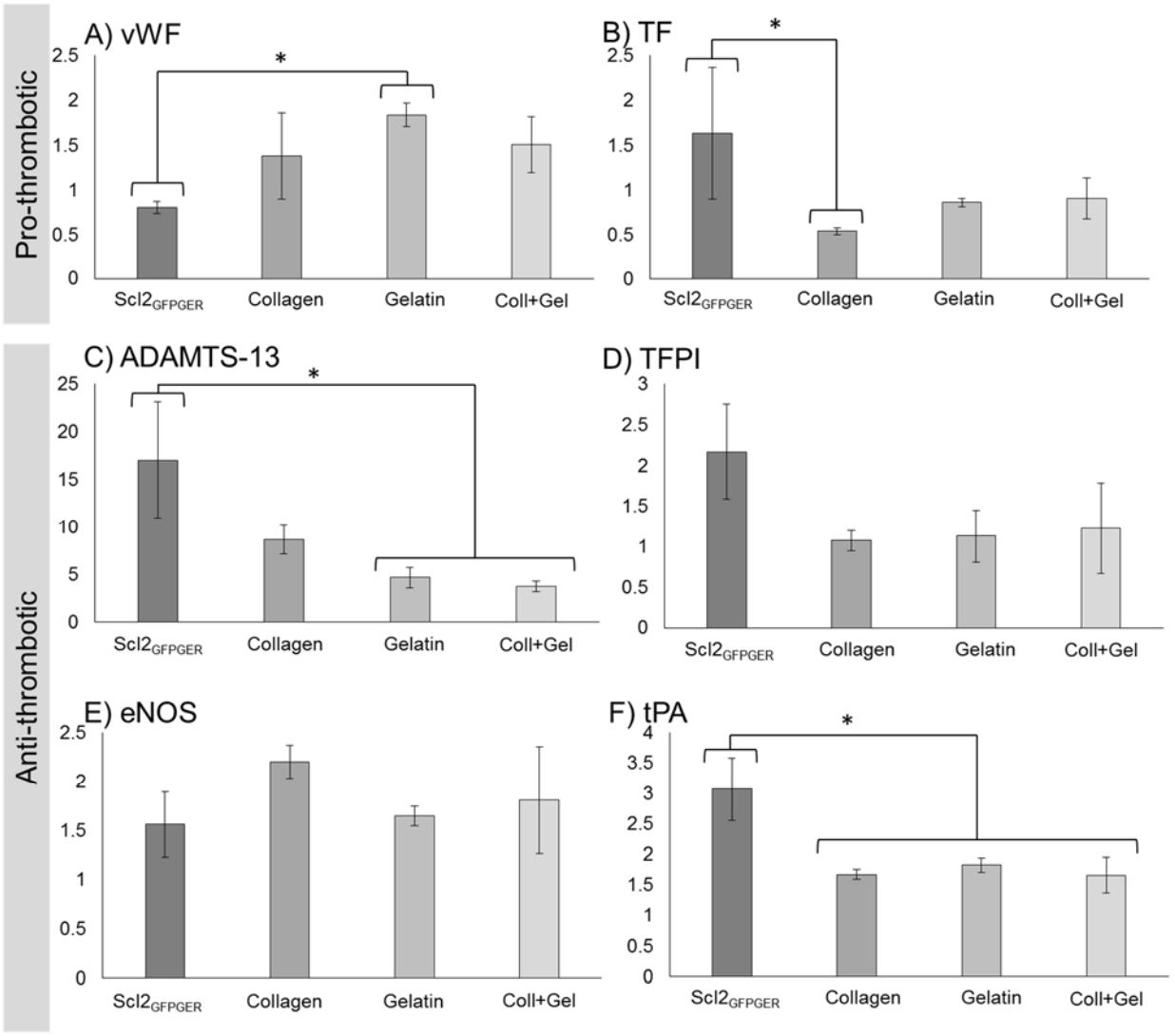

Figure 2.4: HUVEC gene expression of hemostatic regulators. All values have been normalized to TCPS GAPDH. HUVEC gene expression varies on collagen, gelatin, combination, and DC2 hydrogels. Genes investigated were for vWF (A), tissue factor (B), ADAMTS-13 (C), tissue factor pathway inhibitor (D), endothelial nitric oxide synthase (E), and tissue plasminogen activator (F). * represents significance between groups. Significance was determined by a 1-way ANOVA with a post hoc Tukey's test with $p<0.05$ for all comparisons.

Table 2.3: Relative change in gene expression of HUVEC hemostatic regulators. Fold change is represented by: "↓" = 0.5-0.8, "-" = 0.8-1.2, "↑" = 1.2-2, "↑↑" = 2-5, "↑↑↑" = >5.

		PEG-Scl2	PEG-Col	PEG-Gel	PEG-Col/Gel
Prothrombotic	vWF	-	↑	↑	↑
	TF	↑	↓	-	-
Antithrombotic	ADAMTS-13	↑↑↑	↑↑↑	↑↑	↑↑
	TFPI	↑↑	-	-	-
	eNOS	↑	↑↑	↑	↑
	tPA	↑↑	↑	↑	↑

2.3.4 Platelet adhesion

To interrogate the hemostatic functional outcome of integrin targeting, we performed platelet adhesion studies with a protocol adapted from Baloaing et al.[106] The lowest relative levels of platelet adhesion to HUVECs cultured on hydrogel substrates were observed on the PEG-Col and PEG-Scl2$_{GFPGER}$ hydrogels (**Figure 2.5**). The highest relative platelet adhesion was observed on HUVECs cultured on the PEG-Gel hydrogel. HUVECS cultured on the combination PEG-Col/Gel were intermediate to the PEG-Col and PEG-Gel substrates. These results indicate that the HUVEC substrate can indeed be designed to reduce platelet attachment to the endothelial layer by targeting the α1β1 and α2β1.

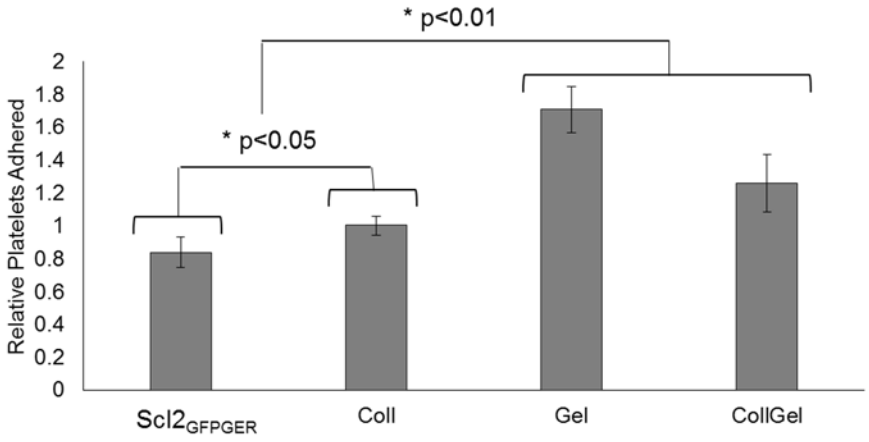

Figure 2.5: Platelet attachment to HUVECs cultured on bioactive hydrogels. Platelets were isolated from whole blood and allowed to adhere to HUVECs after stimulation. Data shown is average ± standard deviation. The * indicated significance between groups, as determined by 1-way ANOVA with a post-hoc Tukey's test.

2.4 Discussion

Endothelialization is a key strategy used to achieve sustained thromboresistance of blood-contacting devices without using anticoagulants. To this end, biomaterials must be designed to achieve both a confluent endothelial layer and a hemostatic phenotype in the adhered cells. Previous studies have investigated endothelial cell hemostatic regulation differences on various ECM components and mimics, but often fail to differentiate the individual and synergistic effects of the integrins under investigation and their effects on endothelial hemostatic regulation.[115,116,119] To elucidate the relationship between select integrin targeting and HUVEC hemostatic regulation, we developed a bioactive hydrogel platform to isolate integrin interactions using PEG-based hydrogels enriched with collagen, gelatin, and the recombinantly expressed collagen-like protein $Scl2_{GFPGER}$.

We first established with integrin antibody blocking that these hydrogels target the desired integrins, α1β1, α2β1, α5β1, and αvβ3 (**Figure 2.3**). Previous studies have demonstrated that

gelatin and collagen bind to these integrins, but a comprehensive blocking study including these proteins and the Scl2$_{GFPGER}$ incorporated into hydrogels had not been previously reported.[81,151] These integrins proved to be the main modes of attachment, with other modalities likely making only minor contributions to attachment but also possibly influencing cell behavior. This is highlighted by the comparison between PEG-Col integrin blocking and PEG-Scl2$_{GFPGER}$ integrin blocking. When blocking the main modes of attachment, α1β1 and α2β1, on the PEG-Col hydrogel (**Figure 2.3A**), approximately 17% of cells remained, indicating that other modes of attachment contribute to cell adhesion and signaling. In comparison, when blocking the same integrins on PEG-Scl2$_{GFPGER}$, cell adhesion was virtually eradicated. This highlights the ability of the PEG-Scl2GFPGER platform to isolate only the integrins α1β1 and α2β1, whereas collagen has other attachment and signaling that can contribute to hemostatic regulation. Additionally, although not statistically different, the α1 integrin blocking appears to have more of an effect on HUVEC attachment on PEG-Scl2$_{GFPGER}$ than on PEG-Col hydrogel (**Figure 2.3A, Figure 2.3D**). This could be due to symbiotic syndecan attachment on collagen that can help to compensate other attachment modalities when α1 is blocked.[82] However, both platforms are demonstrated to mediate HUVEC adhesion primarily through α2β1 interactions. This follows the integrin expression analysis where α2β1was the most highly expressed integrin on the HUVEC surface (**Figure 2.2**). It was also demonstrated that the PEG-Gel platform primarily targeted α5β1 and αvβ3, with each contributing equally to HUVEC attachment (**Figure 2.3B**). This again follows the integrin expression analysis where both integrins had similar expression levels. Similar to PEG-Col, however, some cells remained attached, highlighting minor contributions to attachment and signaling by other attachment modalities.

The other integrins associated with collagen attachment do not appear to be modes of adhesion as demonstrated by no change in attachment when blocking the integrin subunit α2. The PEG-Col/Gel appears to target both the integrins targeted in each PEG-Col and PEG-Gel. This is demonstrated by the reduction in attachment by blocking integrin subunit α2, and the further reduction in attachment by blocking α2+α5+αv (**Figure 2.3C**). Although all of the main integrins that mediate attachment to this combination platform are blocked, 18% of cells remained attached. This indicates that there are other minor modes of attachment that remain in this platform that could affect some intra-cellular signaling. Overall, the integrins interrogated appear to be the main modes of attachment and likely the main mediators of signaling in the HUVECs. Few of the previous assessments of endothelial cell hemostatic regulation have carefully controlled the modes of attachments, often utilizing broad ECM protein coatings.[115] Those that do have more specific targeting often use short peptide sequences such as RGD or other mimics of cell adhesive ligands found in the ECM but lack a thorough investigation of multiple common integrins used in endothelial cell binding to the ECM.[106,116]

Through use of this platform, the data demonstrate that specific integrin targeting modulates HUVEC gene expression of hemostatic regulators (**Figure 2.4**). The hypothesis that specific binding in endothelial cells can affect hemostatic regulator gene expression and functionality is supported by previous studies.[106,119] However, none provided a comprehensive analysis of many integrins and their effects on a broad range of potential hemostatic regulators.[115] Here, we have investigated the effects of binding α1β1, α2β1, α5β1, and αvβ3 on HUVEC expression of vWF, TF, ADAMTS-13, TFPI, eNOS, and tPA. Overall, the HUVECs exhibited generally antithrombotic phenotypes when cultured on the bioactive hydrogel platforms (**Table 2.3**). There were, however, significant differences in the levels of expression of the hemostatic regulators in

cells adhered to different bioactive hydrogels. vWF, a strong prothrombotic factor that directly attaches to platelets, had the lowest expression by targeting α1β1 and α2β1 compared to targeting integrins α5β1 and αvβ3 as well as all integrins in combination. The expression level of vWF is lowest in HUVECs with integrin targets α1β1 and α2β1 on the $Scl2_{GFPGER}$ hydrogel, in which there are no other mechanisms of attachment, like those remaining in collagen. This decrease in vWF on PEG-$Scl2_{GFPGER}$ compared to collagen has been previously reported by Munoz-Pinto et al and serves to confirm this trend.[119] There is an increase in TF expression in HUVECs on PEG-$Scl2_{GFPGER}$ compared to the other platforms, but this is complimented by a similar increase in relative expression of the TF agonist TFPI on PEG-$Scl2_{GFPGER}$. This may possibly offset the effects of each, with no net effect on thrombogenicity. There is also an increase in ADAMTS-13 and tPA on PEG-$SCl2_{GFPGER}$ compared to the other platforms that indicate that by targeting α1β1 and α2β1 alone, there is an increase in anti-thrombotic response in HUVECs. The gene expression of eNOS, a synthesizer of nitric oxide, appears to be most highly expressed on the collagen platform, with the next highest expression on $Scl2_{GFPGER}$. However, there is no significant difference between the groups. Again, in comparing collagen and $Scl2_{GFPGER}$ in hydrogels, Munoz-Pinto et al. found no significant difference in NOS3 expression, a similar synthesizer of NO in endothelial cells.[119] Overall, it appears that by targeting integrins α1β1 and α2β1, HUVECs will exhibit a more thromboresistant phenotype than by targeting the integrins α5β1 and αvβ3 or a combination thereof, though targeting any of these integrins appears to promote thromboresistance.

These gene expression trends are confirmed in the functional assays of platelet adhesion. Previous studies have demonstrated correlation of hemostatic gene expression to the protein expression.[106,119] Therefore it was expected that the platelet adhesion trends would follow the hemostatic regulator gene expression trends. We observe increased platelet attachment to

HUVECs by targeting integrins α5β1 and αvβ3 with PEG-Gel and PEG-Col/Gel hydrogel platforms. Comparatively, there appears to be lower relative platelet attachment to HUVECs when targeting integrins α1β1 and α2β1 with the $Scl2_{GFPGER}$ and collagen hydrogels (**Figure 2.5**). This indicates that the largely thromboresistant phenotype of the HUVECs that was measured when targeting integrins α1β1 and α2β1 has a similar functional outcome, with fewer platelets adhered to these cells. In particular, the gene expression of vWF appears to be most predictive of the trend in adhered platelets (**Figure 2.4A**). This is likely due to the ability of vWF to bind directly to platelets without other intermediaries, but other prothrombotic factors like TF require a cascade to affect platelet activation and aggregation.[30,150] Overall, the results indicate that specific integrins can be used for attachment and thromboresistant signaling in endothelial cells.

These specific integrin targets can be used to tailor biomaterials to not only promote endothelial cell adhesion, they can be used to promote a thromboresistant phenotype in adherent cells. Specifically, previous work has demonstrated that Scl2 proteins can be produced to target specific integrins such as α1β1 and α2β1 while remaining themselves thromboresistant, a distinct advantage over other proteins such as collagen and gelatin.[122] Additionally, they have previously demonstrated increased endothelial cell migration compared to collagen.[54] This creates unique tools to design blood-contacting materials to promote thromboresistance via post-implantation endothelialization. This strategy can be utilized in cardiovascular device design, such as a previously described multi-layer vascular graft.[86] The specific integrin targeting of the naturally thromboresistant $Scl2_{GFPGER}$ incorporated into a hydrogel lining of the graft promotes long term patency via endothelialization. This approach has the potential to enhance many cardiovascular devices.

2.5 Conclusions

We and others have demonstrated that endothelial cell attachment and migration is mediated by the ECM substrate.[28,53,54,87,88,152] The work presented here demonstrates the ability to influence endothelial cell hemostatic regulation through specific integrin targeting. Overall, HUVECs exhibited a more thrombogenic phenotype on bioactive hydrogels that targeted integrins α5β1 and αvβ3. The functional outcome of this increased thrombogenic gene expression *in vitro* is an increase in platelet adhesion. By specifically targeting α1β1 and α2β1, where platelet adhesion was lower, we can promote a more thromboresistant phenotype, ideal for coating blood contacting surfaces in medical devices. This specific targeting can be accomplished through the use of $Scl2_{GFPGER}$, as demonstrated in the antibody integrin blocking study. The ability to target specific integrins enables the design of thromboresistant biomaterials. Future work will include adding other factors to the platform, such as a shear component, to better mimic *in vivo* conditions as well as determine the dominant factor that contributes to endothelial cell hemostatic regulation. The validity of this platform will ultimately be tested by *in vivo* evaluation of endothelial cell behavior with integrin targeting.

CHAPTER III

ELUCIDATING THE ROLE OF GRAFT COMPLIANCE MISMATCH ON INTIMAL HYPERPLASIA USING AN EX VIVO ORGAN CULTURE MODEL

3.1 Introduction

After addressing failures due to thrombosis, we continue to improve the multialyer graft by addressing another critical limitation of synthetic vascular grafts: re-occlusion due to intimal hyperplasia. The high rate of failure due to intimal hyperplasia has been correlated with a compliance mismatch between the grafting material and the native vasculature.[132,140] Despite this strong empirical correlation, the mechanisms by which compliance mismatch leads to intimal hyperplasia are relatively poorly understood. It is theorized that the compliance mismatch leads to a flow disruption at the distal anastomosis, which then leads to low wall shear stress.[132,141] The vessel wall, in response to the low wall shear stress, attempts to correct the flow disruption with intimal thickening, ultimately leading to re-occlusion of the vessel.[140] In order to design vascular grafts with improved patency, the complex cascade of events that begins with changes in the endothelium and initiates the smooth muscle cell phenotypic alterations that typify intimal hyperplasia need to be elucidated.

It has been difficult to directly relate compliance-mismatch and the resulting changes in fluid dynamics to the development of intimal hyperplasia because of confounding factors of graft properties. For example, the often cited high-compliance grafts with improved patency are autografts as compared to the low-compliance synthetic grafts.[140] Isolation of the effect of compliance is ideally conducted on synthetic grafts that can vary compliance independent of other graft variables. We have previously reported on the fabrication of multi-layer vascular grafts with

tunable biomechanical properties and improve compliance matching that enables this investigation.[86] In addition, to elucidate the role of compliance on the change in blood flow, a quantitative prediction of the change in wall shear stress as a function of graft compliance is needed. Computational models have been used to predict changes in blood flow and wall shear stress in stenting of coronary arteries to improve the design iteration process for vascular stents.[153-155] It has also been used to investigate how different anastomosis techniques affect flow between the graft and the native vasculature to determine the optimal surgical method.[156,157] In this study, we propose to use a computational model of the synthetic graft-artery anastomosis to provide a prediction of wall shear stress as a function of graft compliance that can be directly correlated to changes observed in distal arterial remodeling. Finally, evaluation of vascular grafts includes assessment of long-term patency and incidence of intimal hyperplasia using large animal models that can be both time and cost-prohibitive.[158] A method to rapidly screen vascular grafts for early markers of intimal hyperplasia using an *ex vivo* organ culture model would enhance vascular graft development.

In the current study, a unique *ex vivo* organ culture model was developed to analyze the histological changes in grafted porcine carotid arteries in response to an increased compliance matching of the grafts. First, grafts of distinct compliances were fabricated and compliance was evaluated before suturing to the carotid arteries and culturing in the *ex vivo* bioreactor.[86] The distal anastomoses were analyzed after two weeks of culture for changes in the endothelium (VE-Cadherin, vWF, N-Cadherin), VSMC phenotype (SM22α, SMα-actin, N-Cadherin, and proliferation marker Ki67), and extracellular matrix composition (versican, elastin, fibronectin), as early markers of intimal hyperplasia. Finally, these findings were correlated to a predictive computational model of wall shear stress in a grafted carotid artery with increasing compliance of

the graft. This study elucidates not only the intrinsic link between graft compliance mismatch and the development of intimal hyperplasia, it also provides a screening method for synthetic small diameter vascular graft development. It also allowed for the identification of a high compliance graft that limits the development of intimal hyperplasia for the outer layer of the multilayer vascular graft.

3.2 Results and Discussion

3.2.1 Varying graft compliance

We have demonstrated the ability to fabricate multilayer vascular grafts with increasing compliance, exceeding that of the saphenous vein, independent of other factors such as graft chemistry and cellular interactions.[86] For this study, we selected grafts with a low compliance (~2 %/mmHg x 10^{-2}) to mimic the ePTFE clinical control, medium compliance (~5 %/mmHg x 10^{-2}), and high compliance (~8 %/mmHg x 10^{-2}) to closely match the compliance of the native carotid artery to be used in the *ex vivo* bioreactor system. Bionate® thermoplastic poly(carbonate-urethane) was electrospun with careful control of graft thickness and fiber morphology to meet design criteria. Increasing electrospinning collection time from 2 hours to 6 hours resulted in grafts that were 0.4, 0.3, 0.2, and 0.1 mm thick with corollary compliances of 3.4 ± 1.1, 4.1 ± 0.3, 7.3 ± 1.3, and 8.1 ± 0.3 %/mmHg x 10^{-2}, respectively (**Figure 3.1B**). The measured compliance of the ePTFE control, determined by the same methodology, was 1.6 ± 0.2 %/mmHg x 10^{-2}. The grafts retained burst pressures comparable to the saphenous vein and appropriate suture retention strengths (**Figure 3.1 C, D**). Electrospun meshes with target biomechanical properties were then coated with a poly(ethylene glycol)-based hydrogel to ensure thromboresistance in subsequent bioreactor studies.[86]

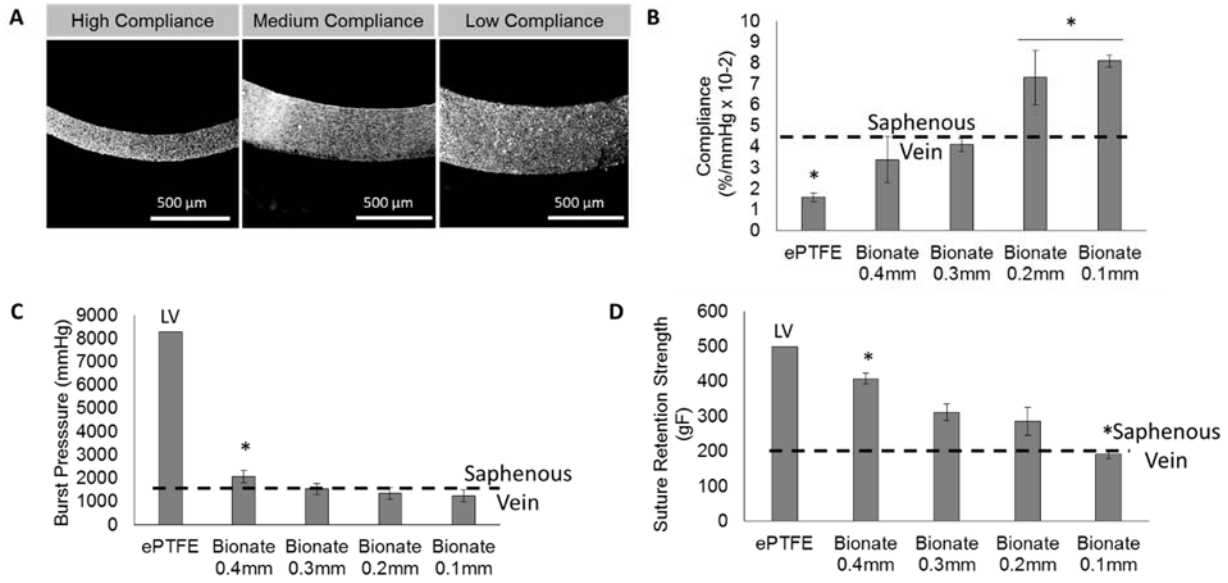

Figure 3.1: A) Effect of modulating collection time on graft thickness as demonstrated by SEM. Compliance (B) and burst pressure (C), and suture retention strength (D) of the low, medium, and high compliance grafts compared to the clinical control ePTFE. Data is represented as average ± standard deviation for n=6. Statistical significance is shown by * showing significance from all other measured values, with $p<0.05$. LV: Literature value from Mun et al. and Mine et al.

3.2.2 Computational modeling

A computational model was created to illustrate the changes in flow as a function of compliance and estimate the resulting changes in wall shear stress at the distal anastomosis of the high, medium, and low compliance grafts (**Figure 3.2**). Turbulent flow was apparent in the low compliance graft model with flow recirculation distal to the graft with a corollary wall shear stress of 0.03 N/m^2 at 80mmHg and 0.03 N/m^2 at 120 mmHg. These values approached zero near the zone of recirculation at the distal anastomosis. The observed turbulence was reduced in the medium compliance model, with the wall shear stress calculated to be 1.04 N/m^2 at 80mmHg and 1.08 N/m^2 at 120mmHg. The high compliance graft eliminated turbulent flow with wall shear stress calculated to be 3.46 N/m^2 at 80mmHg and 3.60 N/m^2 at 120mmHg.

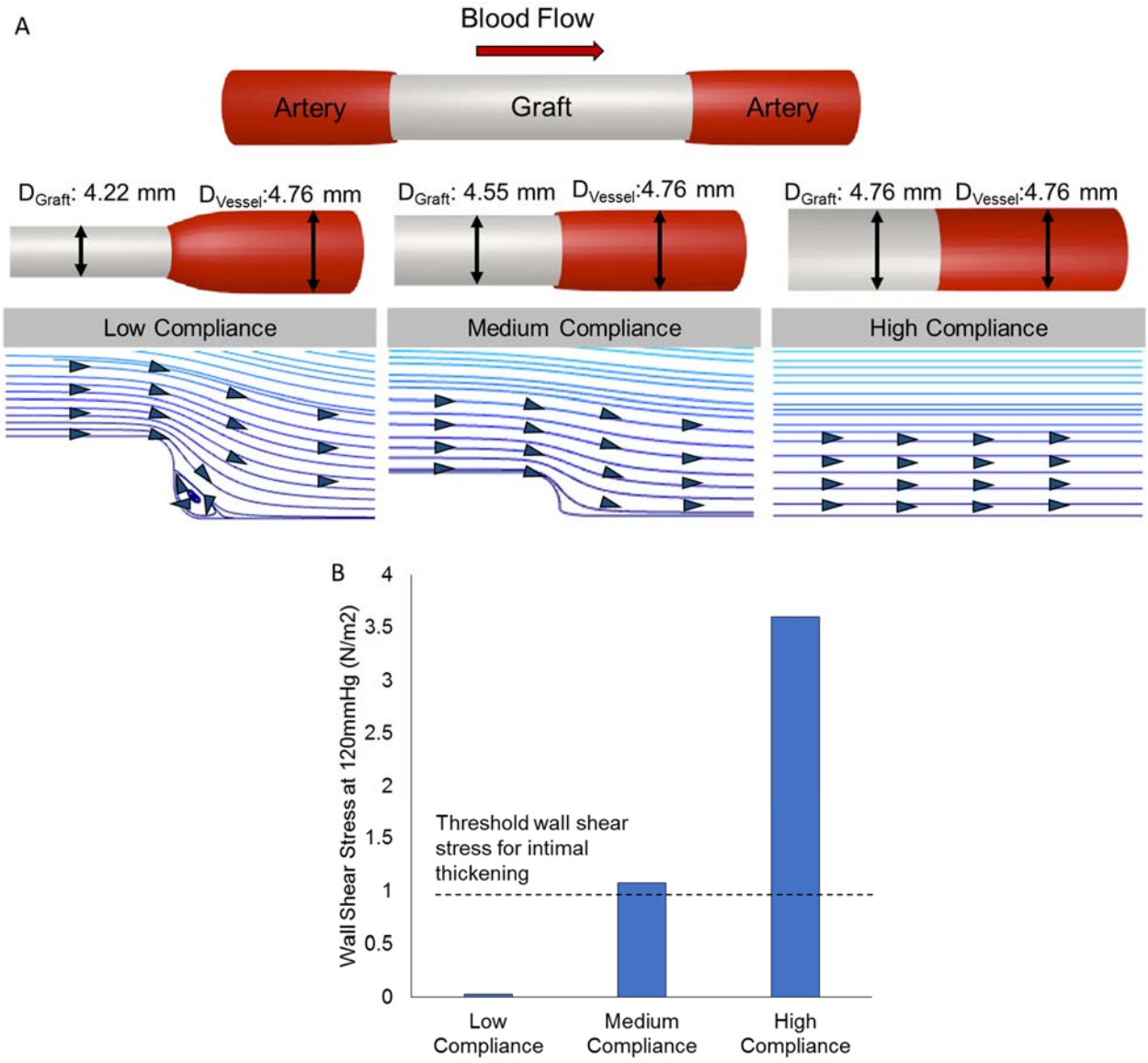

Figure 3.2: A. Effect of compliance on flow patterns and wall shear stress at the distal anastomosis as determined by the computational model made in COMSOL. Linear flow patterns demonstrate decreasing flow disruption with increasing compliance. B. Lower compliance correlates to lower wall shear stress. Threshold from Sho et al. 2004.

The computational model demonstrated the blood flow profile changes and changes in wall shear stress between grafts of different compliances. The differences in compliance lead to differences in dilation that then affect the blood flow profile. Here we are able to demonstrate that

the low compliance grafts have the greatest difference in diameter and therefore the largest effect on the blood flow profile, creating zones of blood recirculation and low wall shear stresses that are associated with the development of intimal thickening in other small animal models [159]. As compliance increases, the dilation changes between the graft and the native artery decrease, preserving flow lines. This in turn increases wall shear stress. Therefore it is expected that grafts with low compliance may induce intimal hyperplasia based on the computational model predictions, and grafts with higher compliance may mitigate those effects.

3.2.4 Ex vivo *bioreactor immunohistochemistry*

The *ex vivo* bioreactor model allows for simplification of a complex *in vivo* system. Porcine carotid arteries sutured to multilayer grafts (**Figure 3.3A**) of low, medium, and high compliance as well as an artery-artery sham control and the ePTFE clinical control were cultured for two weeks. The *ex vivo* bioreactor system subjected the sutured grafts and arteries to physiological pulsatile flow for two weeks in enriched culture medium (**Figure 3.3B**). The analysis of the histology of the arteries sutured to grafts of increasing compliance demonstrate a decrease in markers for intimal hyperplasia (**Figures 3.4-7**). In general, the arteries sutured to the low compliance graft and the ePTFE control exhibited similar staining for early markers of intimal hyperplasia, whereas the arteries sutured to the high compliance grafts displayed similar staining as the artery-artery controls.

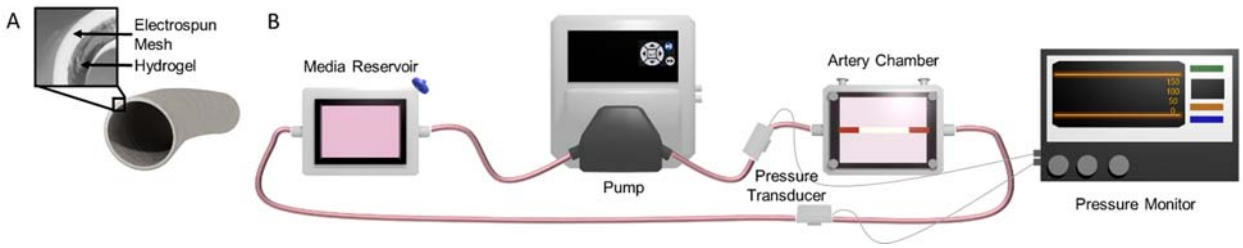

Figure 3.3: A) Inner and outer layers of the multilayer graft. B) Ex vivo organ culture system.

In comparing VSMC phenotype, greater spatial heterogeneity in SMα-actin staining was observed in the lower compliance groups relative to the sham control (**Figure 3.4**). In addition, regions of intense staining for SM22α (**Figure 3.4**) as well as for Ki67 and N-Cadherin (**Figure 3.5**) within the medial layer were noted with increased intensity and frequency with decreasing graft compliance. In contrast, N-Cadherin staining in the endothelium was increased in all synthetic graft groups relative to the sham control (**Figure 3.6**), although the increase was modest for the high compliance group. Similarly, no differences in VE-Cadherin staining were observed across groups. However, vWF staining displayed a clear and consistent increase with higher degrees of compliance mismatch. Furthermore, the low compliance treatment group and ePTFE control group demonstrated vWF staining penetrating into the vessel wall, as is often observed in intimal hyperplasia due to the release of soluble vWF by the endothelium.

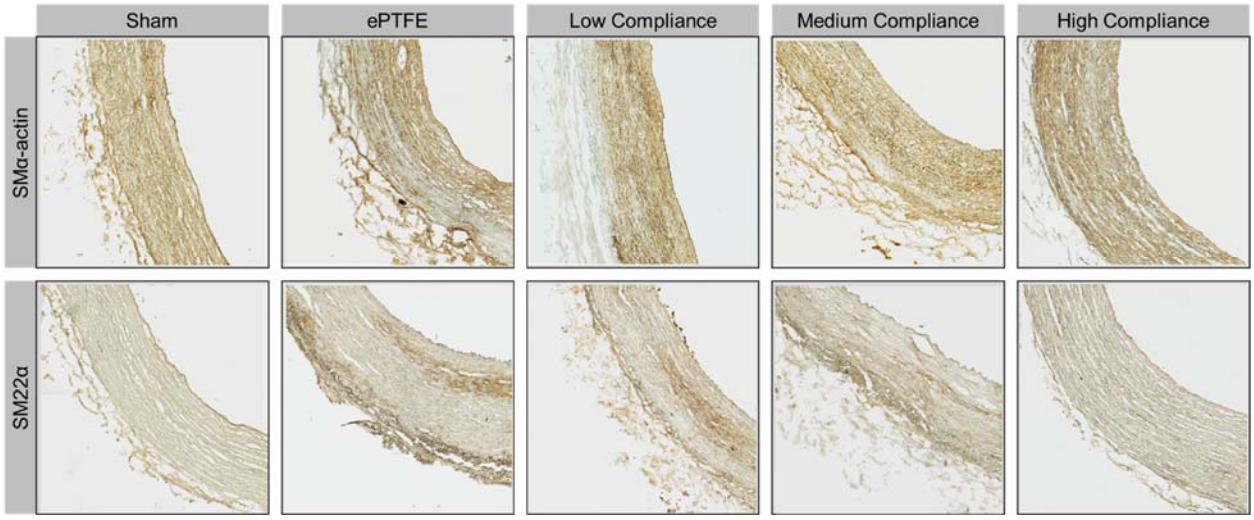

Figure 3.4: The effect of compliance on smooth muscle cells at the distal anastamosis as demonstrated by histological staining of SMα-actin and SM22α at day 14. The images presented are representative of 4 samples.

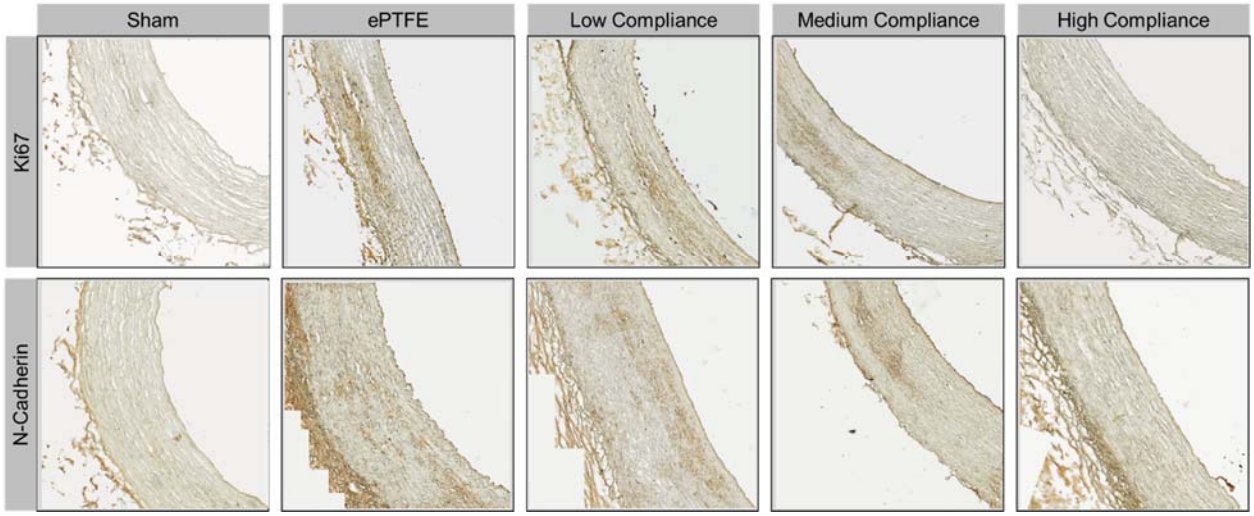

Figure 3.5: The effect of compliance on the smooth muscle cells at the distal anastomosis by histological staining of Ki67 and N-Cadherin at day 14. The images presented are representative of 4 samples.

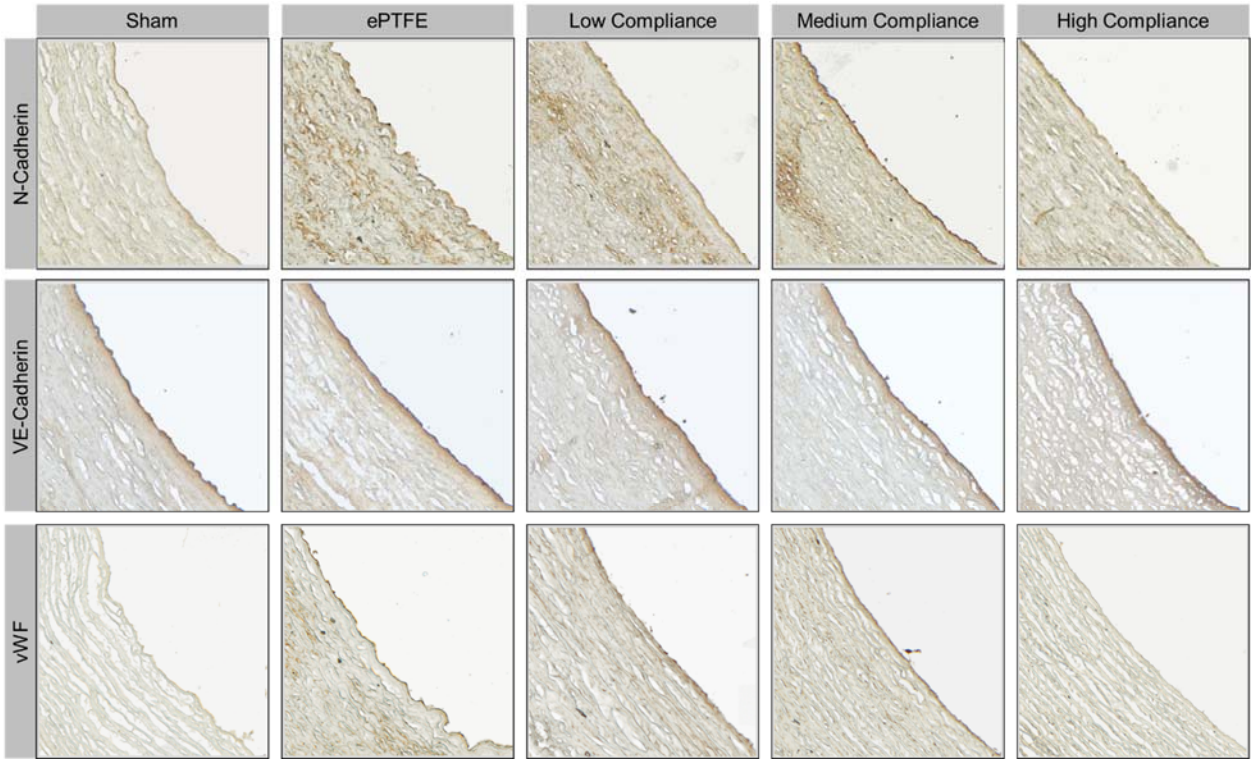

Figure 3.6: The effect of compliance on endothelial cell behavior at the distal anastomosis by histological staining of N-cadherin, VE-Cadherin and vWF at day 14. The images presented are representative of 4 samples. Higher magnification images are provided to enhance the visibility of epithelial staining.

To examine alterations in medial layer extracellular matrix associated with these differences in VMSC and endothelial cell behavior, staining for "acute" markers MMP-1 and versican was conducted (**Figure 3.7**). MMP-1 staining –particularly in the subintimal space – increased as graft compliance decreased. Similarly, versican staining displayed higher subintimal intensity as well as increased spatial variation in the low compliance treatment groups. In contrast, staining for elastin and fibronectin - extracellular matrix markers associated with more progressed states of intimal hyperplasia - showed no apparent differences among groups (**Figure 3.8**).

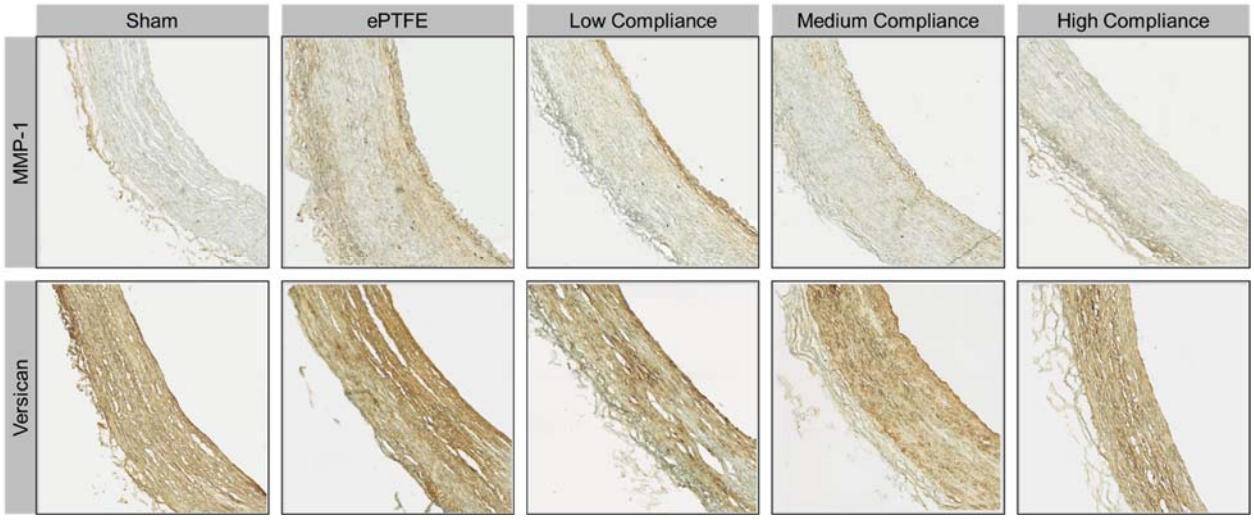

Figure 3.7: The effect of compliance on the extracellular matrix of the vessel media at the distal anastomosis by histological staining of MMP-1 and versican at day 14. The images presented are representative of 4 samples.

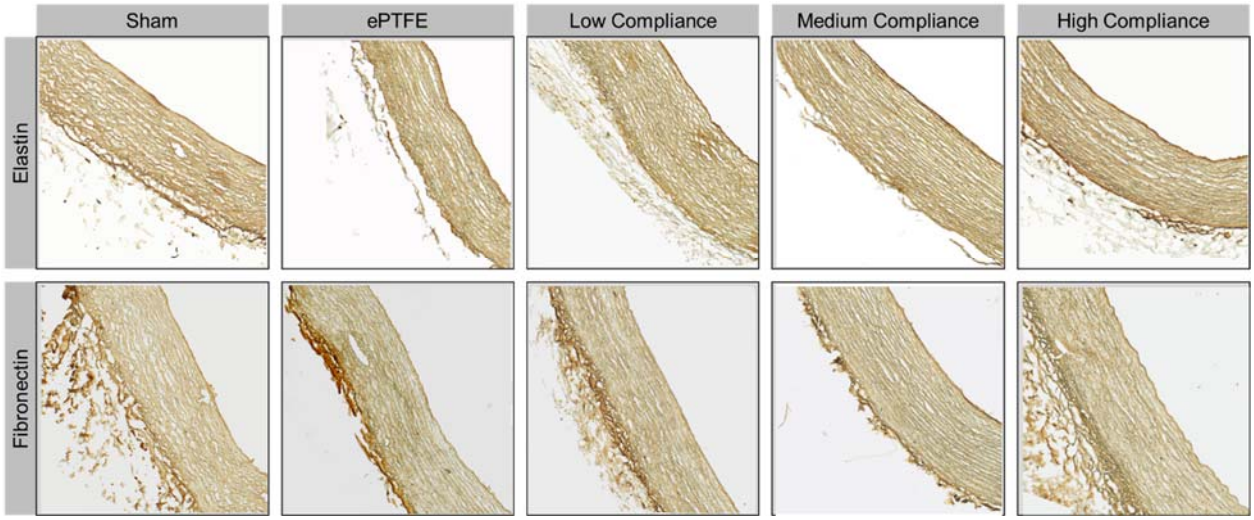

Figure 3.8: The effect of compliance on extracellular matrix proteins at the distal anastomosis by histological staining of elastin and fibronectin at day 14. The images presented are representative of 4 samples.

3.2.3 Biostability of Synthetic Grafts

As a final evaluation prior to proceeding to *in vivo* assessment of intimal hyperplasia using a porcine model, accelerated degradation testing was performed to confirm the biostability of the vascular grafts. Accelerated oxidative degradation in 0.1M $CoCl_2$ and 20% H_2O_2 for 36 days at 37°C was selected for its well-established use in mimicking macrophage-mediated oxidative degradation of polyurethanes.[160] The compliance for the high, medium, and low compliance grafts were not significantly different after degradative treatment, **Figure 3.9A**. Similarly, the burst pressures were not significantly different for the high and medium compliance grafts; however, a small but significant loss of burst pressure was observed for the low compliance graft (**Figure 3.9B**). The suture retention strength for the grafts also remained largely unaltered by degradative treatment (**Figure 3.9C**). No notable change in fiber morphology of the meshes was observed with scanning electron microscopy and no notable change in surface chemistry as monitored with ATR-FTIR spectroscopy was observed after degradative treatment. There was some salt precipitate apparent in the treated samples even after washing and drying. (**Figure 3.9D,E**). Overall, the biomechanical properties of the vascular grafts were retained after accelerated oxidative degradation. These findings in combination with previous studies that confirmed the thromboresistance of the multilayer grafts support the safety of the constructs for long-term implantation studies.[86] Notable for the continuation of this work is that these findings indicate that the compliance would remain constant over the extended *in vivo* evaluation needed to assess intimal hyperplasia.

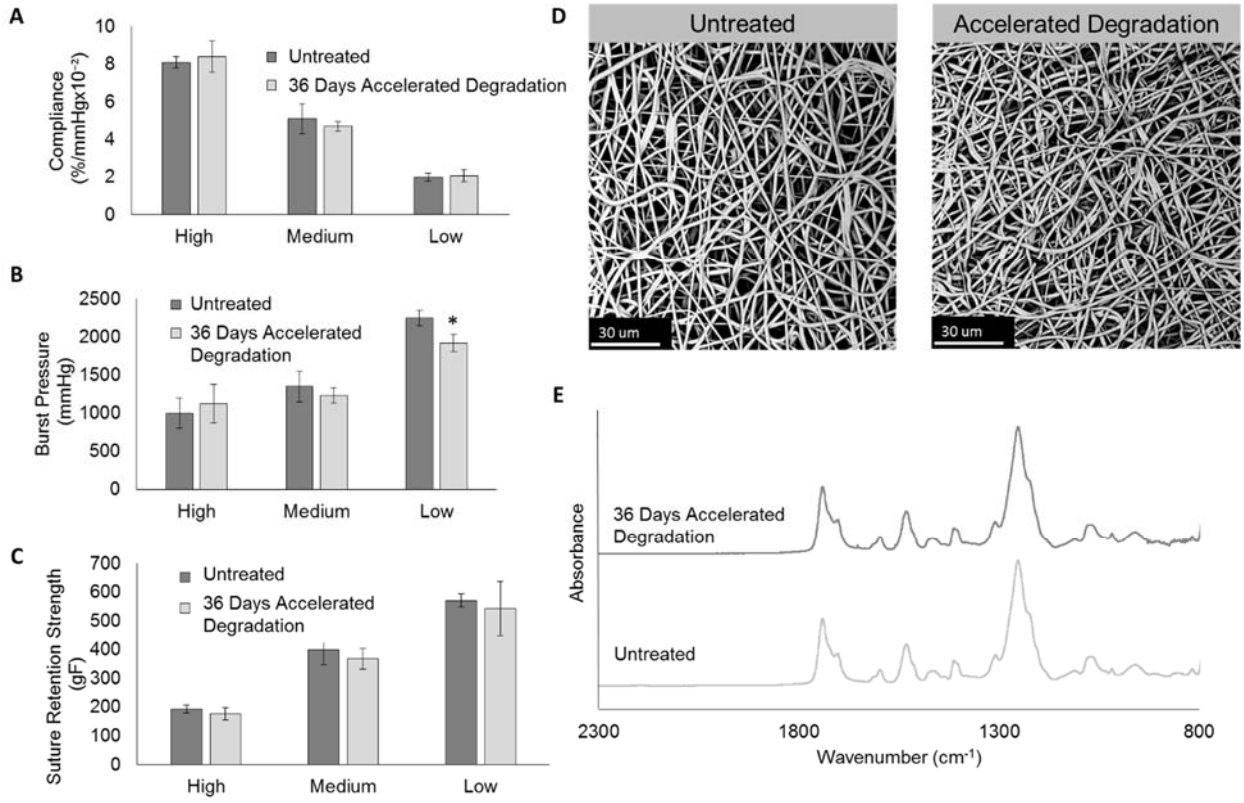

Figure 3.9: The effects of accelerated oxidative degradation for 36 days in 0.1M $CoCl_2$ in 20% H_2O_2 on the compliance (A), burst pressure (B), and suture retention strength (C) of the low, medium, and high compliance multilayered vascular grafts. The effects of oxidative degradation on fiber morphology determined by SEM (D) and surface chemistry determined by ATR (E). Statistical significance is shown by * to show a difference between untreated and degraded groups. Data is represented as average ± standard deviation for an n=4.

3.3 Conclusions

Intimal hyperplasia contributes to the high failure rates of synthetic vascular grafts currently available to clinicians. Elucidating the mechanism that graft compliance mismatch initiates intimal hyperplasia has been clinically difficult due to many confounding factors such as varying graft compositions and confounding diseases. Despite some of these challenges, low wall shear stress has been indicated as a cause of intimal thickening. It has been historically theorized that the

compliance mismatch between the vascular graft and the native vasculature disrupts blood flow and creates zones of blood recirculation. Our ability to fabricate grafts with varying compliance independent of other variables allowed for a direct correlation of changes in wall shear stress due to poor compliance matching and early markers of intimal hyperplasia in a novel *ex vivo* organ culture model. The tools we have developed for these studies not only enable the investigation of intimal hyperplasia, they also allow for efficient future graft design iterations. The computational model also allows for optimization of graft parameters to limit turbulent flow and maintain high wall shear stress at the distal anastomosis. Future versions of the computational model could include more complex arterial geometries to better predict flow and wall shear stress *in vivo*. Finally, the *ex vivo* system can be used to quickly screen vascular graft prototypes for their propensity to induce early markers of intimal hyperplasia. Future work will build on the current studies by examining the long term effects of compliance mismatch in a large animal model and correlate these findings to the *ex vivo* bioreactor screening.

3.4 Materials and Methods

3.4.1 PEGDAA synthesis

Polyethylene glycol diacrylamide (PEGDAA) was synthesized according to a method adapted from Hahn, et al.[149] Briefly, acryloyl chloride (4 molar equivalents) was added dropwise to a solution of PEG diamine (3.4 kDa; 1 molar equivalent) and triethylamine (TEA, 2 molar equivalents) in anhydrous dichloromethane (DCM) under nitrogen. The reaction was stirred for 24 hours, and then washed with 2M potassium bicarbonate (8 molar equivalents). After drying with anhydrous sodium sulfate, the product was precipitated in cold diethyl ether, vacuum filtered, and dried under vacuum.

3.4.2 Multilayer graft fabrication

A 25 wt% solution of Bionate® thermoplastic polycarbonate-urethane (DSM Biomedical) in dimethylacetamide was electrospun with a flow rate of 0.5 ml/hr through a blunted 20G needle. The rotating mandrel for collection was first coated in a PEG sacrificial layer and placed 50 cm from the needle tip. A voltage of 15 kV was applied to the needle and a -5kV voltage was applied to the rotating mandrel. Mesh thickness was varied from 0.1–0.4 mm by adjusting collection time. The rod and mesh were allowed to soak for 1 hour in water to dissolve out the sacrificial PEG layer, and the mesh sleeve was cut into 4 mm long sections. Electrospun mesh sleeves were then taken through a graded ethanol/water soak (70%, 50%, 30%, and 0%; 30 minutes each) to ensure hydration and penetration of the aqueous hydrogel precursor solutions into the mesh prior to hydrogel coating. The pre-wetted meshes were then placed in a cylindrical mold with an inner glass mandrel (4 mm outer diameter). The hydrogel precursor solution (7.2% PEGDAA, 3.6% n-vinyl pyrrolidone (NVP), and 1% Irgacure solution) was pipetted between the mandrel and the hydrated mesh and crosslinked with UV light for 6 minutes in a custom-built UV box. Composite grafts were then soaked for three days with daily solution changes to remove un-reacted NVP.

3.4.3 Computational modeling

Simulations were performed with the software package COMSOL Multiphysics. The geometry used to simulate the graft was an axial model that can be rotated 360 degrees to yield a 3D representation of the grafted vessel. The vessel on each end were modeled with no slip boundaries and a compliance of 9.0 %/mm Hg x 10^{-2}, 10 cm long and 4 mm inner diameter. The graft was modeled with increasing compliances 1.5, 4.0, and 8.5 %/mm Hg x 10^{-2}, 4 cm long and 4 mm inner diameter. Blood flow was modeled using the Carreau Yasuda model of blood viscosity:

$$\mu = \mu_\infty + (\mu_0 - \mu_\infty)[1 + (\lambda\dot{\gamma})^2]^{(n-1)/2}$$

Where

$$\lambda = 3.313s$$

$$n = 0.3568$$

$$\mu_0 = 0.56P$$

$$\mu_\infty = 0.0345P$$

Fluid flow through the fixed inlet was set at physiological parameters at 395 ml/min and pressure varied from 80 to 120 mmHg. Using Fluid-Solid Interaction physics and the Fluid Flow physics, wall shear stress (WSS) was calculated from the flow rate at the walls.

3.4.4 Organ culture

Fresh porcine carotid arteries were purchased from LAMPIRE Biological Laboratories, Inc. (Pipersville, PA). Arteries were dissected in a laminar flow hood to remove excess of connective tissue and rinsed multiple times with PBS containing antibiotics and antimycotics (PBS-PSA, Gibco) to check for leaking or small side branches. Arteries were then sectioned into three pieces distributed as follows: two 2cm length pieces at both ends of the artery and a central 2mm length piece that would be used to assess the initial morphology and protein expression of the artery. The two 2cm segments were then anastomosed using a 7-0 prolene surgical needle (Ethicon) to different grafts; 1) multilayer grafts of low compliance, 2) multilayer grafts of medium compliance, 3) multilayer grafts of high compliance, 4) ePTFE grafts control (GORE-TEX® Stretch Vascular Graft ST04015A) and 5) segments of artery alone, used as negative control. The grafted vessels with a structure of artery-graft-artery or artery-artery-artery were then sealed using surgical glue (Coseal, Baxter) rinsed with PBS-PSA to check for flow and leaking, mounted on a bioreactor chamber (BISS Tissue Growth Technologies) and fixed into place using a sterile nylon thread. The bioreactor system was then washed with PBS-PSA prior to the onset of flow to check

for any leaking. Complete Endothelial Growth Media (EGM; DMEM + 20% BCS+ 2%PSA+ EGF + bFGF + VEGF + Long R3 IGF + Ascorbic Acid + Heparin + Hydrocortisone) was placed inside the artery chambers while the lumen of the grafted vessels was perfused with EGM supplemented with 35 mg/ml of Pharmaceutical Grade Dextran (Dextran T70, Pharmacosmos). Vessels were then cultured with a constant flow rate of 30 ml/min generated by a peristaltic pump (Masterflex L/S 07528-30) for 14 days at 37°C and 5% CO_2 changing media every other day. The peristaltic pump resulted in a pulsatile waveform and pressure in the system was adjusted to achieve ~120 mmHg/80 mmHg peak-to-trough pressures.

Vessels were collected at day 0 or after 14 days of culture and fixed with 10% buffered formalin (Fisher) overnight at 4°C. For the grafted vessels after 14 days of culture, portions of the arteries at both distal and proximal anastomosis sites (2 mm length) were selected for analysis. Day 0 samples and selected 14 days samples were then embedded in OCT and cryosectioned at 5 μm thickness for immunoshistochemical analysis.

3.4.5 Immunohistochemistry

Protein expression was analyzed using standard immunohistochemical techniques. Sections were rehydrated at room temperature for 15 minutes, then endogenous peroxidases were blocked for 10 minutes followed by the addition of the background terminator solution to block nonspecific background staining (BioCare Medical) for 10 minutes. Sections were then incubated with the appropriate primary antibody for 1 hour at room temperature (**Table 3.1**). The binding of the primary antibody was detected by incubating the samples with HRP-conjugated secondary antibodies (Jackson ImmunoResearch) for 1 hour at room temperature followed by the application of the DAB chromogen (Vector Laboratories). Stained sections were imaged using a Zeiss Axiovert microscope.

Table 3.1: Primary antibodies used for histological analysis.

Protein Marker	Clone number	Source
SMα-actin	1A4 (mouse)	SCBT
SM22α	ab14106 (rabbit)	Abcam
Ki67	NB500 (rabbit)	Novus
N-Cadherin	K20 (goat)	SCBT
vWF	H300 (rabbit)	SCBT
VE-Cadherin	C19 (goat)	SCBT
MMP-1	N17-R (rabbit)	SCBT
Versican	12C5 (mouse)	DSHB
Elastin	BA4 (mouse)	SCBT
Fibronectin	EP5 (mouse)	SCBT

*SCBT- Santa Cruz Biotechnology

3.4.6 Oxidative degradation and mechanical testing

Accelerated oxidative degradation testing was utilized to assess the biostability of the electrospun outer layer. Composite vascular grafts of high, medium, and low compliance (n = 4 for each) were placed in an oxidative solution of 0.1M $CoCl_2$ and 20% H_2O_2 for 36 days at 37°C with solution changes every 3 days to maintain a relatively constant concentration of radicals. The effect of the oxidative treatment on the graft compliance, burst pressure, suture retention strength, fiber morphology, and surface chemistry was then characterized. Compliance was measured by first inserting latex tubes into 5 mm long graft segments and connecting to a syringe pump with a flow rate of 2 ml/min. The diameter of the graft was measured using a laser micrometer (1210 Laser Micrometer, Z-Mike) at 80 and 120 mmHg. Compliance (C) was calculated by $C = \Delta D/D_0 \bullet \Delta P = (D_{120} - D_{80})/D_{80} \bullet 40$ as per the Niklason group (ref). Flow rate was then increased to 50 ml/min with obstructed flow until the outer layer burst. The highest pressure measured at the first sign of graft bursting was recorded as the burst pressure. Graft composites were cut lengthwise on one side and a suture was looped through the mesh 2 mm from one end in the center of the

mesh. The un-sutured end was secured in the bottom clamp and the top suture was secured in the upper clamp. Uniaxial strain was applied at a rate of 100 mm/min until the suture was pulled through the mesh. The maximum applied force was recorded as the suture retention strength.

The effect of oxidative degradation on the polyurethane mesh on surface chemistry and topography was determined using attenuated total reflectance- Fourier transform infrared (ATR-FTIR) spectroscopy and scanning electron microscopy (SEM). Meshes were washed and dried under vacuum overnight prior to testing (n = 4). Spectra were recorded using a Nicolet iS10 (Thermo Scientific) FTIR spectrometer at a resolution of 2 cm^{-1} for 64 scans using an ATR accessory with a germanium crystal. The fiber morphology was observed using SEM (Phenom Pro, NanoScience Instruments) at 10 kV accelerating voltage. Specimens approximately 5 mm x 5 mm were cut from each sample and mounted with conducting carbon tape on a cylindrical SEM stub (n = 4). Prior to imaging, the specimens were coated with 4 nm of gold using a sputter coater (Sputter Coater 108, Cressington Scientific Instruments).

CHAPTER IV

INTRODUCTION OF SACRIFICIAL BONDS TO HYDROGELS TO INCREASE DEFECT TOLERANCE DURING SUTURING OF MULTILAYER VASCULAR GRAFTS*

4.1 Introduction

In Chapter II and Chapter III, we described improvements to the cellular interactions and mechanical properties of the multilayer graft, but further improvements to the hydrogel inner layer are required. After implantation as end-to-end anastomosis into the carotid arteries of 6 month old swine, damage to the hydrogel coating of the composite graft was observed, as demonstrated in **Figure 4.1**. The generation of hydrogel particulates during suturing of the grafts represents a significant risk that must be addressed prior to further graft development and assessment. The risks associated with dislodged hydrogel particulates are similar to those of a thrombus or embolus and include stroke, heart attack, and pulmonary embolism.[161] There is a clear need for a hydrogel coating in the multi-layered small diameter vascular graft that does not generate particulates after suturing that can act as emboli downstream. However, no suture damage resistant hydrogels or requisite material properties have been described in literature to the best of our knowledge. We also found that common mechanical properties evaluated in hydrogels such as compressive and tensile modulus, toughness, and elongation did not correlate to particles dislodged during suturing.

---

* Reprinted with permission from "Introduction of sacrificial bonds to hydrogels to increase defect tolerance during suturing of multilayer vascular grafts" by Allison Post, Alysha Kishan, Patricia Diaz-Rodriguez, Egemen Tuzun, Mariah Hahn, Elizabeth Cosgriff-Hernandez, 2018. *Acta Biomaterialia*, 69, 313-322 Copyright (2018) by Acta Materialia Inc.

Due to the lack of hydrogels exhibiting suture damage resistance, we have developed a hydrogel to address this need.

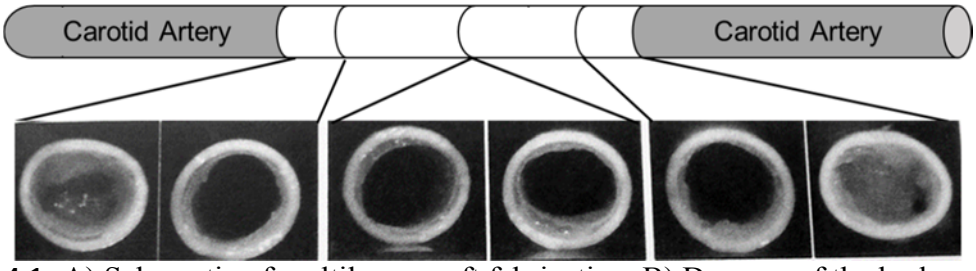

Figure 4.1: A) Schematic of multilayer graft fabrication. B) Damage of the hydrogel at the suture line of multilayer graft composites implanted in porcine animal model.

In order to resist suture damage, the hydrogel must be resistant to crack propagation initiated by passing a suture needle through it. This can be accomplished by increasing the energy required to initiate crack propagation by increasing the secondary force interactions between adjacent polymer chains.[162] Enhancing secondary bonding or sacrificial bonds increases the energy required to initiate crack propagation through a material. Therefore, increasing hydrogen bonding can increase the defect tolerance in the hydrogel coating. We hypothesize that by introducing increased hydrogen bonding in the hydrogel, crack propagation and the associated dislodged particles will decrease. To this end, we enhanced hydrogen bonding by incorporating n-vinyl pyrrolidone (NVP) into the hydrogel to create a clinically relevant graft.

A PEG-based hydrogel with enhanced hydrogen bonding was developed to prevent damage to the hydrogel coating during suturing of our vascular graft. Initially, the mechanical properties of several hydrogel formulations were investigated to identify the impact of hydrogen bonding and

correlation to suture-induced damage. The hydrogel formulation with the fewest dislodged particles was then evaluated to confirm retention of thromboresistance, bioactivity, and biostability as compared to traditional poly(ethylene glycol) diacrylate (PEGDA) hydrogels. Finally, composite grafts were sutured into excised porcine carotid arteries and hydrogel particulate generation was evaluated in an ex vivo model under physiological flow. This study provides a comprehensive evaluation of this new hydrogel as a vascular graft coating that prevents complications associated with suture-induced particulate generation.

4.2 Materials and Methods

4.2.1 Materials

Bionate® Thermoplastic Polycarbonate-urethane was provided by DSM Biomedical (Berkeley, CA). All other chemicals were purchased from Sigma Aldrich (Milwaukee, WI) and used as received unless otherwise noted.

4.2.2 PEGDA and PEGDAA Synthesis

Polyethylene glycol diacrylate (PEGDA) was synthesized according to a method adapted from Hahn, et al.[149] Briefly, acryloyl chloride (4 molar equivalents) was added dropwise to a solution of PEG diol (3.4 kDa; 1 molar equivalent) and triethylamine (TEA, 2 molar equivalents) in anhydrous dichloromethane (DCM) under nitrogen. The reaction was stirred for 24 hours, and then washed with 2M potassium bicarbonate (8 molar equivalents). After drying with anhydrous sodium sulfate, the product was precipitated in cold diethyl ether, vacuum filtered, and dried under vacuum. Polyethylene glycol diacrylamide (PEGDAA) was prepared using a similar method to PEGDA. Briefly, acryloyl chloride was added to a solution of PEG diamine (3.4 kDa) and TEA in anhydrous DCM under nitrogen. The molar equivalent of PEG diamine, TEA, and acryloyl chloride was kept at 1:2:4. After reacting for 24 hours, the solution was similarly washed,

precipitated, and dried to obtain the final product. The chemical structures are shown in **Figure 4.2**.

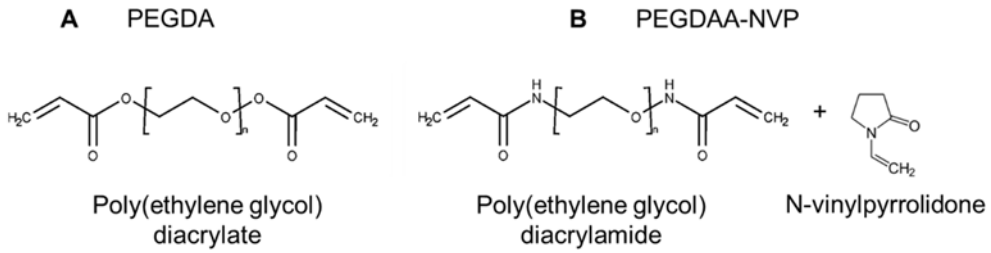

Figure 4.2: Chemical structures of A) poly(ethylene glycol) diacrylate (PEGDA) with an ester linkage, and of B) poly(ethylene glycol) diacrylamide (PEGDAA) with an amide linkage and n-vinylpyrrolidone (NVP).

4.2.3 Hydrogel fabrication and characterization

Several hydrogel compositional variables were tested including the effect of polymer backbone (PEGDA, PEGDAA), molecular weight (10kDa, 6kDa, 3.4kDa), crosslinker (NVP, 4-arm PEG acrylate), and polymer concentration (3.6, 7.2, 10, 20, 30%). As a generalized fabrication method, hydrogel slabs were fabricated by dissolving PEGDA or PEGDAA in deionized water with 1 vol% of the photoinitiator Irgacure 2595 (10mg/ml in 70% ethanol). NVP was incorporated in select precursor solutions at the molar ratios 1:12, 1:24, or 1:54 of PEG:NVP. Samples containing 4-arm PEG-acrylate were prepared with 10% or 20% 4-arm PEG-acrylate added to the 10% precursor solution of PEGDA. Precursor solutions were mixed and pipetted between 1.5 mm glass spacer plates and crosslinked on a UV plate, 6 minutes on each side.

The sol fraction and swelling ratio was determined for each hydrogel composition (n = 6). Briefly, circular hydrogel specimens (D = 8 mm) were dried under vacuum immediately after fabrication and weighed (W_i). Specimens were weighed after swelling in deionized water for 24 h

(W_s), and then weighed again after drying under vacuum for 24 h to assess dry polymer mass (W_d). The sol fraction was calculated as $(W_i-W_d)/W_i$. The equilibrium volumetric swelling ratio, Q, was calculated from the equilibrium mass swelling ratio: $(W_s)/W_d$.

4.2.4 NVP incorporation

An assay developed by El-Rabbat et al. was used to measure the quantity NVP leached out of the hydrogels as an indirect method to determine NVP incorporation into the polymer network.[163] Briefly, 8 mm hydrogel punches (n = 6) were soaked for 3 days with daily solution changes to remove unincorporated NVP. The supernatant was frozen, lyophilized, and re-suspended in 1 ml of glacial acetic acid. NVP was diluted in acetic acid to create the calibration curve. Malonic acid was dissolved at 10 wt% in acetic anhydride at 80°C for 5 minutes to create the working reagent. The working reagent was then added in equal volumes to the re-suspended hydrogel extracts and calibration solutions. The solutions were allowed to stand for 20 minutes at 80°C and then fluorescence read on a plate reader with excitation/emission at 397nm/452nm. The amount of NVP leached out of the gels was calculated using the calibration curve.

4.2.5 Hydrogel mechanical testing

Mechanical testing was performed to determine the effect of compositional variables on the compressive and tensile properties of the hydrogels as well as crack propagation using a single edge notch test. Hydrogels of each composition were fabricated as described above. Compressive modulus was determined using a dynamic mechanical analyzer (DMA) (RSAIII, TA Instruments). Six 8-mm diameter discs were punched from swollen hydrogel sheets and subjected to mechanical testing using the DMA fitted with a parallel-plate compression clamp. Testing was performed under unconstrained compression at room temperature. Dynamic strain sweeps were used to

determine the linear viscoelastic range for each hydrogel formulation. Then, a strain within the upper end of the linear viscoelastic range was used in a constant strain frequency sweep. Tests were conducted between 0.79 and 79 Hz, and the compressive storage modulus was taken at 1.25 Hz.

Tensile testing was performed on hydrogel rings that were fabricated by pipetting the precursor solution into a custom mold with a 3 mm inner diameter and a 5 mm outer diameter. The hydrogel tubes were swollen in deionized water for 24 h and then cut into 3 mm sections. Ring specimens (n = 6) were loaded in tension on an Instron 3324, and the stress and strain were recorded as the rings were pulled at a rate of 6 mm/min until failure. Tensile modulus was determined by the slope of the linear region of the stress-strain curve. Ultimate elongation was measured by the stretched length over the original length as a percent, or $(L/L_0)*100$. Ultimate tensile strength was determined as the force at failure. Toughness was measured as the area under the stress-strain curve.

To determine the fracture toughness of the hydrogel compositions, hydrogel specimens were fabricated (30 mm long, 10 mm wide, 1.5 mm thick) for single edge notch mechanical testing. Hydrogels fabricated with PEG(10k)DA, PEG(6k)DA, and PEG(3.4k)DA, each with and without NVP, were tested (n = 6). Using a razor blade, a notch 5 mm long was cut halfway along the length of the gel. The gels were then loaded into tensile grips of the RSAIII DMA using sandpaper to prevent hydrogel slippage. The gels were pulled in tension at 1 mm/s until the crack had propagated across the gel. The force of crack propagation was recorded and fracture toughness of the gel was calculated by the force over the length of the crack, $G = 2F/h_0$.

4.2.6 Suture-induced damage in hydrogels

Suture-induced damage was determined by the number of particulates dislodged during the pass of a suture needle and thread through a hydrogel slab. Hydrogel slabs were fabricated as described above and soaked in deionized water for 12 h. A 7-0 suture (Ethicon) was passed through the hydrogel to assess the suture-induced damage. Dislodged hydrogel particles were visualized and counted under a stereoscope (National Optical) as a measure of suture-induced damage of the hydrogel.

4.2.7 Bovine aortic endothelial cell (BAEC) adhesion to hydrogels

Bioactivity was conferred to the hydrogels by adding 4 mg/ml of collagen functionalized with acrylate-PEG-NHS linker (JenKem) (functionalization of 10% of the available lysines) to the 10% PEG(3.4k)DA and 20% PEG(3.4k)DAA-NVP hydrogel precursor solutions prior to cure. The hydrogels were soaked for 3 days prior to cell seeding to remove any uncrosslinked NVP. Circular specimens (D = 10 mm) were punched from hydrogel slabs and placed into a 48 well plate. Bovine aortic endothelial cells (BAECs) were cultured in EGM-2 cell media (Lonza), harvested for use at passage P4-P6, and seeded at 10,000 cells per well. Cells were allowed to attach for 3 hours, then washed twice with warm 10 mM phosphate buffered saline (PBS). Specimens were then fixed with 3.7% glutaraldehyde and stained with rhodamine phalloidin (actin/cytoskeleton) and SYBR green (DNA/nucleus). Cell adhesion and spreading were quantified using ImageJ software (n = 4).

4.2.8 Platelet attachment to hydrogels

Platelet attachment was used as an initial measure of thromboresistance of the new hydrogel formulations. 10% PEG(3.4k)DA and 20% PEG(3.4k)DAA-NVP hydrogels were soaked for 3 days prior to cell seeding to remove any uncrosslinked NVP. Circular hydrogel specimens were punched from the hydrogel slabs and placed in a 48 well plate. Platelets were isolated from human whole blood drawn from a volunteer and mixed with ACD via inversion. The mixture was

centrifuged at 990 rpm for 15 minutes to isolate the protein rich plasma (PRP) layer. The PRP layer was removed and prostacyclin was added at 10 μL/mL and centrifuged again at 1500 rpm for 10 min to form a platelet pellet. The pellet was resuspended in CGS buffer for washing and centrifuged again at 1500 rpm for 10 min. The platelets were then resuspended in Tyrode's buffer at half the original volume of PRP. Sudan B Black solution (5% in 70% ethanol) was added to the platelet solution at a 1:10 ratio for 30 minutes at room temperature. The stained platelets were then washed with PBS 3 times by resuspending the pellet in PBS then centrifuging at 1500 rpm for 8 min. Platelets were counted and resuspended at a concentration of 10 x 10^6 platelets/mL in sterile PBS. 500 μL platelet suspension was added in each test well, and platelets were allowed to adhere to substrate for 30 min at 37°C on a shaking incubator. Gels were transferred to new wells and washed twice with PBS, then carefully placed into microcentrifuge tubes and bound cells were lysed with 150 μL DMSO for 15 min at room temperature. 150 μL of PBS was added to each sample and the solution moved to a cuvette for reading on a spectraphotometer (400-650 nm, SpectraMax M2, Molecular Devices).

4.2.9 Fabrication of multilayer vascular graft composites

A 25 wt% solution of Bionate® (DSM) in dimethylacetamide was electrospun with a flow rate of 0.5 ml/hr through a blunted 20G needle. The rotating mandrel for collection was coated in a PEG sacrificial layer and placed 50 cm from the needle tip. A voltage of 15 kV was applied to the needle and a -5kV voltage was applied to the rotating mandrel. The rod and mesh were allowed to soak for 1 hour in water to dissolve out the sacrificial PEG layer, and the mesh sleeve was cut into 4 mm long sections. Electrospun mesh sleeves were then taken through a graded ethanol/water soak (70%, 50%, 30%, and 0%; 30 minutes each) to ensure hydration and penetration of the aqueous hydrogel precursor solutions into the mesh prior to hydrogel coating. The pre-wetted

meshes were then placed in a cylindrical mold with an inner glass mandrel (3 mm OD). Hydrogel solutions were pipetted between the mandrel and the hydrated mesh (4 mm ID) and crosslinked with UV light for 6 minutes in a custom-built UV box.

4.2.10 Accelerated hydrolytic degradation of hydrogel coatings

Hydrolytic degradations of the hydrogels were first compared in accelerated degradation conditions of 50 mM NaOH at 37°C. 8 mm punches were taken from hydrogel slabs after swelling overnight and put under vacuum overnight. Dry weights were recorded, and the hydrogel punches were swollen in water for 1 hour before weighing to determine the swelling ratio. The gels were then transferred to their respective conditions. Swelling ratio (Q) was calculated as *Ws/Wd*. Swollen weights were measured once a day for accelerated degradation of 10% PEG(3.4k)DA, and PEG(3.4k)DAA conditions were measured once a week. Compressive modulus was also recorded at these time points, as described previously.

To evaluate the hydrolytic degradation resistance of the vascular graft composites, multilayer vascular grafts were fabricated with either PEG(3.4k)DAA-NVP or PEG(3.4k)DA precursor solution. The composites were cut into 1cm long sections and incubated in the conditions described above for accelerated hydrolytic degradation. Degradation was measured as a change in luminal diameter. Pictures of the luminal diameter were acquired using a stereoscope (National Optical) and the diameter was measured using ImageJ software.

4.2.11 Bioreactor whole blood study of platelet adhesion of multilayer grafts

The thromboresistance of the multilayer graft was assessed by flowing fresh, heparinized porcine whole blood (Lampire Biological Laboratories) through the lumen of the grafts for extended time periods in a bioreactor. Multilayer grafts with PEGDA or PEG-NVP hydrogel luminal layers (n = 4 per formulation) were fitted onto the graft ports of custom bioreactor graft

chambers and fixed into place using sterile nylon thread. Segments of an ePTFE vascular graft control (GORE-TEX® Stretch Vascular Graft ST04015A) were fitted onto remaining graft ports (n = 4). Prior to the onset of flow, the blood was exposed to 10 μM mepacrine for 30 minutes at 37°C to fluorescently label associated platelets. Samples were perfused with heparinized porcine whole blood for three hours at a flow rate of 100 ml/min/construct generated by a peristaltic pump (Masterflex L/S 07528-30). Grafts were then dismounted from the graft ports and gently rinsed twice with PBS followed by exposure to 10% neutral-buffered formalin. Subsequently, the constructs were cut into two halves using fine-tipped surgical scissors, with the dissection plane slicing the length of each graft. Half of each construct was allocated for fluorescence imaging of adherent platelets, and the remaining half was processed for quantitative assessment of platelet adhesion to the graft lumen. Fluorescence images of platelet adhesion were obtained utilizing a Zeiss Axiovert 200M microscope with a FITC filter set (ex/em 470nm/515nm) and a 20X objective. To quantitatively assess platelet adhesion, the lumen of graft sections were rinsed 3 times with 200 μL of lysis buffer (100 mM TRIZMA-Base, 500 mM LiCl, 10 mM EDTA, 1% LiDS, 5 mM dithiothreitrol). This lysis buffer was collected and associated mepacrine was measured spectrophotometrically (Biotek Synergy HTX plate reader) utilizing a FITC filter set. Sample concentrations were determined relative to a standard curve and then normalized to the luminal surface area of the processed graft section.

4.2.12 Hydrogel particulate capture after suturing composites in ex vivo model

Vascular graft composites, fabricated as described above, were made with either PEG(3.4k)DAA-NVP or PEG(3.4k)DA precursor solution (n = 4). Porcine carotid arteries were acquired from Lampire Biological Laboratories (Pipersville, PA) and used within 48 hours of harvest. The arteries were cleaned and sectioned to 2 cm lengths and sutured to each end of the

grafts. Sham suturing was performed by suturing two carotid artery sections together using 7-0 proline sutures with a tapered needle (Ethicon). The sutured grafts and sham were then placed in a flow loop under physiological pressures (80 mmHg to 120 mmHg) for 30 minutes to further dislodge any hydrogel particulates created during suturing. The flow buffer was collected and filtered for particulates 200μm or larger that were then counted manually. The remaining unfiltered particulates were counted using a Chemtrac particle counter (Atlanta, GA). Grafts were then sectioned to visually inspect suture line damage.

4.2.13 Statistical analysis

The data are displayed as mean ± standard deviation for all measurements with the exception of cell adhesion that is presented as mean ± standard error of the mean. An analysis of variance (ANOVA) comparison was used for multiple composition comparisons with a Tukey's multiple comparison test to analyze the significance of the data. Comparisons in which there are only two compositions were compared using a student's t-test. Linear trends were tested by determining if the slopes of the best fit lines were statistically non-zero using the linear regression function of GraphPad. All tests were carried out at a 95% confidence interval ($p<0.05$).

4.3 Results

4.3.1 Suture-induced damage in hydrogels

Several hydrogel compositional variables were tested, molecular weight (10kDa, 6kDa, 3.4kDa), crosslinker (10%, 20% 4-arm PEG acrylate), and polymer concentration (3.6, 7.2, 10, 20, 30%), in an attempt to identify a correlation between gel mechanical properties and suture-induced damage. Despite the broad range of tensile properties, hydrogel particulates were detected in all PEGDA hydrogels when a suture needle was passed through the hydrogel slabs, **Figure 4.3A**. There was no discernable trend between suture-induced damage and compressive modulus, tensile

modulus, tensile strength, or elongation, **Figure 4.4**. In contrast, copolymerization with NVP resulted in a marked decrease in the total number of dislodged particles in all compositions of PEGDA hydrogels tested, **Figure 4.3B**. Additional mechanical testing of fracture toughness using a single edge notch tensile test identified a marked increase in fracture toughness in PEGDA-NVP hydrogels (**Figure 4.3C**). The force required to propagate the notch across the hydrogel was increased for all PEGDA-NVP compositions and correlated strongly with decreased suture-induced damage as measured by particle generation (**Figure 4.3D**).

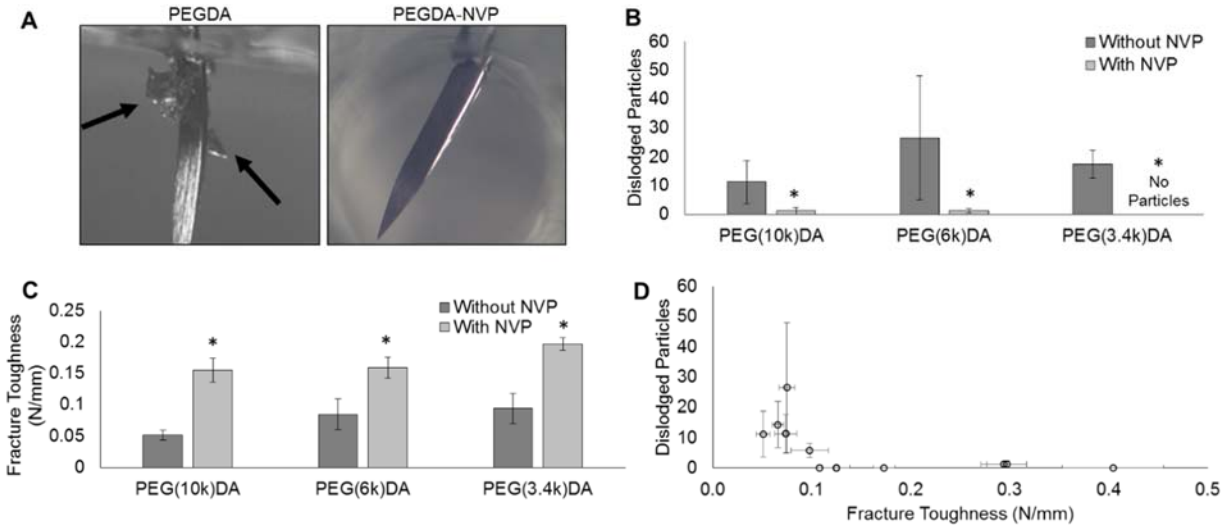

Figure 4.3: A) Images of particles dislodged during suturing for both PEG(3.4k)DA and PEG(3.4k)DA-NVP hydrogel compositions. Black arrows indicate dislodged particles. B) Effect of incorporating NVP into 10% PEGDA hydrogels on suture damage resistance. C) Defect tolerance assessed by fracture toughness. D) Correlation of reduced particle generation during suturing with increasing fracture toughness. All data represents average ± standard deviation of n=6. The * represents a significant difference between groups with and without NVP ($p<0.05$).

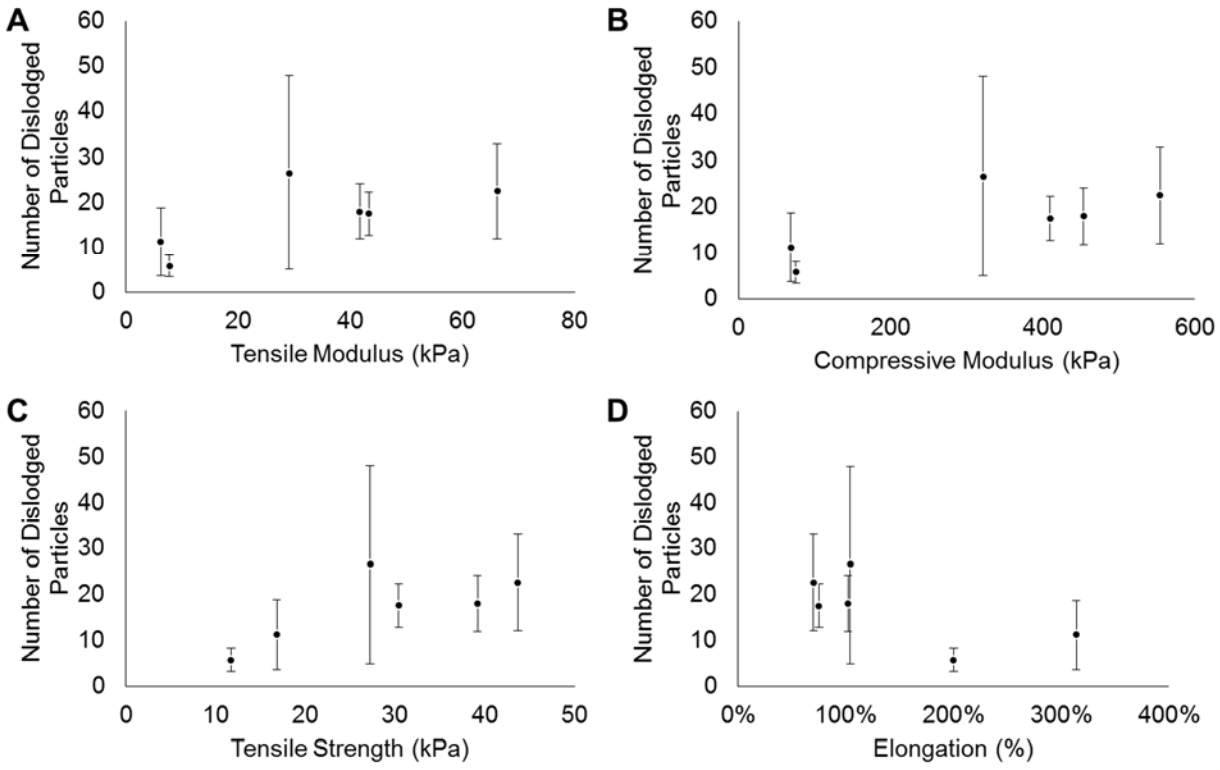

Figure 4.4: A) Images of particles dislodged during suturing for both PEG(3.4k)DA and PEG(3.4k)DA-NVP hydrogel compositions. Black arrows indicate dislodged particles. B) Effect of incorporating NVP into 10% PEGDA hydrogels on suture damage resistance. C) Defect tolerance assessed by fracture toughness. D) Correlation of reduced particle generation during suturing with increasing fracture toughness. All data represents average ± standard deviation of n=6. The * represents a significant difference between groups with and without NVP ($p<0.05$).

4.3.2 Effect of NVP concentration in PEGDA gels

The effect of NVP concentration on the suture damage and compressive modulus of the PEGDA gels was tested (**Figure 4.5**). The number of dislodged hydrogel particles decreased as increasing amounts of NVP were incorporated with particles ultimately eliminated with 54 moles of NVP added to the precursor solution for every 1 mole of PEGDA in solution, **Figure 4.5A**. A concurrent increase in compressive modulus of the 10% PEG(3.4k)DA hydrogels was observed

with increasing amounts of NVP, **Figure 4.5B**. In order to match the original compressive modulus, the polymer content was decreased to 7.2% PEG(3.4k)DA-NVP 1:54, which resulted in a corollary decrease in compressive modulus to approximately 470 kPa (**Figure 4.5C**).

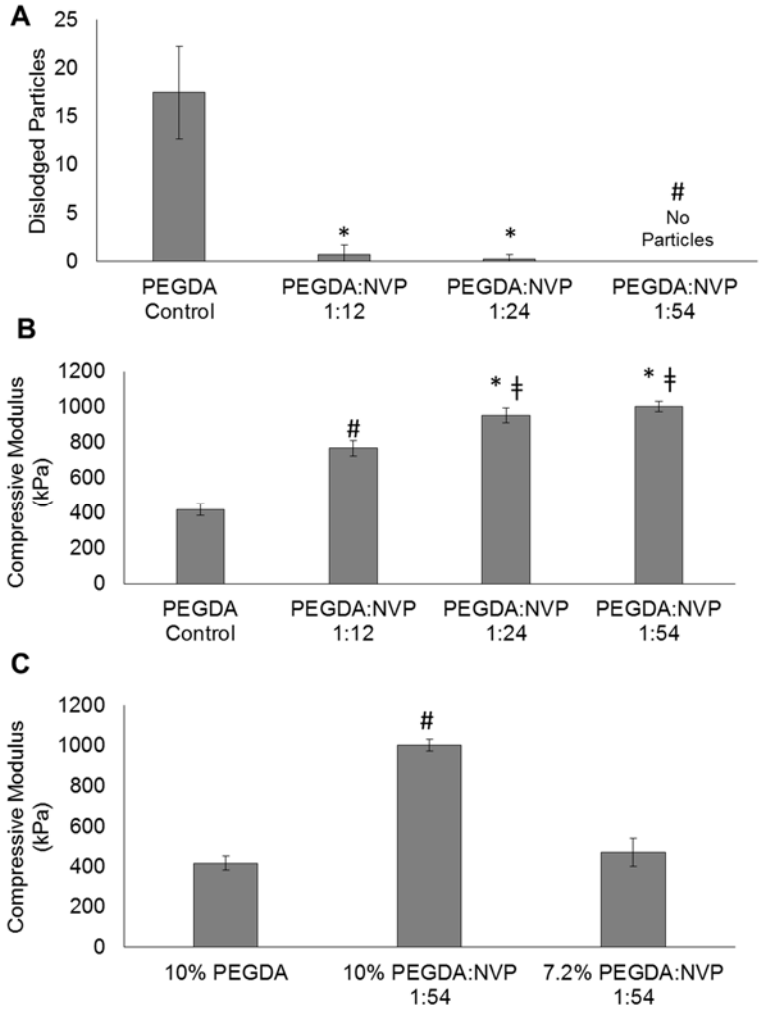

Figure 4.5: Effect of increasing NVP content in 10% PEG(3.4k)DA hydrogels on (A) defect tolerance and (B) compressive modulus. C) Matching modulus of the 10% PEGDA with the PEGDA-NVP formulation by decreasing PEGDA content. Data represents average ± standard deviation of n=6. The * represents a significant difference from the PEGDA Control, the ǂ represents significant difference from the control and PEGDA:NVP 1:12, and the # represents significant difference from all other groups ($p<0.05$) in ANOVA with Tukey's multiple comparison test.

4.3.3 Evaluation of PEGDAA-NVP hydrogel as a candidate luminal layer

Following identification of a method to enhance resistance to suturing damage of PEG-based hydrogels, additional testing was performed to identify and evaluate a candidate hydrogel composition for use as the luminal layer of the multilayer grafts. Previous studies have demonstrated favorable cell adhesion and migration on the 10% PEG(3.4k)DA hydrogels and enhanced hydrolytic stability of PEGDAA hydrogels.[54,86,125] In an effort to match the physical properties and biostability of these previous compositions, a new 7.2% PEG(3.4kDa)DAA-NVP was fabricated and tested in comparison to the 10% PEG(3.4kDa)DA hydrogel. The PEGDAA-NVP formulation displayed comparable compressive modulus and swelling as the PEGDA control with an increase in defect tolerance as indicated by the elimination of suture-induced particles generation, **Figure 4.6**. Biostability of the PEGDAA-NVP was then assessed using accelerated hydrolytic testing. No significant difference in the equilibrium swelling ratio of the PEGDAA-NVP hydrogel was observed; whereas, the PEGDA hydrogels were fully degraded at 5 days.

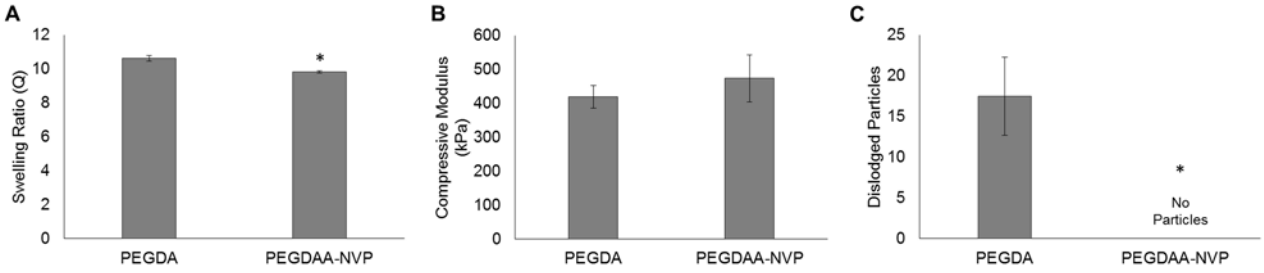

Figure 4.6: Matching swelling (A) and compressive modulus (B) between the original 10% PEG(3.4k)DA formulation and the damage-resistant 7.2% PEG(3.4k)DAA + 1:54 mol NVP hydrogel. C) Effect of decreasing polymer content and adding NVP to improve the defect tolerance of the hydrogel. Data represents average ± standard deviation of n=6. The * represents a significant difference from PEGDA ($p<0.05$) in a student's t-test.

Thromboresistance is another critical property to the success of any blood contacting material and was previously established in the original PEGDA hydrogel coating.[86] As an initial assessment that thromboresistance was retained in the new composition, static platelet attachment was assessed on PEGDAA-NVP hydrogel slabs. A synthetic graft, ePTFE, served as a clinical control and displayed significant platelet attachment, 10.3 ± 4.9 platelets/cm^2. In contrast, a statistically significant decrease in platelet attachment was measured on both the original PEGDA (1.5 ± 1.3 platelets/cm^2) or new PEGDAA-NVP (0.47 ± 0.49 platelets/cm^2) hydrogels. There was no significant difference between the PEGDA or PEGDAA-NVP suggesting that altering the hydrogel formulation to improve defect tolerance had limited impact on platelet attachment.

Finally, the ability to confer bioactivity to the PEGDAA-NVP hydrogels was evaluated by incorporating acrylate-functionalized collagen and assessing endothelial cell adhesion. BAEC attachment studies demonstrated a statistically significant increase in cell attachment and cell spreading with collagen incorporated compared to the hydrogel controls. No significant differences were measured between PEGDA or PEGDA-NVP hydrogel compositions in either number of cells adhered (100 ± 6 cells/mm^2 and 94 ± 6 cells/mm^2) or cell spreading (942 ± 22 μm/cell and 762 ± 35 μm/cell), respectively (**Figure 4.7**). Following these favorable results, this composition was selected for the luminal layer of the multilayer vascular graft.

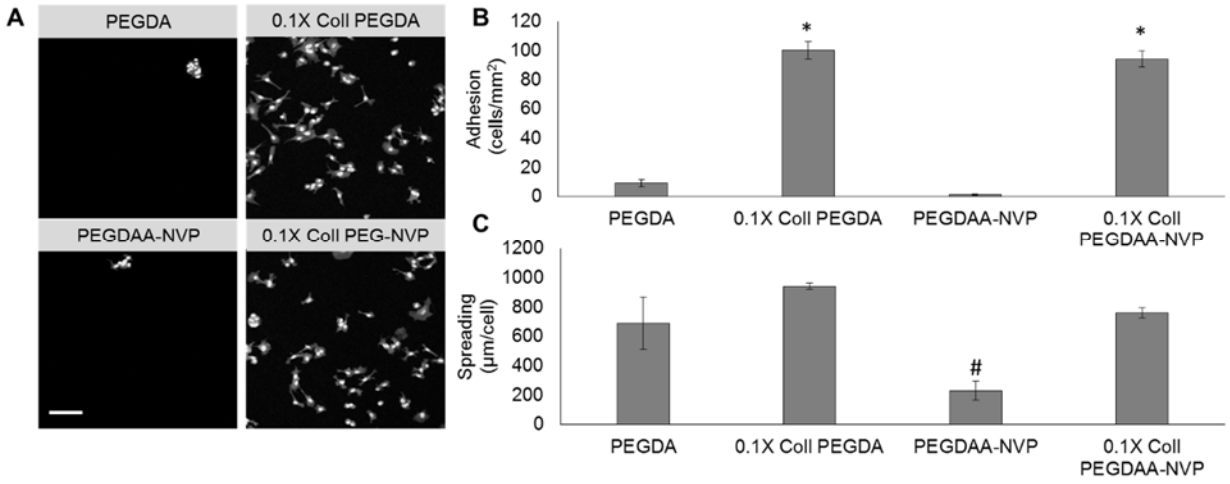

Figure 4.7: A) The effect of hydrogel composition on cell adhesion. Scale bar = 100µm. B) BAEC attachment on both compositions with incorporated functionalized collagen. C) BAEC spreading on both compositions with incorporated functionalized collagen. Data represents average ± standard error of n=4. The * represents a difference between groups with and without collagen ($p<0.05$), and the # represents a significant difference from all others ($p<0.05$) in ANOVA with Tukey's multiple comparison test.

4.3.4 Evaluation of the multilayer vascular graft

Multilayer vascular grafts were fabricated with the new defect-tolerant hydrogel composition (7.2% PEG(3.4kDa)DAA-NVP) and grafts were evaluated for biostability, thromboresistance, and suture-induced damage in comparison to the previous hydrogel composition (10% PEG(3.4 kDa).[86] In order to assess the effects of hydrogel degradation and subsequent swelling on the hydrogel luminal layer, accelerated hydrolytic degradation was performed on composite grafts with either PEGDA or PEGDAA-NVP inner layers. The PEGDA luminal diameter decreased by the first day, and continued to decrease until eventually the PEGDA inner layer delaminated from the outer layer and achieved total dissolution by day 5. The PEGDAA-NVP inner layer demonstrated no change in the luminal diameter over the course of 28 days (**Figure 4.8B**).

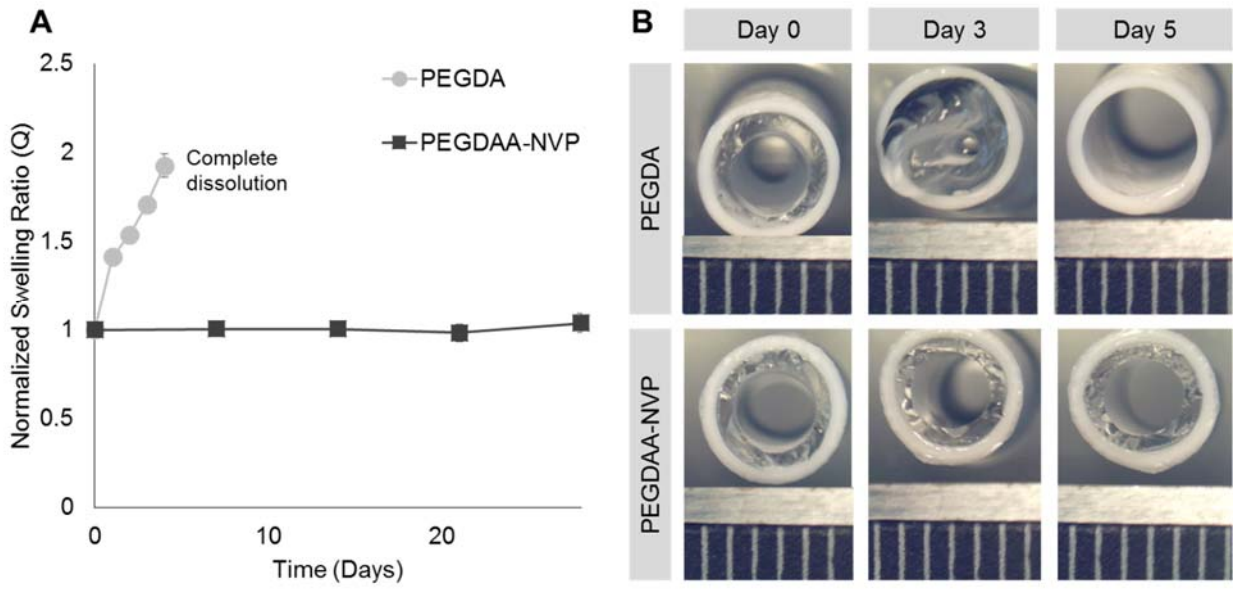

Figure 4.8: A) The effect of hydrogel composition on hydrolytic degradation rate. B) Luminal diameter changes for both compositions; ruler scale is 1mm. Data represents average ± standard deviation of n=4.

Given the low platelet attachment on hydrogels under static conditions described above (**Figure 4.9A**), the multilayer vascular grafts were assessed with whole blood in a pulsatile flow bioreactor. The results of the whole blood attachment studies closely mirror the trends in the platelet attachment study. Low platelet attachment on the PEGDA (0.08 ± 0.02 platelets/cm^2) and PEGDA-NVP (0.1 ± 0.05 platelets/cm^2) composites was observed and the results were statistically different than platelet attachment on the ePTFE graft (0.5 ± 0.2 platelets/cm^2), **Figures 4.9B and 4.9C**.

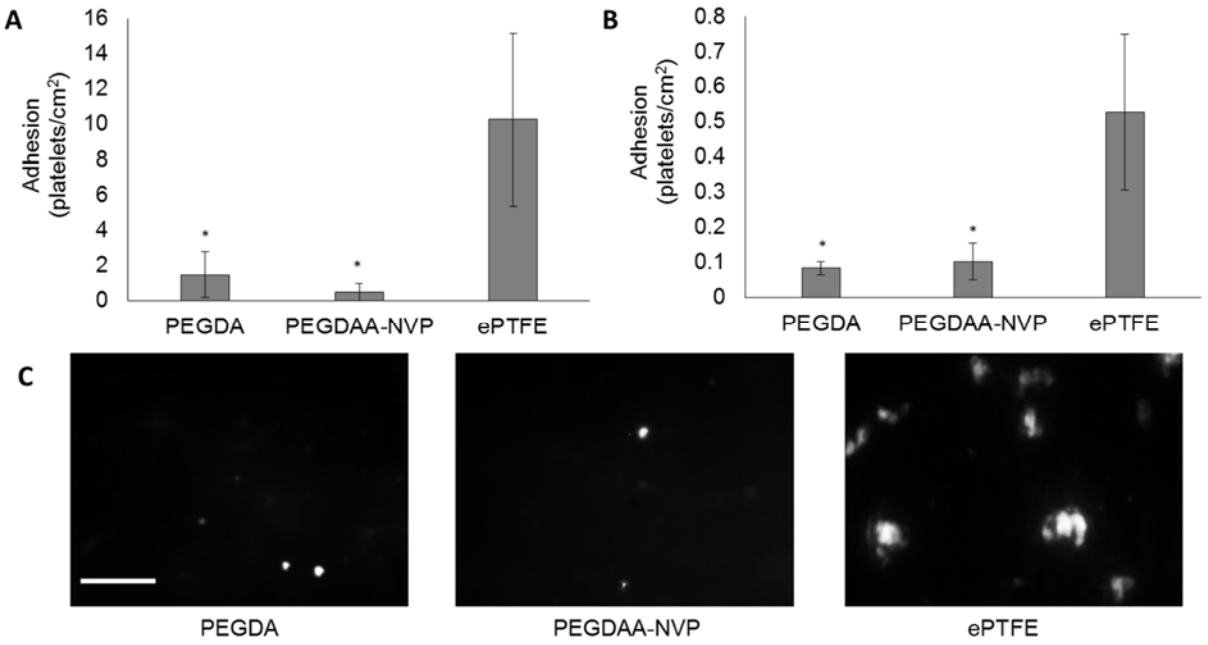

Figure 4.9: A) The effects of hydrogel composition on static platelet adhesion. B) The effects of hydrogel composition on bioreactor whole blood platelet attachment. Scale bar = 100μm. C) Representative images of platelet attachment from the whole blood study. Data represents average ± standard deviation of n=4. The * represents a significant difference from ePTFE control ($p<0.05$) in ANOVA with Tukey's multiple comparison test.

Finally, an *ex vivo* flow loop model was used to provide a more rigorous simulation of the implantation procedure and assess particle generation following suturing of the multilayer grafts, **Figure 4.10A**. The number of dislodged hydrogel particles were counted in both the storage solutions of the sutured grafts and the solutions collected from the flow loop set up. Particulates were identified in all solutions except the sham control. More hydrogel particulates were identified in the storage containers of both formulations than in the flow solutions. There was also a statistically significant increase in particles detected in the solutions of the PEGDA composition than in the PEGDAA-NVP composition, **Figure 4.10B**. Upon investigation of the sutured ends of the grafts, the hydrogel layer of the PEGDAA-NVP composites appeared intact; whereas, marked

damage to the hydrogel layer of the PEGDA composites was noted at the suture line, **Figure 4.10C**.

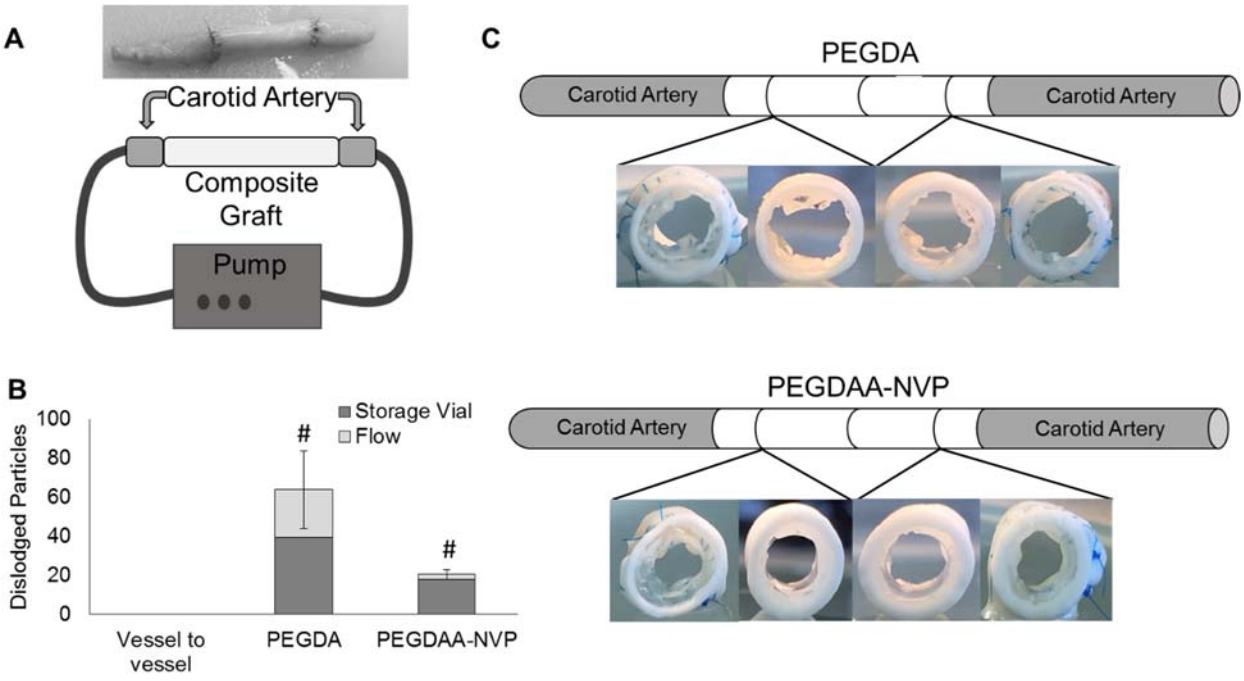

Figure 4.10: A) Composite graft sutured to excised porcine carotid artery segments and diagram of flow loop. B) Effect of composition on the number of particles captured in the flow loop after in vitro suturing. C) Sectioned grafts demonstrating hydrogel suture line damage after in vitro suturing. Data represents average ± standard deviation of n=4. The # represents a difference from all others ($p<0.05$) in ANOVA with Tukey's multiple comparison test.

Additional analysis of the graft indicated damage to the center of both sets of grafts and attributed to forceps gripping of the graft during the suturing procedure. Composite grafts with thinner hydrogel luminal wall thickness did not display this compressive damage, **4.11**.

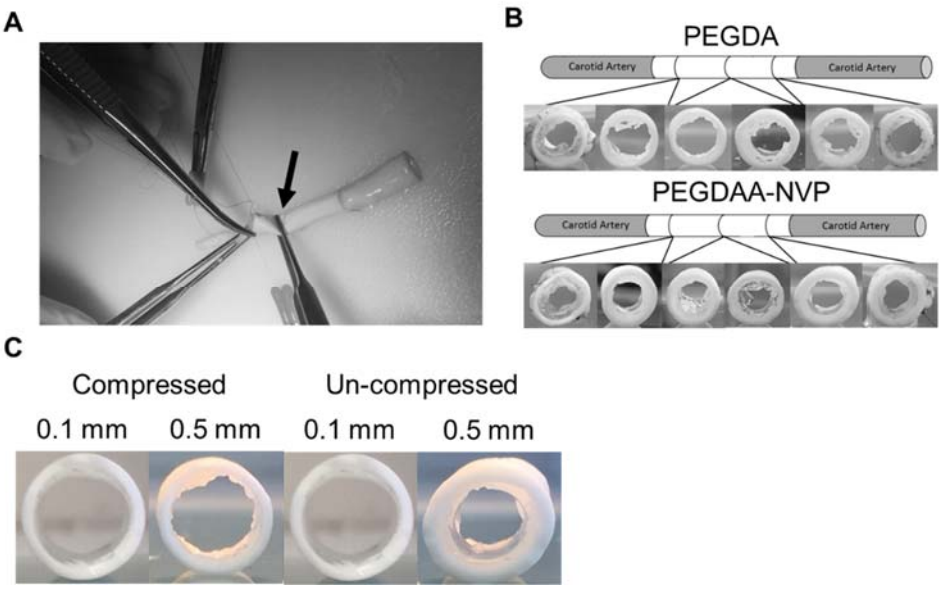

Figure 4.11: A) Suturing of grafts to porcine carotid arteries. Black arrow indicates gripping area. B) Sectioned grafts after suturing demonstrating hydrogel damage. C) Effects of hydrogel inner layer thickness on compression damage during forceps gripping.

4.4 Discussion

The observed suture-induced damage of the hydrogel coating after implantation of the multilayer vascular graft created a clear need for a hydrogel with increased defect tolerance. Hydrogel particulates from suture-induced damage can result in embolisms downstream leading to severe complications and morbidity. To generate a new hydrogel coating that could be used clinically without risk of embolism, traditional hydrogel variables (molecular weight, concentration, crosslinker) were investigated to first identify a correlation between gel mechanical properties and suture-induced particle generation. Despite the large ranges investigated for modulus (6 kPa to 66 kPa), tensile strength (11 kPa to 43 kPa), and elongation (7% to 314%), no strong correlation was observed between these properties and suture damage resistance (**Figure 4.4**).

The mechanical property that could be correlated with defect tolerance was fracture toughness as measured by a single edge notch test. The energy required for crack propagation was a better predictor of hydrogel defect tolerance and particle generation during suturing. Increased fracture toughness was achieved in the PEG-based hydrogels through copolymerization with NVP and attributed to the additional hydrogen bonding sites available upon NVP incorporation. Although there are several possible secondary interactions, one such is water bridging between the carbonyl of the NVP amide and the carbonyls of the ester of PEGDA or amide of PEGDAA, as diagramed in **Figure 4.12**. It has been demonstrated that an increase in secondary force interactions between polymer chains requires greater energy to initiate crack propagation, and this higher initiation energy creates a higher defect tolerance in the crosslinked polymer.[162,164] For our system, the addition of NVP to the PEG-based hydrogels was hypothesized to reduce suture-induced damage by introducing sacrificial, hydrogen bonds that dissipate initial crack energy and potentially reform to limit future crack propagation and fracture.

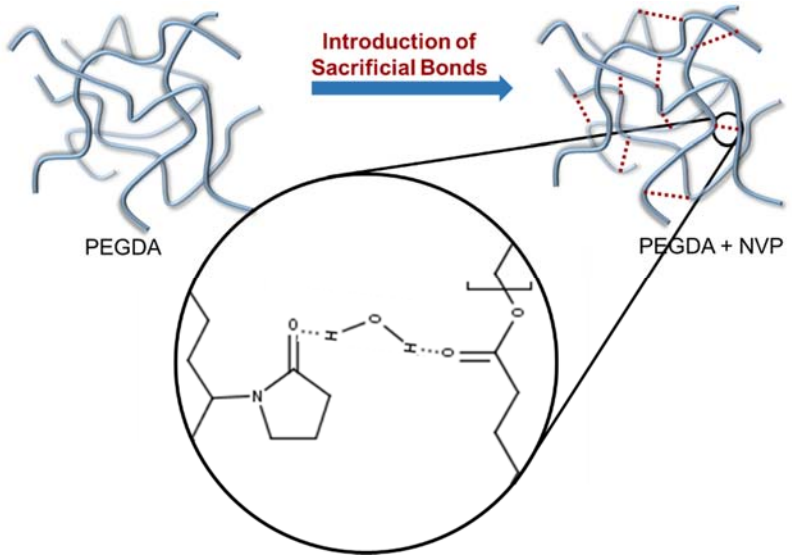

Figure 4.12: The effect of adding n-vinyl pyrrolidone to PEGDA hydrogels on defect tolerance. Fracture energy is increased by introducing sacrificial bonds via increased hydrogen bonding, thereby increasing defect tolerance. The sacrificial hydrogen bonds are created by water bridging of the carbonyl of the PEGDA ester and the carbonyl of the NVP amide groups.

In order to achieve incorporation and total elimination of dislodged hydrogel particulates, relatively large amounts of NVP (54 moles to 1 mole of PEGDA) must be added to the hydrogel precursor solution. During formation of the crosslinked hydrogel network, three simultaneous reactions take place upon UV irradiation of the pre-cursor solution: homopolymerization of the acrylates in PEGDA, homopolymerization of the vinyls in NVP, and copolymerization of the acrylates and vinyls. According to an assay for the detection of tertiary amines developed by El-Rabbat et al., approximately 16 ± 9% of the NVP added is incorporated into the hydrogel network. The high sol fraction (**Figure 4.13**) also supported a low level of NVP incorporation into the network. This result is expected given that the propagation rate (kp) is much higher for acrylate-acrylate reactions (2.165 x 10^4 L/mol·s) then for acrylate-vinyl reactions (0.101 x 10^4 L/mol·s). This strongly favors polymerization of the PEGDA over copolymerization of PEGDA and NVP

due to the limited availability of the acrylate groups for reaction. Therefore, large molar ratios of NVP to PEGDA must be added in order for NVP to be incorporated.

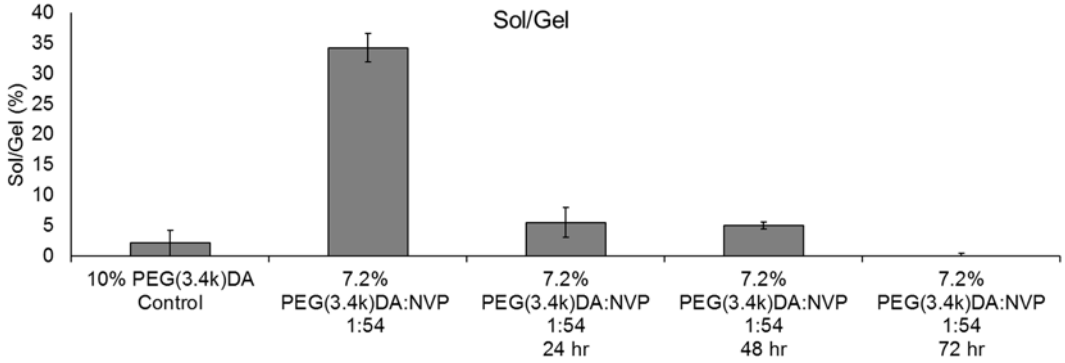

Figure 4.13: Effect of leaching PEGDA-NVP gels on sol/gel.

Although increasing amounts of NVP increased defect tolerance, it also increased the compressive modulus of the resulting hydrogel, **Figure 4.5**. It was hypothesized that the increase in compressive modulus and decrease in swelling ratio was due to an overall increase in polymer concentration in the final gel and corollary decrease in mesh size. However, when overall polymer content (PEGDA and NVP) is kept constant, there is a decrease in compressive modulus and increase in swelling, likely due to the disruption of network formation by NVP, Supplemental Table 1. Based on this finding, modulus was reduced to match the PEGDA control by decreasing the PEGDA concentration of the hydrogel. The resulting hydrogel maintained a similar defect tolerance and similar swelling ratio as the PEGDA hydrogel control. This suggests that the hydrogels mechanical properties can be tailored without altering suture damage resistance, **Figure 4.6**.

In addition to suture damage resistance, it is important the hydrogel coating is resistant to hydrolytic degradation to ensure it remains intact for the lifetime of the graft. In order to accomplish this, the formulation was changed from a PEGDA based hydrogel that contains ester linkages to PEGDAA that contains more hydrolytically stable amide linkages. Previous work in our lab has demonstrated the *in vitro* and *in vivo* hydrolytic stability of the PEGDAA hydrogels.[86] The PEGDAA-NVP displayed a similar resistance to hydrolysis as evidenced by the accelerated hydrolytic degradation study. Stability of the graft inner layer is critical to supporting the endothelial cell layer as well as preventing occlusion of the graft due to increased swelling of the hydrogel, **Figure 4.8**.

Following confirmation that the defect-tolerant hydrogel formulation maintained bioactivity and thromboresistance, a preliminary ex vivo suturing study was performed by suturing the composite graft to excised porcine carotid arteries. Preventing hydrogel damage is critical to the clinical relevance of the multilayered graft, as dislodged hydrogel particulates can act as emboli in the vascular system, and cause downstream heart attacks and strokes. This study demonstrated that significantly fewer particles are dislodged from the PEGDAA-NVP hydrogel coated graft than from the PEGDA hydrogel coated graft, **Figure 4.10**. Upon investigation of the suture line, the PEGDAA-NVP hydrogel appeared intact whereas the PEGDA hydrogel displayed severe damage, **Figure 4.1C**. The dislodged particles in the PEGDAA-NVP hydrogel detected in the storage solutions were attributed to damage of the hydrogel layer at the middle of the graft due to gripping with forceps to stabilize the graft during suturing (**Figure 4.11**). We have confirmed that the gripping damage can be mitigated by using thinner hydrogel coatings in the graft composites. This eliminates all dislodged particles, making the coating efficacious for clinical application.

4.5 Conclusions

Our previous work developing small diameter vascular grafts led to the discovery of the unique problem of particles dislodged from the hydrogel luminal layer during suturing. To address this problem, a new PEGDAA-NVP hydrogel with improved fracture toughness was developed. Increased defect tolerance was achieved through the introduction of sacrificial, hydrogen bonds that enabled suturing of the multilayer vascular graft without particle generation. It was also demonstrated that this modification resulted in no significant increase in thrombogenicity or change in bioactivity compared to a well-characterized PEGDA hydrogel. Therefore, we have successfully addressed the need for a suture-damage resistant hydrogel coating for use in small diameter vascular grafts and highlighted the need for testing the generation of dislodged particles in blood contacting materials. Future work will build upon the current research by testing the initial thromboresistance and long-term stability of the multilayered vascular graft with the new hydrogel inner layer after implantation into a porcine carotid artery model.

CHAPTER V

CONCLUSIONS

5.1 Summary

The work presented here improves many aspects of the multilayer graft, creating potential for safe clinical implementation and long-term patency. Through elucidation of fundamental biological and material relationships, improvements have been made to control cellular interactions, outer layer mechanical properties, and suture damage resistance of the hydrogel inner layer. Not only can these fundamental relationships be applied to the multilayer graft, they have the potential to optimize and improve many cardiovascular devices and constructs.

The first section of this work is dedicated to elucidating integrin-mediated hemostatic control in endothelial cells for improved cellular interactions with the graft inner layer. Endothelial cells have previously been shown to alter expression of hemostatic regulators based on their local substrate, but little work has been done to investigate the hemostatic effect of individual integrin binding in endothelial cells. We first investigated the relative expression of select integrins commonly used for attachment by endothelial cells to the basal lamina (α1β1, α2β1, α5β1, αvβ3). Then, utilizing integrin antibody blocking, we demonstrated that we can target these integrins using bioactive hydrogels enriched with common extracellular matrix proteins and designer collagens. We also showed that hemostatic regulator expression in endothelial cells and the correlating functional assay of platelet adhesion and activation can be modulated by specific integrin targeting. This work demonstrates that by using designer collagen programmed to target α1β1 and α2β1, we can limit endothelial cell thrombogenicity while promoting endothelial adhesion and migration on the hydrogel inner layer of the graft. This understanding of hemostatic

regulation through endothelial cell integrin targeting can be used to make thromboresistant coatings on many types of blood-contacting devices.

The next section describes the process of elucidating the intrinsic relationship between graft compliance and the onset of intimal hyperplasia. Intimal thickening is a common failure mode for synthetic vascular grafts, causing reocclusion at the distal anastamosis. This relationship has been previously difficult to elucidate due to confounding factors, such as differences in material chemistry that can affect cellular interactions between grafts of different compliances. By utilizing electrospinning to fabricate polyurethane grafts, we were able to create grafts of increasing compliance without altering graft material chemistry. This allowed for isolation of compliance as the single influencer of change in the system. Grafts sutured to carotid arteries were cultured for two weeks and interrogated for early markers of intimal hyperplasia. Changes in early markers for intimal hyperplasia that indicate smooth muscle cell proliferation and migration toward the lumen were correlated to changes in wall shear stress as predicted by a computational model of the sutured grafts. Using these systems, we were able to link poor compliance matching to early markers of intimal hyperplasia. This is the first definitive study to identify this relationship, and this bioreactor system is the first presentation of a rapid screening method for small diameter vascular grafts.

The last chapter is dedicated to the discovery and characterization of a suture-damage resistant hydrogel to implement as the inner layer of the multi-layer graft. Initial studies utilizing the multilayer vascular graft found that pieces of the PEGDA hydrogel were dislodged during suturing, creating pseudo-embolisms that can put patients at risk for stroke. In order to address this limitation, we identified a hydrogel formulation and key properties that eliminate particles dislodged during suturing. By introducing sacrificial hydrogen bonds in the hydrogel formulation, we were able to increase the fracture toughness that in turn imparted suture damage resistance to

the hydrogel. Identification of this relationship allows for further hydrogel design and optimization. We demonstrated that introduction of these sacrificial bonds does not affect bioactivity or thromboresistance, retaining properties similar to those of the original hydrogel formulation. By creating a hydrogel layer with suture damage resistance, we have rendered the graft safe for implantation.

With this work, the new vascular graft has 1) improved cellular interactions that promote thromboresistance upon endothelialization, 2) improved compliance matching that has been demonstrated in an *ex vivo* organ culture model to limit early markers of intimal hyperplasia, and 3) improved hydrogel mechanics for a suture damage resistant hydrogel that is requisite for implantation. Overall, this work serves to enhance not only the vascular graft, but provide fundamental insights into material design that can be applied to a number of devices and platforms.

5.2 Significance of Work

Elucidation of endothelial cell hemostatic regulation with integrin-targeting hydrogels

The aim of many blood contacting devices such as vascular grafts is to promote endothelialization to limit thrombogenicity of the material. By elucidating the individual and combinations of integrins that promote not only adhesion and migration but thromboresistance in endothelial cells, we can optimize biomaterial platforms to target these specific integrins. However, few studies have isolated individual integrin binding for the study of their effects on endothelial hemostasis. We established a novel integrin targeting platform using bioactive hydrogels and designer collagens that allows for simple evaluation of this targeting. This is the first reported use of this platform to study integrin targeting effect of hemostasis in endothelial cells. Using this novel platform, we identified integrin combinations that drive endothelial cells into a thromboresistant phenotype. These studies contribute significantly to a growing area of

research with few reports of individual effects of integrins on endothelial cell hemostatic regulation. Overall, this work provides technology and methods for promoting endothelialization of blood-contacting surfaces through priming endothelial cells with a thromboresistant phenotype.

Elucidating the role of graft compliance mismatch on intimal hyperplasia using an ex vivo organ culture model

Although intimal hyperplasia, a prominent failure mode of small diameter vascular grafts, has long been linked to poor compliance matching, there is no single study that definitively links the two. In the work presented here, we offer the first definitive study to elucidate this intrinsic link. In order to do so, we provide the first known description of grafts fabricated with increasing compliance over a wide range without changing material chemistry or fabrication method. The graft compliances range from the clinical standard of ePTFE (low compliance) to compliance of the carotid artery (high compliance, a good native arterial match). Importantly, we confirmed that the high compliance graft that matches compliance of the carotid artery maintains a high burst pressure and suture retention strength. This is the first known report of such a synthetic graft. Using this new library of graft compliances, we established an *ex vivo* organ culture model and computational model to elucidate the definitive link between graft compliance and the onset of intimal hyperplasia. Arteries sutured to low compliance grafts exhibited increased staining for smooth muscle cell proliferation and migration, important early markers of intimal hyperplasia. This link of poor compliance matching causing early markers of intimal hyperplasia contributes significantly to the fields of cardiovascular disease and cardiovascular graft design. Not only did the organ culture system and computational model allow for this elucidation, it introduced a

potential rapid screening method for small diameter vascular grafts using the *ex vivo* organ culture system and computational model.

Introduction of sacrificial bonds to hydrogels to increase defect tolerance during suturing of multilayer vascular grafts

The need for investigation of a suture damage resistant hydrogel emerged from a practical need and an absence of any mention of such a hydrogel in literature. In pursuing a suture damage resistant hydrogel, we identified fracture toughness as a key factor in predicting suture damage resistance. In order to eliminate particles dislodged during suturing, hydrogels required an increase in fracture toughness, accomplished by the introduction of sacrificial bonds. In this work, we present a novel hydrogel formulation that is suture damage resistant without affecting bioactivity or thrombogenicity. This hydrogel is ideal for the multilayered graft, and it can be applied to many other systems and soft tissue applications requiring suturing. Importantly, we identified a key factor for developing suture damage resistance in soft hydrogels that can be applied to many different hydrogel formulations.

5.3 Challenges and Future Work

The work presented here provides significant advancements in the development of the multilayer graft, but extensive investigation remains to be performed in order to make the graft a useful clinical product. In this work we have provide important insight into the influence of integrin attachment on endothelial cell hemostatic regulation. However, this regulation in endothelial cells is influenced by more than just the underlying ECM. These cells receive cues from many other influences, such as shear stress, substrate stiffness, and biochemical factors from blood. Future

work will need to determine which factors or factor combinations dominate endothelial thromboresistance for optimal biomaterial design. This could be accomplished by assessing the hemostatic regulation of endothelial cells under shear stress by applying flow to the system. The effects of varying substrate stiffness could be assessed by increasing and decreasing the compressive modulus of the bioactive hydrogels over a broad range. The ultimate determination will be the evaluation of the endothelial cell behavior *in vivo* on various platforms, as it is difficult to recapitulate all of these factors in a single *in vitro* set up. Not only will their hemostatic regulation be important to monitor, but the efficiency of the coating of the hydrogel inner layer has yet to be evaluated. If the endothelialization process proves to be slow in the *in vivo* evaluation, further modification of the inner layer may be required, such as rolling capture of endothelial progenitor cells to accelerate the endothelialization process.

We have established a significant correlation with the *ex vivo* bioreactor system between compliance matching and early markers of intimal hyperplasia, but further confirmation and correlation is required with an *in vivo* study. To validate the study results, we need to evaluate the presence of early markers of intimal hyperplasia in grafted arteries at 2 weeks *in vivo*. Longer time points will be required to confirm that the early markers of intimal hyperplasia do indeed lead to development of intimal thickening and occlusion in vessels grafted to low compliance grafts. *In vivo* evaluation is also required of the high compliance graft to demonstrate that the accelerated oxidative degradation study correlates to *in vivo* results.

We have developed the new inner layer hydrogel formulation that resists suture damage and compression damage, but it is susceptible to disruption by graft torqueing. In order to address this issue, it is possible to introduce more hydrogen bonding while increasing polymer chain length to resist torqueing damage through increased elongation and toughness. This new formulation with

increased torqueing damage resistance also must be evaluated clinically to ensure that forces recapitulated in the lab assessment of torqueing are representative of what is actually applied by the surgeons performing the grafting procedure. Ultimately, this new layer must also be evaluated *in vitro* for possible changes in bioactivity and thrombogenicity as well as *in vivo* assessment for efficacy as a viable inner layer. Overall, *in vivo* porcine models would confirm 1) that inner layer promotes endothelialization while limiting thrombogenicity, 2) that the outer layer retains its mechanical properties, and 3) that increased compliance matching resists intimal hyperplasia.

Although there is substantial evaluation and development yet to be performed in the multilayered graft, the work presented here has advanced the graft toward the goal of being an off-the-shelf small diameter synthetic vascular graft that has initial and sustained thromboresistance while limiting intimal hyperplasia. First, we provide details of the endothelial cell interactions with the hydrogel inner layer that can be further tailored to tune thromboresistance. Then we provide definitive evidence for the need for compliance matching to limit intimal hyperplasia and demonstrate fabrication of a graft with a high compliance with requisite burst pressure and suture retention strength. Finally, we have developed a suture damage resistant hydrogel that can be further modified for inner layer improvement. These improvements and elucidation of fundamental relationships provide a platform for further development of the multilayer vascular graft.

REFERENCES

1 Lloyd-Jones, D. *et al.* Heart disease and stroke statistics—2010 update A report from the American Heart Association. *Circulation* **121**, e46-e215 (2010).

2 Darling, R. C. & Linton, R. R. Durability of femoropopliteal reconstructions: endarterectomy versus vein bypass grafts. *The American Journal of Surgery* **123**, 472-479 (1972).

3 McKee, J. A. *et al.* Human arteries engineered in vitro. *EMBO reports* **4**, 633-638 (2003).

4 Williams, S. in *FASEB JOURNAL*. A305-A305 (FEDERATION AMER SOC EXP BIOL 9650 ROCKVILLE PIKE, BETHESDA, MD 20814-3998 USA).

5 Axthelm, S. C., Porter, J. M., Strickland, S. & Baur, G. M. Antigenicity of venous allografts. *Annals of surgery* **189**, 290 (1979).

6 Lehalle, B., Geschier, C., Fieve, G. & Stoltz, J. Early rupture and degeneration of cryopreserved arterial allografts. *Journal of vascular surgery* **25**, 751-752 (1997).

7 Carpenter, J. P. & Tomaszewski, J. E. Human saphenous vein allograft bypass grafts: immune response. *Journal of vascular surgery* **27**, 492-499 (1998).

8 Iaffaldano, R. A., Lewis, B. E., Johnson, S. A., Piffare, R. & McKieman, T. L. Patency of cryopreserved saphenous vein grafts as conduits for coronary artery bypass surgery. *CHEST Journal* **108**, 725-729 (1995).

9 Kader, K. N. *et al.* eNOS-overexpressing endothelial cells inhibit platelet aggregation and smooth muscle cell proliferation in vitro. *Tissue engineering* **6**, 241-251 (2000).

10 Rodgers, G. M. Hemostatic properties of normal and perturbed vascular cells. *The FASEB Journal* **2**, 116-123 (1988).

11 Cummings, C. L., Gawlitta, D., Nerem, R. M. & Stegemann, J. P. Properties of engineered vascular constructs made from collagen, fibrin, and collagen–fibrin mixtures. *Biomaterials* **25**, 3699-3706 (2004).

12 Rowe, S. L. & Stegemann, J. P. Interpenetrating collagen-fibrin composite matrices with varying protein contents and ratios. *Biomacromolecules* **7**, 2942-2948 (2006).

13 Wise, S. G. *et al.* A multilayered synthetic human elastin/polycaprolactone hybrid vascular graft with tailored mechanical properties. *Acta biomaterialia* **7**, 295-303 (2011).

14 Wissink, M. *et al.* Improved endothelialization of vascular grafts by local release of growth factor from heparinized collagen matrices. *Journal of Controlled Release* **64**, 103-114 (2000).

15 Wu, H.-C. *et al.* Coculture of endothelial and smooth muscle cells on a collagen membrane in the development of a small-diameter vascular graft. *Biomaterials* **28**, 1385-1392 (2007).

16 L'HEUREUX, N. *et al.* A human tissue-engineered vascular media: a new model for pharmacological studies of contractile responses. *The FASEB Journal* **15**, 515-524 (2001).

17 L'Heureux, N., Germain, L., Labbé, R. & Auger, F. A. In vitro construction of a human blood vessel from cultured vascular cells: a morphologic study. *Journal of vascular surgery* **17**, 499-509 (1993).

18 L'heureux, N., Pâquet, S., Labbé, R., Germain, L. & Auger, F. A. A completely biological tissue-engineered human blood vessel. *The FASEB Journal* **12**, 47-56 (1998).

19 Niklason, L. *et al.* Functional arteries grown in vitro. *Science* **284**, 489-493 (1999).

20 Greenwald, S. & Berry, C. Improving vascular grafts: the importance of mechanical and haemodynamic properties. *The Journal of pathology* **190**, 292-299 (2000).

21 Greisler, H. P. *et al.* Enhanced endothelialization of expanded polytetrafluoroethylene grafts by fibroblast growth factor type 1 pretreatment. *Surgery* **112**, 244-254; discussion 254-245 (1992).

22 Heise, M. *et al.* PEG-hirudin/iloprost coating of small diameter ePTFE grafts effectively prevents pseudointima and intimal hyperplasia development. *European journal of vascular and endovascular surgery* **32**, 418-424 (2006).

23 Sarkar, S., Sales, K. M., Hamilton, G. & Seifalian, A. M. Addressing thrombogenicity in vascular graft construction. *Journal of Biomedical Materials Research Part B: Applied Biomaterials* **82**, 100-108 (2007).

24 Bohl, K. S. & West, J. L. Nitric oxide-generating polymers reduce platelet adhesion and smooth muscle cell proliferation. *Biomaterials* **21**, 2273-2278 (2000).

25 Jun, H.-W., Taite, L. J. & West, J. L. Nitric oxide-producing polyurethanes. *Biomacromolecules* **6**, 838-844 (2005).

26 Kibbe, M., Billiar, T. & Tzeng, E. Inducible nitric oxide synthase and vascular injury. *Cardiovascular research* **43**, 650-657 (1999).

27 Salacinski, H. J. *et al.* The mechanical behavior of vascular grafts: a review. *Journal of biomaterials applications* **15**, 241-278 (2001).

28 Michiels, C. Endothelial cell functions. *Journal of cellular physiology* **196**, 430-443 (2003).

29 Pearson, J. D. Endothelial cell function and thrombosis. *Best Practice & Research Clinical Haematology* **12**, 329-341 (1999).

30 van Hinsbergh, V. W. in *Seminars in immunopathology*. 93-106 (Springer).

31 Semenza, G. L. Vascular responses to hypoxia and ischemia. *Arteriosclerosis, thrombosis, and vascular biology* **30**, 648-652 (2010).

32 Bae, J.-S., Yang, L. & Rezaie, A. R. Receptors of the protein C activation and activated protein C signaling pathways are colocalized in lipid rafts of endothelial cells. *Proceedings of the National Academy of Sciences* **104**, 2867-2872 (2007).

33 Bajzar, L., Morser, J. & Nesheim, M. TAFI, or plasma procarboxypeptidase B, couples the coagulation and fibrinolytic cascades through the thrombin-thrombomodulin complex. *Journal of Biological Chemistry* **271**, 16603-16608 (1996).

34 Bos, G. W., Poot, A. A., Beugeling, T., van Aken, W. G. & Feijen, J. Small-Diameter Vascular Graft Prostheses: Current Status. *Archives of Physiology and Biochemistry* **106**, 100-115, doi:10.1076/apab.106.2.100.4384 (1998).

35 Fukudome, K. *et al.* The endothelial cell protein C receptor cell surface expression and direct ligand binding by the soluble receptor. *Journal of Biological Chemistry* **271**, 17491-17498 (1996).

36 Ishii, H., Salem, H. H., Bell, C. E., Laposata, E. A. & Majerus, P. W. Thrombomodulin, an endothelial anticoagulant protein, is absent from the human brain. *Blood* **67**, 362-365 (1986).

37 Majerus, E. M., Zheng, X., Tuley, E. A. & Sadler, J. E. Cleavage of the ADAMTS13 propeptide is not required for protease activity. *Journal of Biological Chemistry* **278**, 46643-46648 (2003).

38 Medcalf, R. Fibrinolysis, inflammation, and regulation of the plasminogen activating system. *Journal of Thrombosis and Haemostasis* **5**, 132-142 (2007).

39 Osterud, B., Bajaj, M. & Bajaj, S. Sites of tissue factor pathway inhibitor (TFPI) and tissue factor expression under physiologic and pathologic conditions. On behalf of the Subcommittee on Tissue factor Pathway Inhibitor (TFPI) of the Scientific and Standardization Committee of the ISTH. *Thrombosis and haemostasis* **73**, 873-875 (1995).

40 Parmar, K. M. *et al.* Integration of flow-dependent endothelial phenotypes by Kruppel-like factor 2. *The Journal of clinical investigation* **116**, 49-58 (2006).

41 Ramesh, S. *et al.* Antiphospholipid antibodies promote leukocyte–endothelial cell adhesion and thrombosis in mice by antagonizing eNOS via β2GPI and apoER2. *The Journal of clinical investigation* **121**, 120-131 (2011).

42 Sakata, Y., Curriden, S., Lawrence, D., Griffin, J. H. & Loskutoff, D. J. Activated protein C stimulates the fibrinolytic activity of cultured endothelial cells and decreases antiactivator activity. *Proceedings of the National Academy of Sciences* **82**, 1121-1125 (1985).

43 Shim, K., Anderson, P. J., Tuley, E. A., Wiswall, E. & Sadler, J. E. Platelet-VWF complexes are preferred substrates of ADAMTS13 under fluid shear stress. *Blood* **111**, 651-657 (2008).

44 Valentijn, K. M. *et al.* Multigranular exocytosis of Weibel-Palade bodies in vascular endothelial cells. *Blood* **116**, 1807-1816 (2010).

45 Van Hinsbergh, V. *et al.* Activated protein C decreases plasminogen activator-inhibitor activity in endothelial cell-conditioned medium. *Blood* **65**, 444-451 (1985).

46 Jokinen, J. *et al.* Integrin-mediated Cell Adhesion to Type I Collagen Fibrils. *Journal of Biological Chemistry* **279**, 31956-31963, doi:10.1074/jbc.M401409200 (2004).

47 BARANSKA, P., JERCZYNSKA, H., PAWLOWSKA, Z., KOZIOLKIEWICZ, W. & CIERNIEWSKI, C. S. Expression of integrins and adhesive properties of human endothelial cell line EA. hy 926. *Cancer Genomics-Proteomics* **2**, 265-269 (2005).

48 Szmitko, P. E. *et al.* New markers of inflammation and endothelial cell activation part I. *Circulation* **108**, 1917-1923 (2003).

49 Wu, M. D. K. K. & Thiagarajan, M. D. P. ROLE OF ENDOTHELIUM IN THROMBOSIS AND HEMOSTASIS. *Annual Review of Medicine* **47**, 315-331, doi:10.1146/annurev.med.47.1.315 (1996).

50 Otsuka, F. *et al.* The importance of the endothelium in atherothrombosis and coronary stenting. *Nature Reviews Cardiology* **9**, 439-453 (2012).

51 Sumpio, B. E., Timothy Riley, J. & Dardik, A. Cells in focus: endothelial cell. *The International Journal of Biochemistry & Cell Biology* **34**, 1508-1512, doi:http://dx.doi.org/10.1016/S1357-2725(02)00075-4 (2002).

52 Aird, W. C. Endothelial cell heterogeneity. *Cold Spring Harbor perspectives in medicine* **2**, a006429 (2012).

53 Lamalice, L., Le Boeuf, F. & Huot, J. Endothelial Cell Migration During Angiogenesis. *Circulation Research* **100**, 782-794, doi:10.1161/01.RES.0000259593.07661.1e (2007).

54 Browning, M. B. *et al.* Endothelial cell response to chemical, biological, and physical cues in bioactive hydrogels. *Tissue Engineering Part A* **20**, 3130-3141 (2014).

55 Iivanainen, E., Kähäri, V. M., Heino, J. & Elenius, K. Endothelial cell–matrix interactions. *Microscopy research and technique* **60**, 13-22 (2003).

56 Cines, D. B. *et al.* Endothelial cells in physiology and in the pathophysiology of vascular disorders. *Blood* **91**, 3527-3561 (1998).

57 Davis, G. E. & Senger, D. R. Endothelial extracellular matrix biosynthesis, remodeling, and functions during vascular morphogenesis and neovessel stabilization. *Circulation research* **97**, 1093-1107 (2005).

58 Deanfield, J. E., Halcox, J. P. & Rabelink, T. J. Endothelial function and dysfunction testing and clinical relevance. *Circulation* **115**, 1285-1295 (2007).

59 Lerman, A. & Zeiher, A. M. Endothelial function cardiac events. *Circulation* **111**, 363-368 (2005).

60 Urbich, C. & Dimmeler, S. Endothelial Progenitor Cells: Characterization and Role in Vascular Biology. *Circulation Research* **95**, 343-353, doi:10.1161/01.res.0000137877.89448.78 (2004).

61 Esmon, C. T. Protein C anticoagulant pathway and its role in controlling microvascular thrombosis and inflammation. *Critical care medicine* **29**, S48-S51 (2001).

62 White, T. A. *et al.* Endothelial-derived tissue factor pathway inhibitor regulates arterial thrombosis but is not required for development or hemostasis. *Blood* **116**, 1787-1794 (2010).

63 Packham, M. A. Role of platelets in thrombosis and hemostasis. *Canadian journal of physiology and pharmacology* **72**, 278-284 (1994).

64 da Silva, M. L. & Cutler, D. F. von Willebrand factor multimerization and the polarity of secretory pathways in endothelial cells. *Blood* **128**, 277-285 (2016).

65 Broberg, M. & Nygren, H. Von Willebrand factor, a key protein in the exposure of CD62P on platelets. *Biomaterials* **22**, 2403-2409 (2001).

66 Feys, H., Anderson, P., Vanhoorelbeke, K., Majerus, E. & Sadler, J. Multi-step binding of ADAMTS-13 to von Willebrand factor. *Journal of Thrombosis and Haemostasis* **7**, 2088-2095 (2009).

67 Turner, N. A., Nolasco, L., Ruggeri, Z. M. & Moake, J. L. Endothelial cell ADAMTS-13 and VWF: production, release, and VWF string cleavage. *Blood* **114**, 5102-5111 (2009).

68 YEH, H. C. *et al.* Disulfide bond reduction of von Willebrand factor by ADAMTS-13. *Journal of Thrombosis and Haemostasis* **8**, 2778-2788 (2010).

69 Warner, T. D., Armstrong, P. C., Chan, M. V. & Knowles, R. B. (Taylor & Francis, 2016).

70 Booyse, F. M., Aikens, M. L. & Grenett, H. E. Endothelial Cell Fibrinolysis: Transcriptional Regulation of Fibrinolytic Protein Gene Expression (t-PA, u-PA, and PAI-1) by Low Alcohol. *Alcoholism: clinical and experimental research* **23**, 1119-1124 (1999).

71 Hynes, R. Cell–matrix adhesion in vascular development. *Journal of Thrombosis and Haemostasis* **5**, 32-40 (2007).

72 Bouïs, D., Hospers, G. A., Meijer, C., Molema, G. & Mulder, N. H. Endothelium in vitro: a review of human vascular endothelial cell lines for blood vessel-related research. *Angiogenesis* **4**, 91-102 (2001).

73 Olivero, D. K. & Furcht, L. T. Type IV collagen, laminin, and fibronectin promote the adhesion and migration of rabbit lens epithelial cells in vitro. *Investigative Ophthalmology & Visual Science* **34**, 2825-2834 (1993).

74 Raines, E. W. The extracellular matrix can regulate vascular cell migration, proliferation, and survival: relationships to vascular disease. *International journal of experimental pathology* **81**, 173-182 (2000).

75 Zamir, E. & Geiger, B. Molecular complexity and dynamics of cell-matrix adhesions. *Journal of Cell Science* **114**, 3583-3590 (2001).

76 Hynes, R. O. The Extracellular Matrix: Not Just Pretty Fibrils. *Science* **326**, 1216-1219, doi:10.1126/science.1176009 (2009).

77 van Hinsbergh, V. W. The endothelium: vascular control of haemostasis. *European Journal of Obstetrics & Gynecology and Reproductive Biology* **95**, 198-201 (2001).

78 Herbst, T. J., McCarthy, J. B., Tsilibary, E. C. & Furcht, L. T. Differential effects of laminin, intact type IV collagen, and specific domains of type IV collagen on endothelial cell adhesion and migration. *The Journal of Cell Biology* **106**, 1365-1373, doi:10.1083/jcb.106.4.1365 (1988).

79 Ricard-Blum, S. The Collagen Family. *Cold Spring Harbor Perspectives in Biology* **3**, a004978, doi:10.1101/cshperspect.a004978 (2011).

80 Hay, E. D. *Cell Biology of Extracellular Matrix*. Second Edition edn, (Springer US, 1991).

81 Heino, J. The collagen receptor integrins have distinct ligand recognition and signaling functions. *Matrix Biology* **19**, 319-323, doi:http://dx.doi.org/10.1016/S0945-053X(00)00076-7 (2000).

82 Vuoriluoto, K. *et al.* Syndecan-1 supports integrin α2β1-mediated adhesion to collagen. *Experimental Cell Research* **314**, 3369-3381, doi:http://dx.doi.org/10.1016/j.yexcr.2008.07.005 (2008).

83 Pankov, R. & Yamada, K. M. Fibronectin at a glance. *Journal of cell science* **115**, 3861-3863 (2002).

84 Durbeej, M. Laminins. *Cell and Tissue Research* **339**, 259-268, doi:10.1007/s00441-009-0838-2 (2009).

85 Couchman, J. R., Chen, L. & Woods, A. Syndecans and cell adhesion. *International review of cytology* **207**, 113-150 (2001).

86 Browning, M. *et al.* Multilayer vascular grafts based on collagen-mimetic proteins. *Acta biomaterialia* **8**, 1010-1021 (2012).

87 Mahabeleshwar, G. H. *et al.* Integrin affinity modulation in angiogenesis. *Cell Cycle* **7**, 335-347, doi:10.4161/cc.7.3.5234 (2008).

88 Mehta, D. & Malik, A. B. Signaling Mechanisms Regulating Endothelial Permeability. *Physiological Reviews* **86**, 279-367, doi:10.1152/physrev.00012.2005 (2006).

89 Morgan, M. R., Humphries, M. J. & Bass, M. D. Synergistic control of cell adhesion by integrins and syndecans. *Nature Reviews Molecular Cell Biology* **8**, 957-969 (2007).

90 Hasan, S. S. & Siekmann, A. F. The same but different: signaling pathways in control of endothelial cell migration. *Current opinion in cell biology* **36**, 86-92 (2015).

91 Shattil, S. J. & Ginsberg, M. H. Perspectives series: cell adhesion in vascular biology. Integrin signaling in vascular biology. *Journal of Clinical Investigation* **100**, 1-5 (1997).

92 Giancotti, F. G. Complexity and specificity of integrin signalling. *Nature Cell Biology* **2**, E13-E14 (2000).

93 Short, S. M., Talbott, G. A. & Juliano, R. L. Integrin-mediated signaling events in human endothelial cells. *Molecular Biology of the Cell* **9**, 1969-1980 (1998).

94 Kreidberg, J. A. Functions of α3β1 integrin. *Current Opinion in Cell Biology* **12**, 548-553, doi:http://dx.doi.org/10.1016/S0955-0674(00)00130-7 (2000).

95 Legate, K. R., Wickström, S. A. & Fässler, R. Genetic and cell biological analysis of integrin outside-in signaling. *Genes & Development* **23**, 397-418, doi:10.1101/gad.1758709 (2009).

96 Ivaska, J. & Heino*, J. Adhesion receptors and cell invasion: mechanisms of integrin-guided degradation of extracellular matrix. *Cellular and Molecular Life Sciences CMLS* **57**, 16-24, doi:10.1007/s000180050496 (2000).

97 Niu, G. & Chen, X. Why integrin as a primary target for imaging and therapy. *Theranostics* **1**, 30-47 (2011).

98 Ataya, B., Tzeng, E. & Zuckerbraun, B. S. Nitrite-generated nitric oxide to protect against intimal hyperplasia formation. *Trends in cardiovascular medicine* **21**, 157-162, doi:10.1016/j.tcm.2012.05.002 (2011).

99 Geiger, B., Spatz, J. P. & Bershadsky, A. D. Environmental sensing through focal adhesions. *Nat Rev Mol Cell Biol* **10**, 21-33 (2009).

100 Schwartz, M. A. Integrin signaling revisited. *Trends in Cell Biology* **11**, 466-470, doi:http://dx.doi.org/10.1016/S0962-8924(01)02152-3 (2001).

101 Clark, E. A. & Brugge, J. S. Integrins and signal transduction pathways: the road taken. *Science* **268**, 233 (1995).

102 Hodivala-Dilke, K. M., Reynolds, A. R. & Reynolds, L. E. Integrins in angiogenesis: multitalented molecules in a balancing act. *Cell and Tissue Research* **314**, 131-144, doi:10.1007/s00441-003-0774-5 (2003).

103 Zhao, X. & Guan, J.-L. Focal adhesion kinase and its signaling pathways in cell migration and angiogenesis. *Advanced Drug Delivery Reviews* **63**, 610-615, doi:http://dx.doi.org/10.1016/j.addr.2010.11.001 (2011).

104 Zaidel-Bar, R., Itzkovitz, S., Ma'ayan, A., Iyengar, R. & Geiger, B. Functional atlas of the integrin adhesome. *Nat Cell Biol* **9**, 858-867, doi:http://www.nature.com/ncb/journal/v9/n8/suppinfo/ncb0807-858_S1.html (2007).

105 Bernfield, M. *et al.* Biology of the syndecans: a family of transmembrane heparan sulfate proteoglycans. *Annual review of cell biology* **8**, 365-393 (1992).

106 Balaoing, L. R. *et al.* Laminin peptide-immobilized hydrogels modulate valve endothelial cell hemostatic regulation. *PloS one* **10**, e0130749 (2015).

107 Kainulainen, V. *et al.* Suppression of syndecan-1 expression in endothelial cells by tumor necrosis factor-α. *Journal of Biological Chemistry* **271**, 18759-18766 (1996).

108 Chaterji, S., Lam, C. H., Ho, D. S., Proske, D. C. & Baker, A. B. Syndecan-1 regulates vascular smooth muscle cell phenotype. *PloS one* **9**, e89824 (2014).

109 Fears, C. Y., Gladson, C. L. & Woods, A. Syndecan-2 is expressed in the microvasculature of gliomas and regulates angiogenic processes in microvascular endothelial cells. *Journal of Biological Chemistry* **281**, 14533-14536 (2006).

110 Alexopoulou, A. N., Multhaupt, H. A. & Couchman, J. R. Syndecans in wound healing, inflammation and vascular biology. *The international journal of biochemistry & cell biology* **39**, 505-528 (2007).

111 Caplan, M. R. & Shah, M. M. Translating biomaterial properties to intracellular signaling. *Cell biochemistry and biophysics* **54**, 1-10 (2009).

112 Carey, D. J. Control of growth and differentiation of vascular cells by extracellular matrix proteins. *Annual review of physiology* **53**, 161-177 (1991).

113 Leitinger, B. & Hohenester, E. Mammalian collagen receptors. *Matrix Biology* **26**, 146-155, doi:http://dx.doi.org/10.1016/j.matbio.2006.10.007 (2007).

114 Senger, D. R. *et al.* The α1β1 and α2β1 Integrins Provide Critical Support for Vascular Endothelial Growth Factor Signaling, Endothelial Cell Migration, and Tumor Angiogenesis. *The American Journal of Pathology* **160**, 195-204, doi:http://dx.doi.org/10.1016/S0002-9440(10)64363-5 (2002).

115 McGuigan, A. P. & Sefton, M. V. The influence of biomaterials on endothelial cell thrombogenicity. *Biomaterials* **28**, 2547-2571 (2007).

116 Genové, E., Shen, C., Zhang, S. & Semino, C. E. The effect of functionalized self-assembling peptide scaffolds on human aortic endothelial cell function. *Biomaterials* **26**, 3341-3351 (2005).

117 Gillis, C., Bengtsson, L. & Wiman, B. Secretion of prostacyclin, tissue plasminogen activator and its inhibitor by cultured adult human endothelial cells grown on different matrices. *European journal of vascular and endovascular surgery* **11**, 127-133 (1996).

118 Damsky, C. H. & Werb, Z. Signal transduction by integrin receptors for extracellular matrix: cooperative processing of extracellular information. *Current Opinion in Cell Biology* **4**, 772-781, doi:http://dx.doi.org/10.1016/0955-0674(92)90100-Q (1992).

119 Munoz-Pinto, D. J. *et al.* Collagen-mimetic hydrogels promote human endothelial cell adhesion, migration and phenotypic maturation. *Journal of Materials Chemistry B* **3**, 7912-7919 (2015).

120 Wissink, M. *et al.* Relation between cell density and the secretion of von Willebrand factor and prostacyclin by human umbilical vein endothelial cells. *Biomaterials* **22**, 2283-2290 (2001).

121 Xu, Y., Keene, D. R., Bujnicki, J. M., Höök, M. & Lukomski, S. Streptococcal Scl1 and Scl2 proteins form collagen-like triple helices. *Journal of Biological Chemistry* **277**, 27312-27318 (2002).

122 Seo, N. *et al.* An Engineered α1 Integrin-binding Collagenous Sequence. *The Journal of Biological Chemistry* **285**, 31046-31054, doi:10.1074/jbc.M110.151357 (2010).

123 Humtsoe, J. O. *et al.* A Streptococcal Collagen-like Protein Interacts with the α2β1 Integrin and Induces Intracellular Signaling. *Journal of Biological Chemistry* **280**, 13848-13857, doi:10.1074/jbc.M410605200 (2005).

124 Messent, A. J. *et al.* Effects of collagenase-cleavage of type I collagen on alpha2beta1 integrin-mediated cell adhesion. *Journal of cell science* **111**, 1127-1135 (1998).

125 Browning, M. B., Russell, B., Rivera, J., Höök, M. & Cosgriff-Hernandez, E. M. Bioactive hydrogels with enhanced initial and sustained cell interactions. *Biomacromolecules* **14**, 2225-2233 (2013).

126 Cosgriff-Hernandez, E. *et al.* Bioactive hydrogels based on designer collagens. *Acta biomaterialia* **6**, 3969-3977 (2010).

127 Davis, G. E. Affinity of integrins for damaged extracellular matrix: αvβ3 binds to denatured collagen type I through RGD sites. *Biochemical and biophysical research communications* **182**, 1025-1031 (1992).

128 Grover, C. N. *et al.* Crosslinking and composition influence the surface properties, mechanical stiffness and cell reactivity of collagen-based films. *Acta biomaterialia* **8**, 3080-3090 (2012).

129 Zhang, J. C., Wojta, J. & Binder, B. R. Growth and fibrinolytic parameters of human umbilical vein endothelial cells seeded onto cardiovascular grafts. *The Journal of thoracic and cardiovascular surgery* **109**, 1059-1065 (1995).

130 Balcells, M. & Edelman, E. R. Effect of pre-adsorbed proteins on attachment, proliferation, and function of endothelial cells. *Journal of cellular physiology* **191**, 155-161 (2002).

131 Clowes, A. W. Intimal hyperplasia and graft failure. *Cardiovascular Pathology* **2**, 179-186 (1993).

132 Lemson, M., Tordoir, J., Daemen, M. & Kitslaar, P. Intimal hyperplasia in vascular grafts. *European Journal of Vascular and Endovascular Surgery* **19**, 336-350 (2000).

133 Mills, B., Robb, T. & Larson, D. F. Intimal hyperplasia: slow but deadly. *Perfusion* **27**, 520-528, doi:10.1177/0267659112452316 (2012).

134 Rzucidlo, E. M., Martin, K. A. & Powell, R. J. Regulation of vascular smooth muscle cell differentiation. *J Vasc Surg* **45 Suppl A**, A25-32, doi:10.1016/j.jvs.2007.03.001 (2007).

135 Chen, P. Y., Qin, L., Li, G., Tellides, G. & Simons, M. Fibroblast growth factor (FGF) signaling regulates transforming growth factor beta (TGFbeta)-dependent smooth muscle cell phenotype modulation. *Scientific reports* **6**, 33407, doi:10.1038/srep33407 (2016).

136 Newby, A. C. & Zaltsman, A. B. Molecular mechanisms in intimal hyperplasia. *J Pathol* **190**, 300-309, doi:10.1002/(SICI)1096-9896(200002)190:3<300::AID-PATH596>3.0.CO;2-I (2000).

137 Davies, M. G. & Hagen, P. O. Pathobiology of intimal hyperplasia. *The British journal of surgery* **81**, 1254-1269 (1994).

138 Jennette, J. C. & Stone, J. R. in *Cellular and Molecular Pathobiology of Cardiovascular Disease* 197-219 (Academic Press, 2014).

139 Miyachi, H., Takahashi, M. & Komori, K. A Novel Approach against Vascular Intimal Hyperplasia Through the Suppression of Girdin. *Annals of vascular diseases* **8**, 69-73, doi:10.3400/avd.ra.14-00129 (2015).

140 Salacinski, H., Tiwari, A., Hamilton, G. & Seifalian, A. Cellular engineering of vascular bypass grafts: role of chemical coatings for enhancing endothelial cell attachment. *Medical and Biological Engineering and Computing* **39**, 609-618 (2001).

141 Haruguchi, H. & Teraoka, S. Intimal hyperplasia and hemodynamic factors in arterial bypass and arteriovenous grafts: a review. *Journal of Artificial Organs* **6**, 227-235 (2003).

142 Anderson, J. M. *et al.* Recent advances in biomedical polyurethane biostability and biodegradation. *Polymer International* **46**, 163-171 (1998).

143 Stokes, K., McVenes, R. & Anderson, J. M. Polyurethane elastomer biostability. *Journal of biomaterials applications* **9**, 321-354 (1995).

144 Lim, S.-T. *et al.* Nuclear-localized focal adhesion kinase regulates inflammatory VCAM-1 expression. *The Journal of Cell Biology* **197**, 907-919, doi:10.1083/jcb.201109067 (2012).

145 Rana, D. & Matsuura, T. Surface modifications for antifouling membranes. *Chemical reviews* **110**, 2448-2471 (2010).

146 Dong, B., Manolache, S., Wong, A. C. & Denes, F. S. Antifouling ability of polyethylene glycol of different molecular weights grafted onto polyester surfaces by cold plasma. *Polymer Bulletin* **66**, 517-528 (2011).

147 Harding, J. L. & Reynolds, M. M. Combating medical device fouling. *Trends in biotechnology* **32**, 140-146 (2014).

148 Gillis-Haegerstrand, C., Frebelius, S., Haegerstrand, A. & Swedenborg, J. Cultured human endothelial cells seeded on expanded polytetrafluoroethylene support thrombin-mediated activation of protein C. *Journal of vascular surgery* **24**, 226-234 (1996).

149 Hahn, M. S. *et al.* Photolithographic patterning of polyethylene glycol hydrogels. *Biomaterials* **27**, 2519-2524 (2006).

150 Ruggeri, Z. Von Willebrand factor, platelets and endothelial cell interactions. *Journal of Thrombosis and Haemostasis* **1**, 1335-1342 (2003).

151 Plant, A. L., Bhadriraju, K., Spurlin, T. A. & Elliott, J. T. Cell response to matrix mechanics: focus on collagen. *Biochimica et Biophysica Acta (BBA)-Molecular Cell Research* **1793**, 893-902 (2009).

152 Hynes, R. O. Integrins: Versatility, modulation, and signaling in cell adhesion. *Cell* **69**, 11-25, doi:10.1016/0092-8674(92)90115-S.

153 Antoniadis, A. P. *et al.* Biomechanical modeling to improve coronary artery bifurcation stenting: expert review document on techniques and clinical implementation. *JACC: Cardiovascular Interventions* **8**, 1281-1296 (2015).

154 Karanasiou, G. S. *et al.* Stents: biomechanics, biomaterials, and insights from computational modeling. *Annals of biomedical engineering* **45**, 853-872 (2017).

155 Lally, C., Dolan, F. & Prendergast, P. Cardiovascular stent design and vessel stresses: a finite element analysis. *Journal of biomechanics* **38**, 1574-1581 (2005).

156 Ballarin, F. *et al.* Fast simulations of patient-specific haemodynamics of coronary artery bypass grafts based on a POD–Galerkin method and a vascular shape parametrization. *Journal of Computational Physics* **315**, 609-628 (2016).

157 Lei, M., Giddens, D., Jones, S., Loth, F. & Bassiouny, H. Pulsatile flow in an end-to-side vascular graft model: comparison of computations with experimental data. *Journal of Biomechanical Engineering* **123**, 80-87 (2001).

158 Rashid, S. T., Salacinski, H. J., Hamilton, G. & Seifalian, A. M. The use of animal models in developing the discipline of cardiovascular tissue engineering: a review. *Biomaterials* **25**, 1627-1637 (2004).

159 Sho, E. *et al.* Arterial enlargement, tortuosity, and intimal thickening in response to sequential exposure to high and low wall shear stress. *Journal of vascular surgery* **39**, 601-612 (2004).

160 Dempsey, D. K. *et al.* Comparative analysis of in vitro oxidative degradation of poly (carbonate urethanes) for biostability screening. *Journal of Biomedical Materials Research Part A* **102**, 3649-3665 (2014).

161 Jaff, M. R. *et al.* Management of Massive and Submassive Pulmonary Embolism, Iliofemoral Deep Vein Thrombosis, and Chronic Thromboembolic Pulmonary Hypertension. *A Scientific Statement From the American Heart Association* **123**, 1788-1830, doi:10.1161/CIR.0b013e318214914f (2011).

162 Myllymäki, T. T. T., Lemetti, L., Nonappa & Ikkala, O. Hierarchical Supramolecular Cross-Linking of Polymers for Biomimetic Fracture Energy Dissipating Sacrificial Bonds and Defect Tolerance under Mechanical Loading. *ACS Macro Letters* **6**, 210-214, doi:10.1021/acsmacrolett.7b00011 (2017).

163 El-Rabbat, N., Askal, H. F., Khashaba, P. Y. & Attia, N. N. A validated spectrofluorometric assay for the determination of certain macrolide antibiotics in pharmaceutical formulations and spiked biological fluids. *Journal of AOAC International* **89**, 1276-1287 (2006).

164 Nakajima, T. Generalization of the sacrificial bond principle for gel and elastomer toughening. *Polym J*, doi:10.1038/pj.2017.12 (2017).

165 Greenfield, N. J. & Fasman, G. D. Computed circular dichroism spectra for the evaluation of protein conformation. *Biochemistry* **8**, 4108-4116 (1969).

166 Abraham, L. C., Zuena, E., Perez-Ramirez, B. & Kaplan, D. L. Guide to collagen characterization for biomaterial studies. *Journal of Biomedical Materials Research Part B: Applied Biomaterials* **87**, 264-285 (2008).

167 Lopes, J. L., Miles, A. J., Whitmore, L. & Wallace, B. A. Distinct circular dichroism spectroscopic signatures of polyproline II and unordered secondary structures: Applications in secondary structure analyses. *Protein Science* **23**, 1765-1772 (2014).

168 Chi, E. Y., Krishnan, S., Randolph, T. W. & Carpenter, J. F. Physical Stability of Proteins in Aqueous Solution: Mechanism and Driving Forces in Nonnative Protein Aggregation. *Pharmaceutical Research* **20**, 1325-1336, doi:10.1023/A:1025771421906 (2003).

169 von Hippel, P. H. & Wong, K.-Y. The effect of ions on the kinetics of formation and the stability of the collagen-fold. *Biochemistry* **1**, 664-674 (1962).

170 Post, A. *et al.* Introduction of sacrificial bonds to hydrogels to increase defect tolerance during suturing of multilayer vascular grafts. *Acta biomaterialia* **69**, 313-322 (2018).

171 Emsley, J., Knight, C. G., Farndale, R. W., Barnes, M. J. & Liddington, R. C. Structural basis of collagen recognition by integrin α2β1. *Cell* **101**, 47-56 (2000).

APPENDIX I

DESIGNER COLLAGEN PRODUCTION, CHARACTERIZATION, AND OPTIMIZATION

A.1 Introduction

Streptococcal collagen-like proteins, or Scl2, are recombinant proteins that mimic the triple helical structure of collagen but do not require post-translational modification for helix formation.[121] Although they mimic the structure of collagen, the Scl2 proteins are devoid of the native binding sites associated with collagen.[121] Therefore, the bioactivity of the Scl2 protein can then be customized by site-directed mutagenesis to introduce peptide sequences for specific cell surface receptor targeting.[122] For example, the collagen-derived peptide binding sequence GFPGER targets the integrins α1β1 and α2β1 and has been incorporated into Scl2 to tailor bioactivity.[122,123] Scl2 proteins with this targeting sequence are known as $Scl2_{GFPGER}$ proteins, and the binding of integrins to this peptide sequence is strengthened by the triple helical structure of the $Scl2_{GFPGER}$ protein.[124] This protein is naturally thromboresistant, even with the integrin targeting sequence, making it ideal for incorporation into the multilayer vascular graft to promote endothelialization.[86] Although production of this protein can be simple and high through-put with recombinant expression in *E. coli*, there have been inconsistencies in the protein batches that were discovered through irregularities in cell binding to the protein in hydrogels. Batch variability must be reduced in order to have consistent results in investigating the protein's effects and to make the production process appropriate for commercialization. Reducing batch variability required identification of the factors that affect the structure and bioactivity of the protein. The work presented here describes the production methods and processes that can affect the protein structure and ultimately the protein's ability to bind cells in 3D matrices.

A.2 $Scl2_{GFPGER}$ Evaluation

$Scl2_{GFPGER}$ protein structure and stability are key to its function of binding the targeted integrins α1β1 and α2β1.[122,123] The structure of the protein can be characterized several ways, including molecular weight and monomer content by SDS-PAGE, presence and tightness of the triple helix by circular dichroism, and aggregation by solubility assessment. The stability of the protein can be evaluated by measuring the melting curve, again using circular dichroism. Each of these measures may be useful predictors of the success of the batch in promoting cell binding. However, the protein functionality is ultimately assessed by cell adhesion on protein coats and $Scl2_{GFPGER}$ enriched hydrogels, depending on the intended application. For $Scl2_{GFPGER}$ incorporated into 3D structures, hydrogel evaluation is especially important, as the surface presentation of the protein is different than that of a protein coat.

A.2.1 $Scl2_{GFPGER}$ Molecular Weight and Monomer Content

Although the structure of the $Scl2_{GFPGER}$ protein is similar to that of collagen, the protein is only roughly one third of the size of collagen, about 35 kDa compared to collagen's 110 kDa. The molecular weight can be assessed using non-denaturing SDS-PAGE. The same gel can be used to assess monomer presence and content, giving an approximate indication of the fraction of the protein batch is in fact a true $Scl2_{GFPGER}$ protein with a stable triple helix. The bands indicating the triple helix and the monomer are shown in **Figure A.1** below.

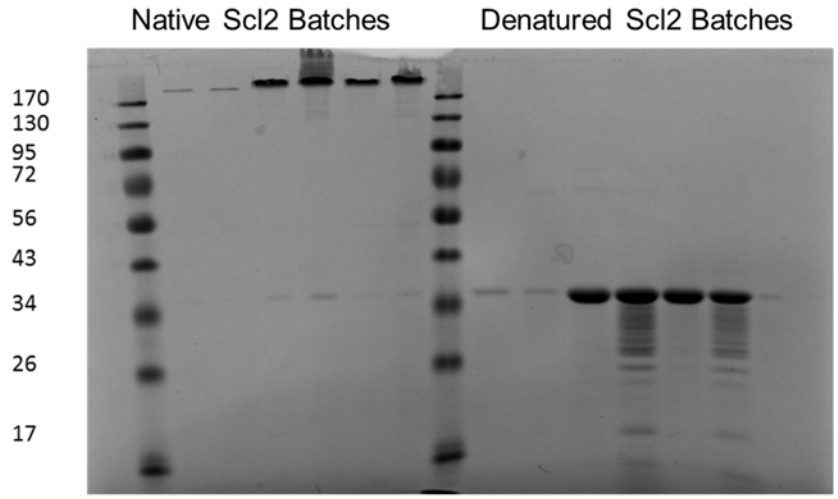

Figure A.1: Characterization of Scl2-2 protein monomer content and molecular weight using SDS-PAGE. Scl2 batches are compared between native conformation and denatured conformation. Native structure appears around 170kDa, and monomers appear around 34kDa.

A.2.2 Scl2$_{GFPGER}$ Triple Helix

Although SDS-PAGE can indicate the fraction of the protein batch that is in a triple helical form based on the expected molecular weight, it cannot disseminate the tightness of the triple helix. This can be characterized use circular dichroism (CD). CD is a measure of the difference in absorption between the left- and right-handed light of circularly polarized light.[165] CD is commonly used to characterize the secondary structure of proteins, with different peaks at various wavelengths indicating structures such as beta sheets and alpha helices. Examples of these different structures are shown in **Figure A.2** below.

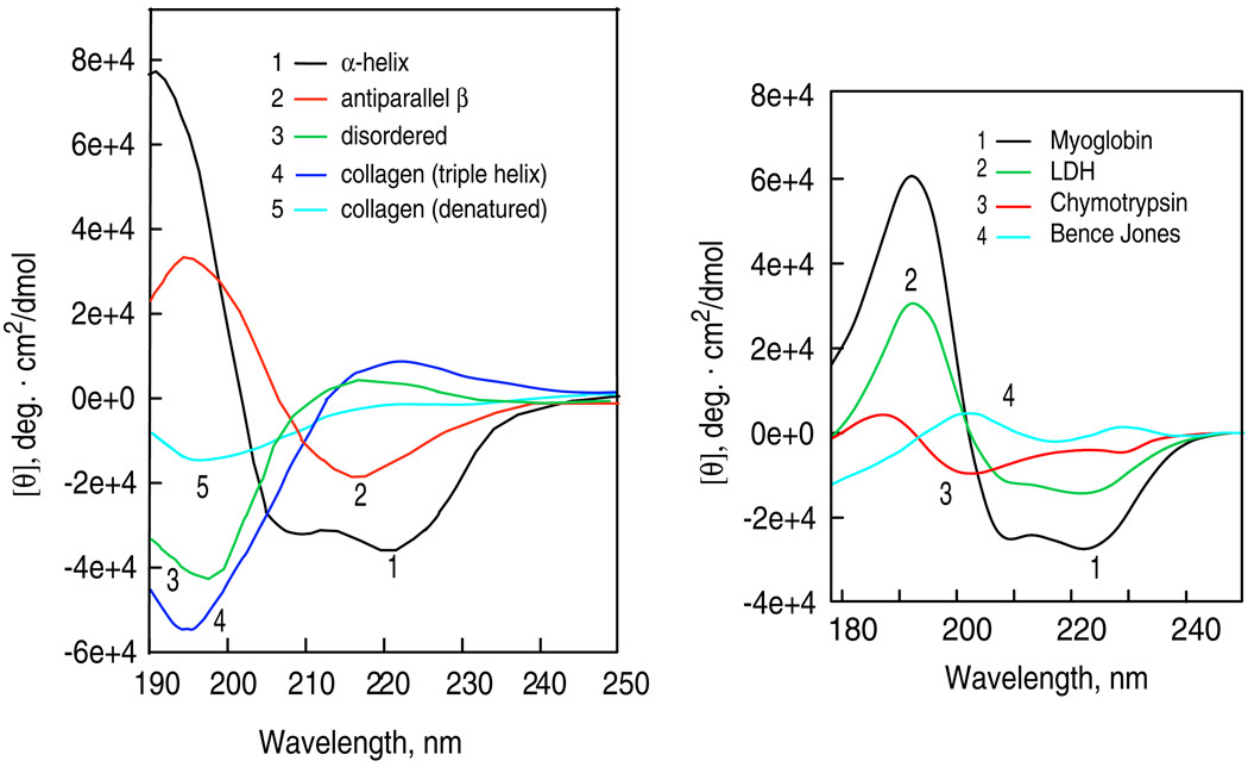

Figure A.2: Representative CD spectra of various protein conformations. Adapted from Greenfield et al 2009.

The presence of a triple helix is indicated by a peak in the CD spectra at 220nm.[166] The height of this peak can be a relative measure of the tightness of the helix. Additionally, the tightness of the alpha strand helices that make up the triple helix may have a relative measure by comparison of the shift in the valley of the peak around 200nm.[167] An example of these comparisons and shifts are shown in **Figure A.3** below.

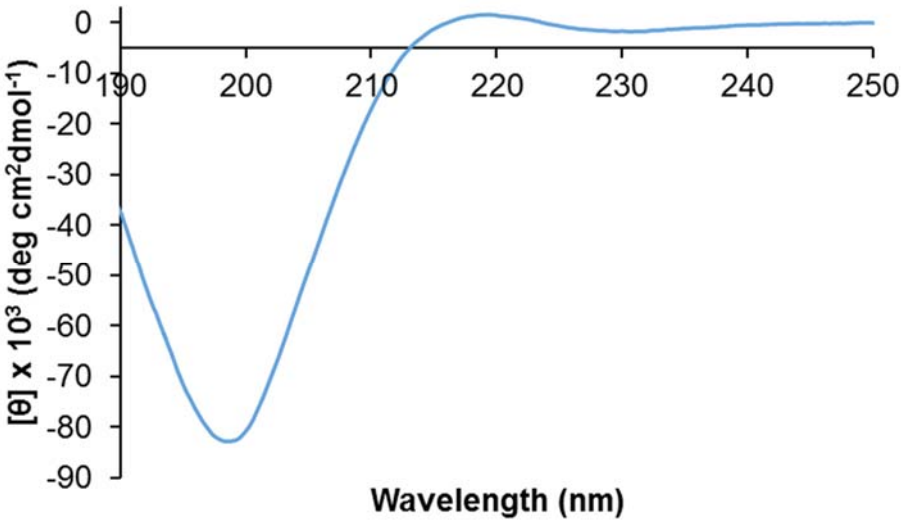

Figure A.3: Representative CD spectra of Scl2-2. The peak at 220nm demonstrated the presence and tightness of the triple helix based on the relative height of the peak. The valley around 200nm represents the alpha strand twisting and tightness based on the horizontal shift of the peak.

A.2.3 Scl2$_{GFPGER}$ Aggregation and Solubility

Another assessment of the structure of the Scl2 protein is its solubility. In the production process of the protein, there are opportunities for the proteins to loosen its triple helix then entangle with other loosened proteins, creating irreversible protein aggregates in non-native conformations.[168] These aggregates are theorized to preclude cell adhesion due to disruption and blocking of binding sites. Scl2 aggregates are visible in solution as they do not readily dissolve, especially when the protein is at a high concentration. Therefore the presence of aggregates can be identified by attempting to dissolve the protein. If aggregates of the protein are identified after protein isolation but before lyophilization, they can be "spun out" via centrifugation, leaving only soluble protein in solution. The supernatant can then be used for freezing and lyophilization.

In general, dissolution of the protein, similar to collagen, can be improved by the addition of salts and by altering pH.[168,169] The ideal salt molarities and pH ranges to retain protein structure are ultimately determined by the overall charge of the protein.[168] The salt ions can modulate the strength of the electrostatic interactions between charged groups in the protein that ultimately dictate the protein conformation.[168,169] In studies examining the effects of neutral salts on the structure of collagen, it was shown that salts competitively reorganize the water involved in stabilizing the collagen helix, contributing to the triple helix stability.[169] Use of buffers such as PBS can therefore contribute to the stability of the triple helices in solution. Although low pH has been demonstrated to increase solubility of collagen by loosening the structure, it has been previously demonstrated that low pH destabilized the triple helix of Scl2 proteins by shifting the melting curve dramatically (**Figure A.4**).[124] Therefore, lowering pH can contribute to improved dissolution of Scl2 proteins within a specific range, but lowering the pH too far can decrease the melting point beyond practical levels. Another method to protect protein structure is the introduction of a stabilizer into solution. One such stabilizer is sucrose, and it protects protein structure by preventing unfolding through preferential surface exclusion, or negative binding. As the surface area of the protein increases, as is what occurs during unfolding, the protein is pushed back towards the native, folded state through increased negative binding.

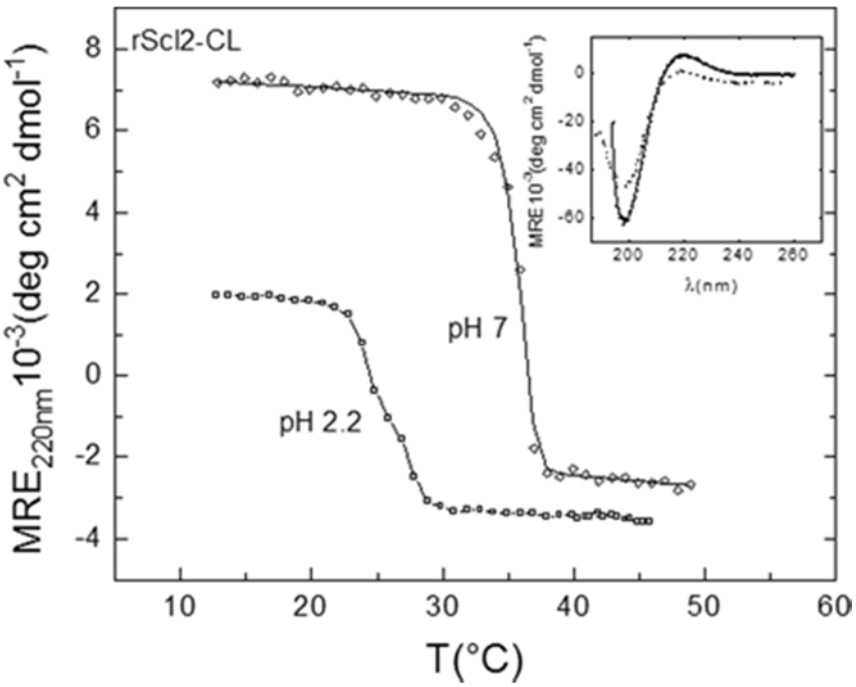

Figure A.4: The melting temperature of Scl2 is lowered by lowering the pH of the solvent. From Mohs et al. 2007.

A.2.4 Scl2$_{GFPGER}$ Stability

The overall thermodynamic stability of the Scl2$_{GFPGER}$ triple helix can be assessed by monitoring the denaturation in the triple helix in a neutral buffer over a temperature range to find the melting temperature. This can be accomplished with CD analysis by measuring the height of the peak at 220nm over the specified temperature range. The melting temperature of Scl2 proteins is typically observed around 35°C (**Figure A.5**), but batch variability or low pH of the solvent can lead to lower melting temperatures that reduce Scl2$_{GFPGER}$ stability.

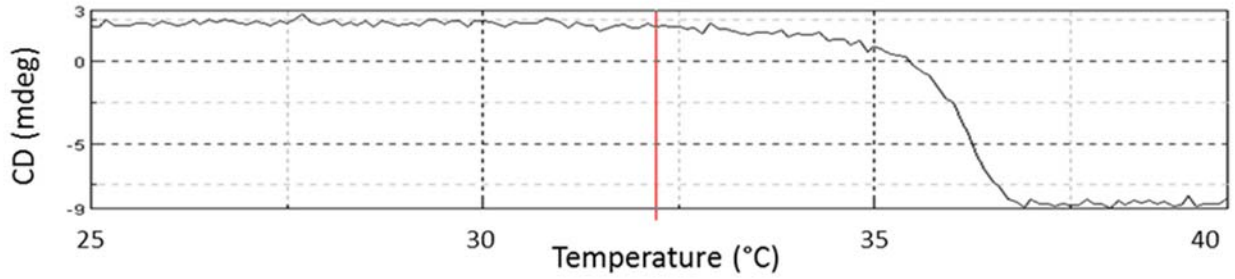

Figure A.5: Representative CD spectra of the Scl2-2 melting curve.

A.2.5 Cell Adhesion on Scl2$_{GFPGER}$ Protein Coats

Protein structure and stability characterization can give clues as to the functionality of the protein, but protein batch success can ultimately only be tested via cell adhesion to determine its binding affinity. Using low protein concentrations (2-10μg per 96 well), well plates can be coated with the protein, blocked with BSA to limit non-specific binding, then exposed to cells to determine attachment differences between different proteins and batches.

In order to assess Scl2$_{GFPGER}$ protein functionality with cell adhesion, the cells used in the adhesion study must present the targeted integrins, α1β1 and α2β1, in relatively high abundance. C2C12 cells are commonly used with induced overexpression of these integrins. Most endothelial cells also express these integrins, and these are the cells we commonly use in our studies. However, if there is ever a question of appropriate integrin expression, use of C2C12 cells is a method to ensure attachment is possible. Although there are observable differences in attachment between protein types, such as between the collagen and Scl2$_{GFPGER}$ shown below (**Figure A.6**), there is too much variability in the test to effectively determine differences between adhesion in batches that later arise when the protein is incorporated into a 3D matrix. Protein coat attachment is ultimately not predictive of cell attachment to Scl2$_{GFPGER}$ hydrogels.

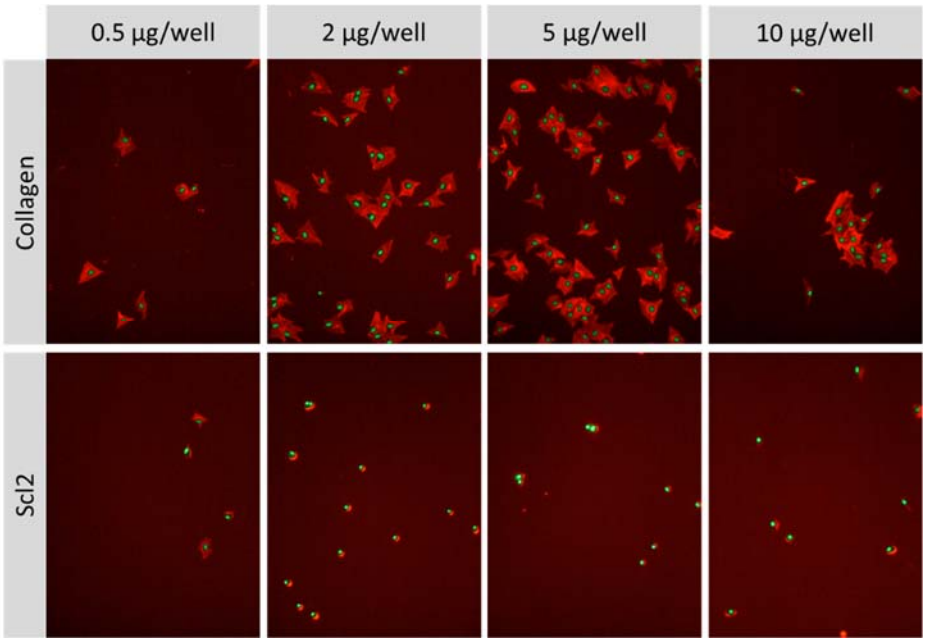

Figure A.6: Endothelial cell attachment on collagen and Scl2-2 protein coats at various protein concentrations.

A.2.6 Cell Adhesion on Hydrogels

A more discerning test of $Scl2_{GFPGER}$ function is to incorporate it into hydrogels, where surface presentation is more random and perhaps less concentrated. The $Scl2_{GFPGER}$ protein is incorporated into 3D structures, as it cannot form 3D structures independently. In order to covalently incorporate the protein into a hydrogel, a common application in our lab, the protein must first by functionalized with a linker. Previous work has determined the optimal functionalization density for maximum cell adhesion without significant protein loss to be 0.1X, or functionalization of 10% of the lysines present in the protein.[54] This previous work also demonstrated that FTIR spectra can be used to determine the relative functionalization of the protein, and must be confirmed for protein incorporation into the hydrogel (**Figure A.7**).[54]

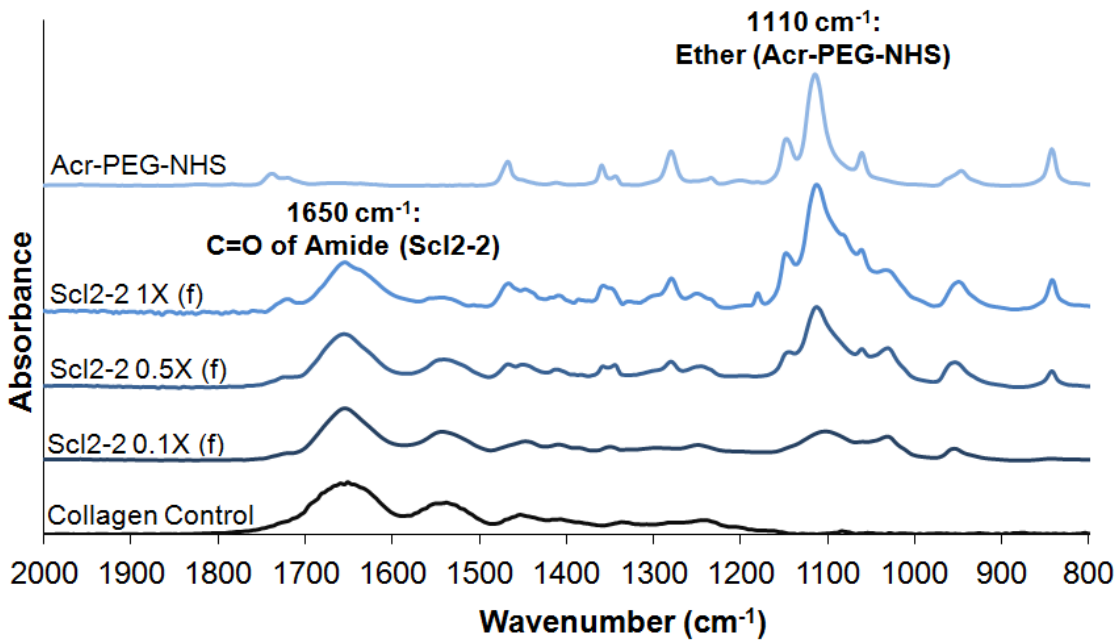

Figure A.7: FTIR spectra of Scl2-2 and collagen functionalization with the PEG-based linker Acr-PEG(3500)-NHS. The functionalization increases from 10% of the available lysines (0.1X) to 100% of the available lysines (1X). The peak at 1110 represents the PEG backbone, and the peaks at 1650 represent the amines of the protein. Adapted from Browning et al 2013.

Cell attachment is performed as previously described.[170] Briefly, once the protein is incorporated into the PEGDA hydrogel, it is soaked overnight with 3 PBS changes. Then the hydrogel slab is punched into rounds and placed into a 48 well plate. Cells are then seeded at 10,000 cells/well, allowed to adhere for 3 hours, rinsed with PBS to remove non-adherent cells, and fixed with 3.7% glutaraldehyde. Hydrogel slab cell attachment provides a clear picture of Scl2$_{GFPGER}$ batch functionality differences (**Figure A.8**).

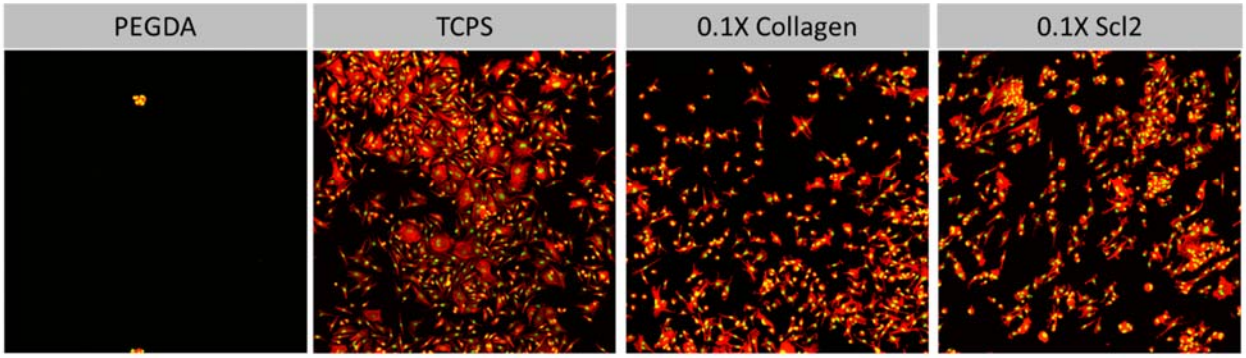

Figure A.8: Endothelial cell adhesion on collagen and Scl2-2 hydrogels.

A.3 Expression system effects

$Scl2_{GFPGER}$ protein is produced through the recombinant expression of the protein in *E. coli*, as described previously.[121] Briefly, *E. coli* are grown out in LB media until the absorbance measurement OD600 falls between 0.6 and 0.8. Then expression of the protein in the *E. coli* is induced by the addition of IPTG. After expression of $Scl2_{GFPGER}$, the *E. coli* are spun down for collection (8000 rpm, 4˚C, 15 min) then frozen to encourage disruption of the bacterial membranes. The thawed *E. coli* are then sonicated or French pressed in order to release the cellular contents. The cellular waste is then removed via centrifugation (20000g, 4˚C, 30 min), and the $Scl2_{GFPGER}$ protein is then isolated using nickel columns. Different strains of *E. coli* can be used for protein expression, and they each have different effects on Scl2-2 protein structure.

The Topp 3 system was used initially to express $Scl2_{GFPGER}$. This system is characterized by considerable variability in protein production. In fact, the product is no longer manufactured due to concerns about the protein production consistency (REF). BL21 is the new recommended system and is thought to have more consistency between batches (REF). Yet another system, the Clear Coli system, provides cleaner protein with much lower LPS content (REF). Creating protein

with lower endotoxin levels could help limit the amount of post-process cleaning required for making the protein safe in animal studies. However, in switching to the Clear Coli system, the structure and stability of $Scl2_{GFPGER}$ is greatly affected.

Characterization of the protein made using the Clear Coli system reveals high monomer content, a less stable triple helix, and lower cell attachment as compared to $Scl2_{GFPGER}$ made via expression in Topp 3 (**Figure A.9**). In the non-denaturing SDS-PAGE, there is an obvious band at around 40-55kDa in the Clear Coli $Scl2_{GFPGER}$, indicating a denatured form of the $Scl2_{GFPGER}$ protein. Upon further investigation, we discovered that the melting temperature of Clear Coli $Scl2_{GFPGER}$ is much lower than that of the Topp 3 $Scl2_{GFPGER}$, 32˚C and 37˚C, respectively. When the protein is incorporated into hydrogels, there is an obvious difference in cell adhesion, with little to no adhesion observed in the Clear Coli $Scl2_{GFPGER}$ hydrogels.

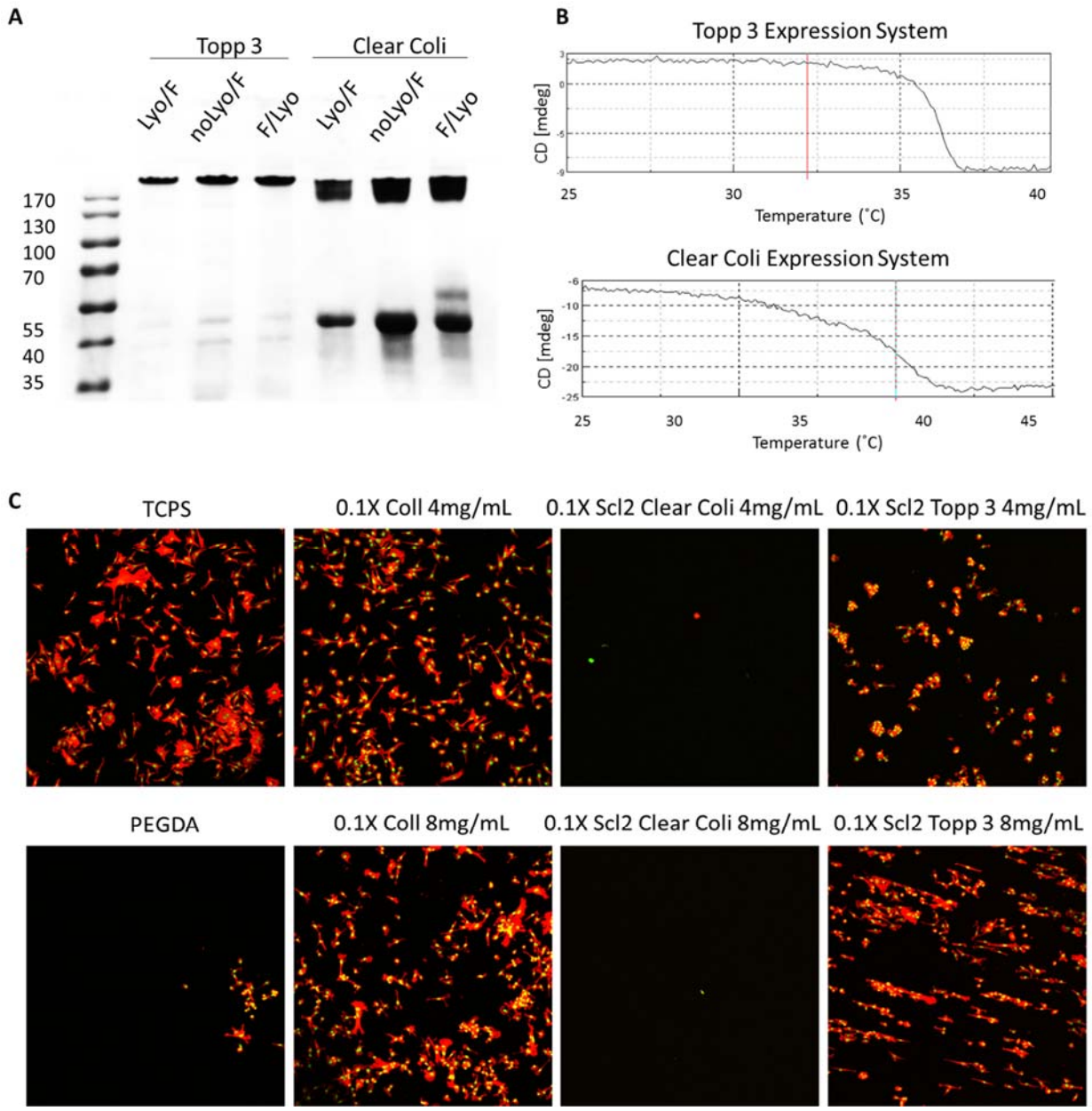

Figure A.9: Comparison of Scl2-2 expression systems using protein characterization in SDS-PAGE with lyophilized, non-lyophilized and functionalized, and functionalized and lyophilized protein (A), CD (B), and cell attachment (C).

A.4 LPS Removal Effects

Lipopolysaccharides, or LPS, are endotoxins that are structural components of the outer cell membrane of all gram-negative bacteria, and they appear in the $Scl2_{GFPGER}$ proteins due to the expression method. Endotoxins elicit an immune response, therefore they must be removed for the protein to be used in animal models. There are several methods for LPS removal. In detergent removal, the protein is washed with Triton X-114 to degrade the LPS, followed by dialysis to remove the detergent .This is generally considered an efficient method of LPS removal with very little loss of protein. However, the $Scl2_{GFPGER}$ structure is sensitive to harsh detergents, and the protein tends to unfold, as shown in **Figure A.10**. This unfolding can increase the monomer content of the batch as well as create the opportunity for protein aggregation as discussed earlier.

Another method for LPS removal is column purification. An example of such a column is the Pierce High Capacity Endotoxin Removal Spin Column. The porous cellulose beads in the column have been surface modified with polylysine that has a high affinity for endotoxins. This removal method is much less damaging to the protein with little change in the protein structure and function. The column removal is also less efficient, however, and requires many passes through the column in order to reduce the LPS to acceptable levels for animal use. The many passes through the column results in significant protein loss, but yields a clean, stable protein.

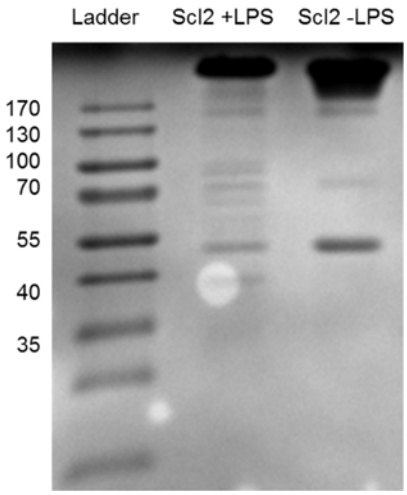

Figure A.10: Effect of detergent LPS removal on protein structure and monomer content.

A.5 Globular Domain Removal Effects

The $Scl2_{GFPGER}$ proteins are comprised of a rounded globular domain and a long collagenous tail, forming a lollipop structure. The globular domain has a diameter that is roughly 3.9-6.4nm, and the collagen like tail is approximately 45.5nm long.[121] Removal of the globular domain is thought to increase solubility of the $Scl2_{GFPGER}$ protein as well as lower any possible remaining immunological concerns, as the globular domain has more bacterial-specific peptide sequences that can be recognized as "non-self" by other animal species. Globular domain removal is achieved by enzymatic cleavage, and slightly reduces the molecular weight of the $Scl2_{GFPGER}$ protein. Removal of the globular domain does not appear to have large effects on the triple helix, melting temperature, or cell adhesion in hydrogels, as shown below.

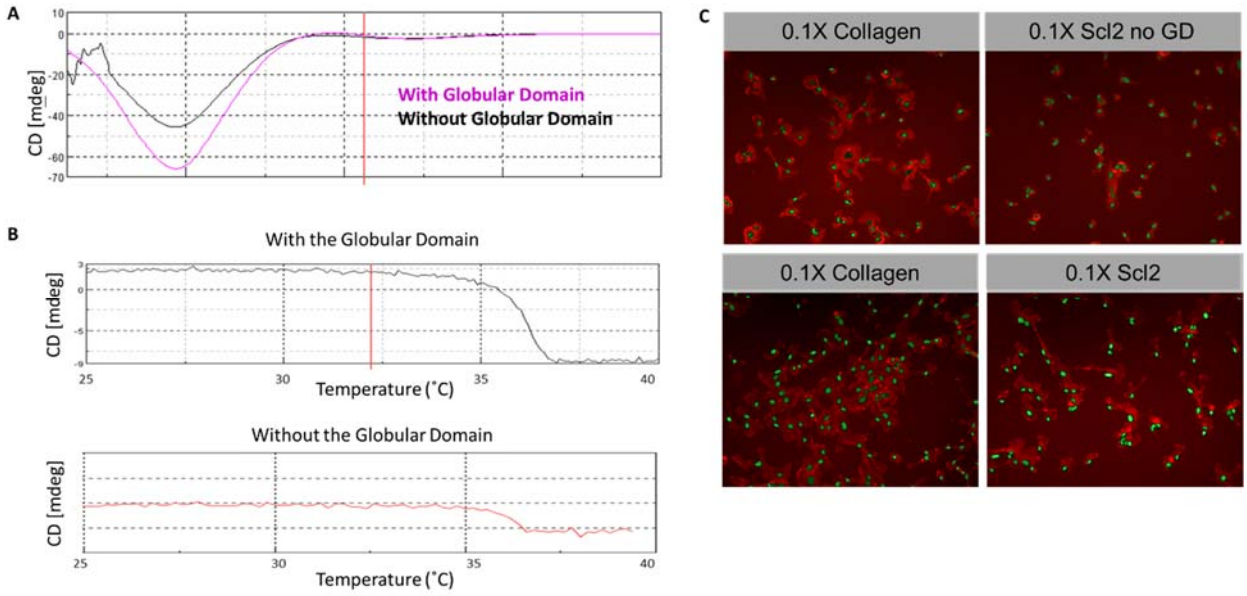

Figure A.11: Comparison of Scl2-2 with and without the globular domain in CD for triple helix (A), CD for melting curve (B), and cell attachment (C).

A.6 pH Effects on Conformation and Function

Enzymatic cleavage of the globular domain can be performed in different pH conditions, depending on the enzyme used for cleavage. Typically we have used pepsin as the cleaving enzyme, and pepsin has optimum activity at a pH of 2.5. This pH can still alter Scl2$_{GFPGER}$ protein structure, similar to the detergent washes described above for LPS removal. Even small changes in protein conformation can affect binding affinity of targeted integrins on the cell surface.[171]### The enzyme has also shown to be effective at a pH of 4, and although the condition is still harsh, the effects of the low pH on the protein structure are hypothesized to be minimal enough to allow for endothelial cell attachment to Scl2$_{GFPGER}$ hydrogels.

A.7 Conclusions and Future Work

The work presented here demonstrates many ways to characterize Scl2 protein structure and function. Using various assessment tools, we can analyze protein monomer content and aggregation, triple helix formation and stability, and batch affinity for cell attachment. We have also identified several production and isolation processes that can affect Scl2 structure and function. Although there has been extensive characterization of the $Scl2_{GFPGER}$ protein structure, it is difficult to identify a single predictor of protein functionality in hydrogels. Without knowing the strongest predictor of protein batch success, batches cannot be effectively screened before use in hydrogels. This work, however, has created a system for possible discovery of that predictor.

The specific integrin targeting of $Scl2_{GFPGER}$ can be used to control cell fate through intracellular signaling initiated by integrin attachment. With the demonstrated potential for targeted binding and control, this protein has been used in many bioengineering applications, such as cardiovascular, orthopedic, and wound healing biomaterial design. Therefore, future optimization of $Scl2_{GFPGER}$ production is crucial for many applications in tissue engineering and biomaterial design. Future work with the Scl2 family of proteins will require identifying the best expression and isolation parameters to produce consistent batches of protein. Once batch consistency and functional predictability has been established, then fermenter scale up of the production process can increase batch yield. This would be ideal for commercialization and large experimental studies.